Novel Light-Matter Interaction in Quasi-One-Dimensional Graphene Nanomaterials for Photonics

Thesis by

Deepan Kishore Kumar

In Partial Fulfillment of the Requirements for

the Degree of

Doctor of Philosophy

CALIFORNIA INSTITUTE OF TECHNOLOGY

Pasadena, California

2021

(Defended May 21, 2021)

Deepan Kishore Kumar
ORCID: 0000-0003-0236-8805

ACKNOWLEDGEMENTS

I am deeply grateful for being given the opportunity to explore the frontiers of science in Professor Nai-Chang Yeh's group at Caltech. The intellectual stimulation and adventures in last few years have been unmatched in the pursuit of bold ideas, equipped with only curiosity that showed the way forward, to explore a new paradigm in solar energy harvesting and silicon nanophotonics with 2D nanomaterials. This work could have not happened anywhere, if not for Prof. Nai-Chang's infinite enthusiasm for physics and willingness to challenge the status-quo with a deep sense of engagement in student's wellbeing above everything.

The feedback and encouragement from my committee members - Prof. Amnon Yariv, Prof. Alireza Marandi, Prof. Andrei Faraon, and Prof. Mohammad Mirhosseini – has certainly helped me refine and evolve my understanding of coherent interaction in non-linear systems, and I hope to continue collaborating with their groups in the years to come.

I am also grateful for the support from many scientists like Dr. Jay Winkler (Beckman Institute Laser Resource Center), Dr. Baolai Liang and Dr. Aziz (UCLA CNSI), Dr. Andres and Dr. Giada (Beckman Imaging facility), Dr. Philip Hon (Northrop Grumman), Prof. George Rossman (GPS, Caltech) for teaching me valuable optical experimental skills and accommodating my endless stream of questions that has kept this research endeavor fruitful -- you all make science accessible to the broader community and have been wonderful collaborators.

I am also very grateful to Dr. Ali Ghaffari for providing me not just TAship, nearly every quarter even though the pandemic, for APh 109, but also for sharing his invaluable perspective of life in teaching, research, and mentorship. The work done with Dorte, Stella, and others has helped in accelerating research, and helped me to grow as a mentor and collaborator.

I am also deeply thankful for the support net of Dr. S.M., Dr. A.M., and Dr. J.W., for being instrumental in supporting my wellbeing. To the countless friends who shared my happiness

and pains, thank you for everything, you all have been the fuel for my soul, and I thank you for the inspiring me.

I have been most fortunate to learn science from teachers who were boundlessly passionate about teaching and mentoring and really inspired me, directly or indirectly, to continue on a life-long pursuit of scientific inquiry: Dr. Srinivasa Raghavan, Dr. Sundaram Swaminathan, Dr. Ravi Kant Mittal have been my guiding north stars to venture deeper into science from an early stage starting from Indian School Muscat, Oman and the Birla Institute of Technology and Science, Pilani.

I am also thankful for the wonderful interactions with The Yeh Group: Duxing Hao, Jacob Bagley, Dr. Marcus Teague, Steve Lu, Akiyoshi Park, Dr. Chen-Chih Hsu, Dr. Kyle, Dr. Vincent, and others who all share a common curiosity for pure or applied physics, and are all just wonderful people with whom I shared my lab years.

Last and most importantly, none of this would have been possible without the infinite support from my family and their love – I am an incredibly lucky person because of you all.

Dedicated to

அம்மா (Vijayalakshmi)

அப்பா (Kishore Kumar)

அக்கா (Krithikaa)

ABSTRACT

Nonlinear light-matter interaction in two-dimensional (2D) materials like graphene with unique nanostructured quasi-one-dimensionality (quasi-1D) holds the potential to address major technology opportunities in photonics from on-chip photo detection, modulation of light, and even possibly coherent light sources. In this work, we propose to use graphene, a gapless two-dimensional nanomaterial, for both nano-photonic applications and potentially energy harvesting by nano-structuring the material into nearly quasi-one-dimensional effective optical cavities with defects that act like color centers. These defects are naturally formed during its synthesis or can be engineered in the material by selective plasma radiation, are found to support a broad spectral distribution of color centers that exhibit excitation dependent photoluminescence. Through detailed investigation on the temperature and power dependence of photoluminescence from such defects, excitation dependent photoluminescence emission, we have established that these graphene nanomaterials with metastable energy states can support material excitations (*e.g.*, excitons) that are strongly coupled to the optical modes confined within the nanostructured cavities to produce polaritonic quasiparticles, leading to many interesting nonlinear behaviors. In particular, the manifestation of blue-shifted photoluminescence, polariton lasing-like emission, multimode lasing-like emission, and distinct interference fringes, all points to the presence of novel light-matter interaction in quasi-one-dimensional graphene. Such novel light matter interactions can be exploited, among other applications, within photonic integrated circuits (PIC) by directly synthesizing graphene on silicon from a low temperature, single-step, plasma-enhanced chemical vapor deposition (PECVD) with feedstock gases of methane and hydrogen.

TABLE OF CONTENTS

LIST OF ILLUSTRATIONS

Number *Page*

Chapter 1

INTRODUCTION TO NANOSCALE LIGHT MATTER INTERACTION

In this thesis, we demonstrate a direct, single-step, low-temperature plasma enhanced chemical vapor deposition (PECVD) method that is capable of synthesizing quasi-one-dimensional graphene nanomaterials directly on silicon and silicon oxide substrates apart from traditional copper substrates. The observation of lasing-like emission, or possible amplified spontaneous emissions, in the infrared to visible light range from the quasi-1D-graphene-on-silicon systems, can be a step towards broad applications in photonics and optoelectronics. The current industrial need for high-quality graphene is evident from a survey of graphene quality being commercially sold reported by Alessandro et al [2]. Towards addressing the industrial need for bulk quantities of graphene nanomaterials, we also develop transfer techniques using scalable processes based on spin-coating or ink-jet printing with organic solvent assisted colloidal suspensions of multi-layer high-quality graphene. These transferred graphene nanomaterials, with well-preserved quasi-1-dimensiaonlity can help develop highly sensitive photodetectors, or light-modulators, and broadband light sources for printed electronics, integrated optical sensors, electrochemical sensors etc. In order to understand many of the novel light-matter interactions reported in this thesis, we study the effects of temperature, power, wavelength of excitation laser, and th role of defects on the nanoscale scattering of light. These preliminary studies indicate the possibility of using these quasi-1D-graphene nanomaterials for solar energy harvesting (due to the presence of optically active defect centers), among other directions.

The review by A. C. Ferrari at al [6], laid out the state of the art in mono-layer graphene photonics and optoelectronics. Graphene as a light source was always limited to graphene oxide having a complete bandgap showing broadband photoluminescence, however synthesis of graphene oxide had no direct route except for oxygen plasma treatment of multilayer graphite, as the etching effect of oxygen plasma on monolayer graphene would lead to complete removal of the carbon atoms from graphene. The ability to engineer such

defect states from plasma processing is the key to integrating nanomaterials for integrated devices that can exploit strong light matter interaction. In particular, we note that the Dirac electrons in graphene with a vanishing effective mass have been predicted by Zeiegler and Mikhailov [7] to be strongly nonlinear with up-conversion and frequency multiplication effects, which can help explain some of our experimental findings in quasi-1D graphene nanomaterials.

Plasmonic mode confinement of propagating optical modes offers unprecedented access to integrating optics to nanoscale devices by exploiting collective electronic excitations. This ability to concentrate light and/or produce high local-field intensities is typically been the domain of dielectric lenses and resonators. With nanostructures of quasi-1d-graphene there may be a unique opportunity to leverage deep-subwavelength mode confinements to possibly realize nanoscale control of excitons or other quasiparticle interactions. Surface plasma polaritons, for instance, can propagate back and forth between metallic nanostructure terminations, acting like an effective Fabry-Perot resonator, picking up a phase on multiple reflections. Such subwavelength regimes can be probed by near field scanning optical microscopes (NSOM), as an example. With nanostructured gapless material like quasi-1D-graphene, we also need to consider nonlinear effects like Second Harmonic Generation (SHG), from broken inversion symmetry at interfaces along the width of the nanomaterial.

Lastly, we also need to consider the ability to engineer the radiative decay rates of ‘emitters’ like embedded quantum dots, or topological defects within quasi-1D-graphene for useful for photonic applications such as plasmonic nanoscale lasers, sensing or lithography [1]. The strongly confined plasmonic fields can alter the radiative and non-radiative decay rates of such emitters and also alter the emission directionality.

1.1 Gedanken Experiment on Nanoscale Photon Trapping

From the early demonstration of light induced electrochemical effects on platinum electrodes in solution by Becquerel* in 1839, and later in solid state materials like selenium (where a direct photoconductivity effect was observed by W. Smith), to the widely accepted understanding of the photoelectric effect formulated by Einstein in the 1900s, the scientific enterprise has focused primarily on light interaction with semiconducting (direct or indirect bandgap) materials. These well-defined crystalline semiconducting materials, like silicon, GaAs, CdSe, CIGS, *etc*., all rely on the excitation of ground state electrons from the valence band to an excited state within the conduction band by broadband solar illumination, which provides the energy needed for this transition or other electron-electron scattering pathways for hot electron generation and multiplication. In order to enhance the efficiency of light coupling to matter, and to overcome the fundamental limitation of the detailed balance limit set by accounting for various thermodynamic factors within bandgap semiconductors, there has been a substantial progress on reaching power conversion efficiency towards 46% in multi-junction solar cell devices.

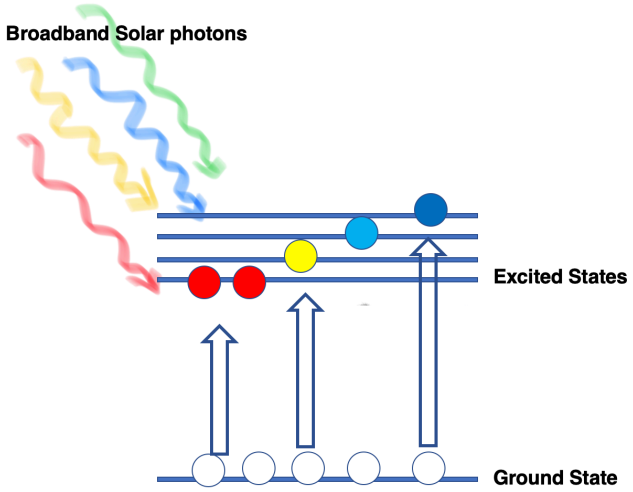

Figure 1.1: Conceptual sketch of photoexcitation in a conventional multi-junction semiconductor

For this thesis work, rather than epitaxially growing perfectly crystalline bandgap semiconductors, we consider growing nearly perfect nanostructured that can act as *effective*

optical cavities with some color centers that can interact with the light trapped in the subwavelength cavities. Is there a way, then, to harvest the trapped photons near the color center through the creation of some quasi particles like plasmon polaritons or exciton polaritons? Is it also possible to achieve a coherent state of quasiparticles within these optical cavities so that ultra-high efficiency conversion from the photon-hybridized quasiparticle states to the ground state can take place? Moreover, if one could extract the excited charge carriers from such a macroscopically occupied regime before their radiative relaxation back to the ground state, then it would be feasible to have a *nearly*-coherent current output. Being able to mimic collective quasiparticle interactions and possibly to realize the regime of polariton lasing would be an important step towards creating coherent states for efficient on-chip integrated silicon photonics applications like modulation, or tunable light emission, etc.

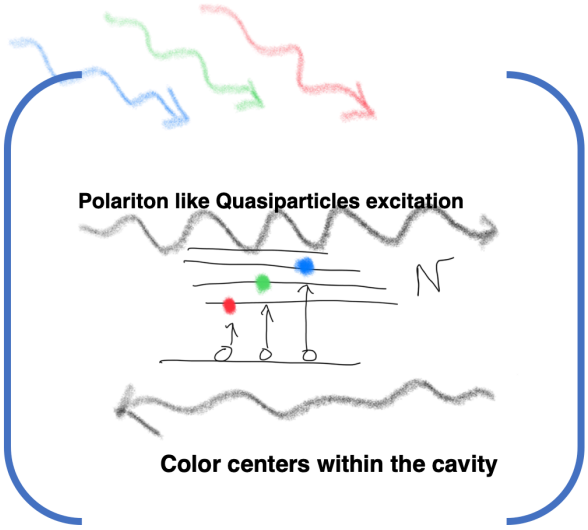

Figure 1.2: Trapping photons with a broadband cavity with N-color centers

The regime of local condensation of polaritons and its competing effect of "polariton lasing" (as any stimulated emission of a locally condensed state will kill global condensation) seem to hold the promise of creating a photo-excited coherent state that would allow for efficient photon to electron conversion through an intermediate virtual/hybridized state.

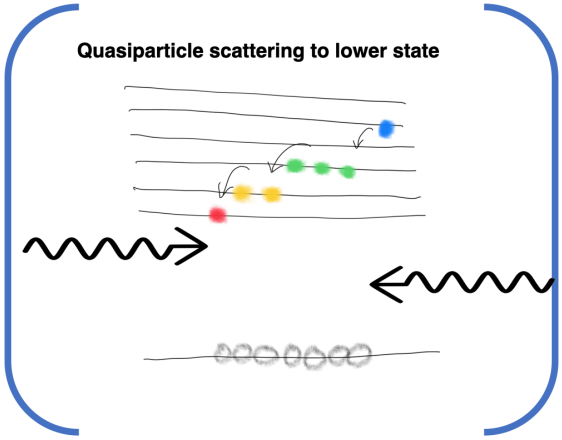

Figure 1.3: Collective scattering to lower excited state under strong correlation regime

Therefore, it seems like an interesting proposition to synthesize materials that can act like *effective* optical cavities or coupled resonators to trap photons beyond a few picoseconds. Such a resonator may allow for the thermalization of the excited quasiparticles to create a coherent state by scattering off phonons or other quasiparticles through strong correlations or long-range interactions. In Figures 1.2 and 1.3, the fuzzy colors in the excited states are to indicate polariton rather than pure electronic excitations, the latter would have been represented by discrete circles as shown in Figure 1.1. This system, which necessarily needs lifetimes beyond tens of picoseconds, may then allow for a collective occupation of the thermalized bosonic system of quasiparticles at a hybridized state, similar to the lower polariton branch in the cavity QED regime. Such quasiparticles could be mediated by plasmon polaritons, exciton polaritons, plasmon-exciton polaritons (recently named as "plexcitons"), or phonon polaritons, all of which are bosonic rather than fermionic quasiparticles, by coupling to photons and being able to interact with each other.

We explore the use of vertically grown, turbostratic, graphene nanomaterials that can be engineered to contain topological defects (*e.g.*, sp^3 defects, vacancy defects, Stone-Wales defects, or isolated carbon domain of polyacene) and functional groups (like C=O, C-X, *etc*.) that act like color centers, or more simply like two-level systems. This graphene

metamaterial, by virtue of being a perfect broadband absorber, should be able to support cavity modes between or within the vertical graphene nanostructures. Such a multimode resonator should in-principle be able to support quasiparticle lasing and coherent excited states for energy harvesting. The Gedanken experiment here serves to invite the reader to imagine these cooperative interactions between photons and defects which are the color centers within a network of coupled nanoscale optical cavities.

To further elucidate the breadth of light-matter interactions in graphene nanomaterials, experiments in demonstrating the use of these materials for on-chip photo detection by directly growing or depositing the photosensitive material on CMOS substrates are described. Throughout this thesis, we adopt and develop scalable experimental processes from synthesis, to spin coating by vacuum deposition, and CMOS processes for device fabrication. These approaches ensure that our graphene technologies are commercially viable.

1.2 Einstein Coefficients in Light-matter interaction

When studying the equilibrium between blackbody radiation and the transition rate between different energy levels, Einstein noticed a special case, which was an inevitable outcome of Planck's equation. The work published in 1917 is briefly revisited here to develop the theory of lasing from first principles so as to motivate the remainder of the thesis on studying novel light-matter interaction effects in graphene.

Consider the rate of transition between two discreet energy levels. For convenience, we will discuss atomic energy levels here, although the same analysis applies to other bosonic systems as well. Let's say we have N_n atoms at energy level n, and N_m atoms at energy state of m. If these atoms were in thermal equilibrium with thermal radiation, then the relative number of atoms in such states would be given by:

$$\frac{N_m}{N_n} = e^{-\Delta E_{mn}/kT}$$

where ΔE_{mn} is the energy difference between *m* and *n* states. Next, we consider how these atoms interact with blackbody radiation with which they attain equilibrium. Note, instead of considering blackbody radiation, one could also consider an externally applied radiation / pump that causes a spread of excited states to be created through quasiparticle scattering. Photons with the exact energy difference would convert atoms in level *n* to level *m* at a rate given by:

$$R_{n\to m} = N_n B_{nm} u_V (h\upsilon_{mn})$$

$$\Delta E_{mn} = h\upsilon_{mn}$$

B_{nm} is the proportionality constant describing the "ease" of this excitation process. u_V is the blackbody energy density that we previously derived. Next, Einstein examined the inverse process, where atoms from state *m* convert to state *n*. Here we account for spontaneous emission given by $N_m A_{mn}$ where A_{mn} is another proportionality constant. It was then assumed, in order to derive the correct result, a second light emission process dependent on the light intensity (the so-called stimulated emission) for which Einstein assigned the rate:

$$N_m B_{mn} u_V (h\upsilon_{mn})$$

The rate for this process then follows:

$$R_{m\to n} = N_m B_{mn} u_V (h\upsilon_{mn}) + N_m A_{mn}$$

Equating these rates, we find the blackbody energy density as:

$$u_V (h\upsilon_{mn}) = \frac{A_{mn}/B_{nm}}{e^{h\upsilon_{mn}/kT} - B_{mn}/B_{nm}}$$

This derivation by Einstein so far could only be in agreement with the Planck formulation if and only if B_{mn} was finite and equal to B_{nm}. It also turns out that the ratio A_{mn}/B_{nm} was frequency dependent:

$$\frac{A_{mn}}{B_{nm}} = 8\pi {\upsilon_{mn}}^3 / c^3$$

As we can now see from the above derivation, the denominator for u_V $(h\upsilon_{mn})$ has the -1 term in the denominator of the Bose Einstein Distribution from the stimulated emission process that Einstein assumed. Also, the ratio of the stimulated emission to the spontaneous emission is equal to the occupation probability $f_{Bose-Einstein}$. The rate of absorption is higher by a factor of $e^{h\upsilon/kT}$ times $\frac{f_{Bose-Einstein}}{1-f_{Bose-Einstein}}$ than the rate of stimulated emission. A similar derivation is also done in EE/ APh 131 Light Interactions with Atomic Systems taught by Prof. Yariv at Caltech. Some caveats to note from the above derivations are: photon emitted by spontaneous radiation has no directionality, and can go in any random direction, whereas photons emitted by stimulated emission must be emitted in the same optical mode as that of the stimulating photons in order to conserve momentum. This implies that a stimulated photon is identical to the stimulating photon with regard to polarization, frequency, direction and phase. This perhaps is the hallmark signature of bosonic interaction where indistinguishability is protected. The next caveat is that the relative strength so the two processes (*i.e.*, spontaneous and stimulated emission), when expressed through the Bose Einstein distribution, retain the same form when a chemical potential is associated with the light – *i.e.*, light in a cavity. This consideration now gives rise to the prospects of laser action: if the chemical potential is higher than the photon energy, we will be in a regime where stimulated emission will be higher than absorption, which causes light amplification in the material.

1.3 Basic structure of a Defect in a Cavity

Most experimental work to probe strong light-matter interaction is studied in various types of optical resonators, or waveguides that can strongly couple photons with atoms, or nitrogen-vacancy (NV) color centers in diamond, and other similar two-level systems like excitons. A conceptual illustration of a cavity quantum electrodynamic (QED) system is shown in Figure 2.1, where the system comprises a single mode of the electromagnetic field in a cavity with a decay rate κ and a coupling strength *g* to a two-level system with a spontaneous decay rate γ.

It should be noted that such the "optical cavities" in the cavity QED systems need not be typical resonators such as a sawtooth resonator, a whispering gallery mode resonator, photonic crystals, *etc*. Such *effective* optical cavities may be formed by quasi-1D graphene nanomaterials that could be treated as effective multi-mode coupled resonators with deep-sub-wavelength confinement of optical modes or by quantum confinement effects within the length scales of the quasi-1D nanostructures. The refractive index mismatch at the interfaces of the quasi-1D-graphene, including the interface with air and the interface with the underlying substrate, may be treated as mirrors that confine optical modes.

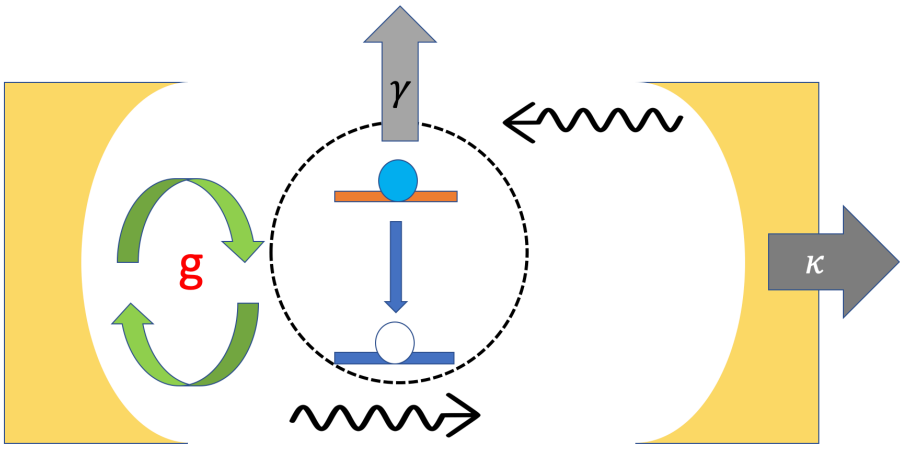

Figure 1.4: An optical cavity with a two-level system, such as a defect.

The material parameters that are of interest here, are *N* two-level (or *m* energy states, *m* >2) system (which can be introduced by defect engineering various functional groups or topological defects), the lifetime τ of such defects, and the Rabi splitting Ω_R under a strong correlation regime where we can upper and lower polariton energy levels splitting from such defect states.

$$\tau = \frac{1}{\gamma}$$

Optical mode confinement can be achieved through quasiparticles such as plasmon polaritons or excitons polaritons that propagate along the length of the quasi-1D graphene nanomaterials. High harmonic generation, enhanced Raman scattering, chemical reaction rates enhancements, observation of Bose condensation and coherent emission, *etc*., are a few well documented effects under the strong coupling regime [10]. In this regime, the physics of the system can be described by hybrid eigenmodes of the coupled system, such as the upper and lower polaritonic modes. When *g* becomes non-negligible, we see the ultra-strong coupling, common for organic materials in optical cavities with high quality factors (high-Qs) [15][16].

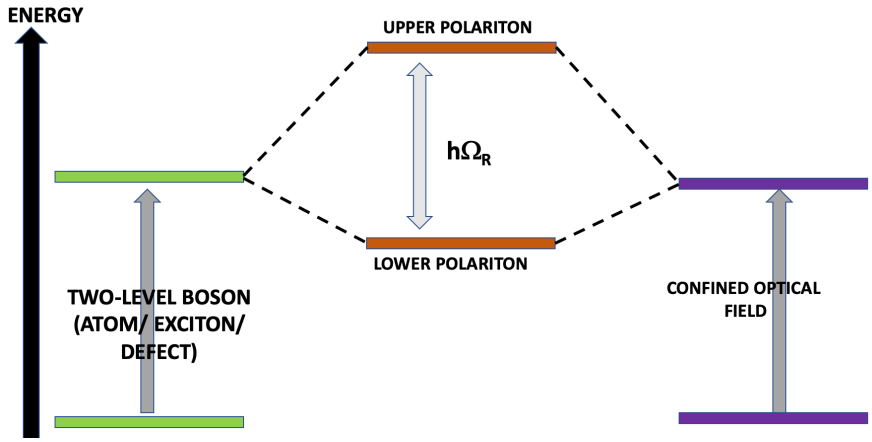

Figure 1.5: Hybridization of energy states within a cavity

In Figure 1.5, we depict the hybridized states of an exciton within a typical optical cavity. The cavity here again, could support plasmon polariton of the optical field which then

interact with the defects in the graphene nanomaterial. The light-matter interaction strength is denoted by g, and is related to the vacuum Rabi oscillation as $g \equiv \Omega_R / v$, where v is the transition frequency of the two-level system. If $g > \gamma$ (the decay rate of the excited state) or g > cavity losses (κ), then the system is said to be strong-coupling regime.

In case of a simple model of a single-photon mode coupled to a two-level system is the Jaynes–Cummings model [20]:

$$H = \omega \hat{a}^{\dagger} \hat{a} + \varepsilon \sigma^{+} \sigma^{-} + g(\sigma^{+} \hat{a} + H.c.).$$

Here $\hat{a}^{\dagger}$ and $\hat{a}$ represent the photon creation and annihilation operators, respectively, and we have taken $\hbar = 1$ for simplicity. The two-level system (*e.g.*, a saturable molecular transition) with energy ε splitting is described through Pauli matrices $\sigma^{\pm}$, which correspond to raising or lowering the transition between the two states such that σ^{+} (σ^{-}) creates (annihilates) an exciton. The last term g ($\sigma^{+}\hat{a}$ + *H.c.*) describes the coherent coupling between the photon and exciton, where *H.c.* represents the Hermitian conjugate. The above Hamiltonian conserves n_{ex}, the number of photons plus excitons, the eigenstates at fixed $n_{ex} > 1$ can be found as the eigenvalues of a 2 × 2 matrix:

$$h_{n_{ex}} = n_{ex}\omega + \begin{pmatrix} \epsilon - \omega & g\sqrt{n_{ex}} \\ g\sqrt{n_{ex}} & 0 \end{pmatrix}$$

The energy for the eigenstates is given by:

$$E^{\pm}_{n_{ex}} = (n_{ex} - 1)\omega + \frac{1}{2}\left[\epsilon + \omega \pm \sqrt{(\epsilon - \omega)^2 + 4g^2 n_{ex}}\right]$$

If $\varepsilon = \omega$, these modes are the symmetric and antisymmetric superposition of exciton and photon, and the transition from the $n_{ex} = 0$ ground state to the first excited state $n_{ex} = 1$ is split by $2g$—the vacuum Rabi splitting. As the field strength scales as $1/\sqrt{V}$ for mode volume V, one approach to increase g is to decrease V. Generally, V is limited by the wavelength of light, λ^3; however, for evanescent fields (*e.g.*, the plasmonic resonance in the gap between a gold nanoparticle and a metal film), V can be smaller. An alternative approach to increase the Rabi splitting is coupling many particles to the same cavity mode. In our system, we would perhaps have mode volumes much smaller than λ^3 due to deep-subwavelength confinement and strong mode reduction effects associated with graphene plasmons. Additionally, the number of color centers, or defects, can be distributed throughout the quasi-1D cavity or engineered to be locally clustered. For an N exciton system, the Rabi splitting scales as $g \rightarrow g\sqrt{N}$. The photon-exciton interaction is proportional to the inverse of the Bohr radius of the exciton (a_b), and the Coulomb interactions between excitons is proportional to $E_b\, a_b^2$ where E_b is the binding energy. This interaction scaling makes it easier to achieve ultra-strong coupling of photons with organic material or defects in organics than in semiconducting quantum wells (such as the GaAs/InGaAs systems).

Eli Yablonovitch originally proposed the use of photonic crystals to suppress spontaneous emission [11][12] in 1987. Photonic crystals with defects provide for extremely small mode volumes and large Q. In the case of quasi-1D graphene nanostructures, with defects, the mode volume is typically confined to the region containing the sparse topological defects (which we will refer as Type 1 defects) or can be engineered to expand the mode volume by introducing "Type 2 defects" through plasma irradiation-induced damages. The general Purcell enhancement factor (P) of the spontaneous emission is given by:

$$P = \frac{3}{4\pi^2}\frac{\lambda^3}{n}\frac{Q}{\boldsymbol{V}}$$

This Purcell enhancement comes from the coupling to those continuum modes that make up the quasi-modes (cavity modes with dissipation) of the resonator, and the spontaneous

emission is directed to the quasi-mode. Quantum dots or local topological defects could strongly couple to the cavity modes, when the "pseudo-atom"-field coupling strength ***g*** is faster than other dissipative rates and larger than 1/T, where **T** is the interaction time. In Cavity QED, the dissipation of the atomic states is characterized by the population relaxation of the excited atomic-like states, and the atomic-like dephasing rates $\gamma_{\parallel}$ and $\gamma_{\perp}$.

The extremely small effective mode volumes (***V***) in nanostructured quasi-1D-graphene can be attributed to the geometric volume reduction of the electromagnetic modes that allows for large Purcell enhancement effects.

1.4 Lasing and Dicke Superradiance

In this thesis, we also report some signatures that may be attributed to multi-mode polariton lasing-like phenomena from infrared to visible light in quasi-1D graphene nanomaterials at room temperature when the materials are illuminated by high power CW lasers. Although the underlying mechanism for such findings is still unclear and will require more rigorous experiments to pinpoint the physical origin (*e.g.*, polaritons localization, population inversion, ultra-low lasing threshold, *etc*.) of the lasing-like emission, the frequency comb like behavior with a frequency separation on the order of tens of THz and linewidths of a few THz seems to suggest that the behavior may be primarily associated with electronic transitions.

In contrast, in the limit of low laser power excitations, photoluminescence (PL) with temperature independent (from 15 K to 300 K) long carrier lifetimes (~ 10 ns) from the quasi-1D graphene nanomaterials may be attributed to excitons trapped by defects that are effectively zero-dimensional (0D) objects (*e.g.*, the presence of C=O defects with energies on the order of 2.2 eV, and other topological defects with higher energies). These defect sites are effective 0D color centers that produce excitons with temperature independent radiative lifetimes as predicted by theory, and these 0D excitons interact strong with photons that are trapped in the effective optical cavity of the quasi-1D graphene

nanomaterials, leading to coherent polaritons emission spectra, including novel emission spectral gap, spectral blue shift, as well as spatial interference fringes in PL studies.

It is also important to make the distinction between a pure excitonic excitation and a polaritonic excitation in this thesis for two main reasons. First, a pure excitonic excitation from defects in the graphene nanomaterials would not be sensitive to the geometry of the material. However, in our experiments described in Chapter 3, the lifetime of excited quasiparticle states is found to be strongly dependent on the length-to-width aspect ratios of the quasi-1D structures. For instance, when the quasi-1D structure is destroyed in either deliberately crushed graphene nanomaterials or heavily doped materials, the resulting quasiparticle lifetimes are much reduced, indicating a dependence on the geometry of the nanomaterial. This strong photonic sensitivity to material confinement seems consistent with a quasiparticle nature of hybridized material and photon excitations.

1.5 Self-organization in driven dissipative system

Spontaneous emergence of spatio-temporal order – pattern formation – in non-equilibrium systems represents a key mechanism of self-organization in nature (L.M. Pismen, [13],[21]). Kerr frequency combs in the dissipative soliton regime are a beautiful example of such self-organizing driven dissipative systems, where there is a double balance between nonlinearity and dispersion as well as dissipation and gain. Different physical systems are described by similar order parameter equations and therefore may share similar pattern formation properties. The two types of pattern formations that are distinguished are localized (coherent) structures and extended (possibly periodic) solutions. Much of the spatial pattern forming can be understood using the complex Ginsburg-Landau equation (cGLE) [12] to describe the behavior of the system in the vicinity of an instability and symmetry-breaking. The cGLE for order parameter $\psi(r, t)$ takes a general form :

$$i\partial_t\psi = c_1\nabla^2\psi + c_2|\psi|^2\psi + c_3\psi$$

,

where c_1, c_2, c_3 are complex parameters. For an equilibrium condensate system, c_1, c_2, c_3 are real, leading to the well-known nonlinear Schrödinger's equation (also known as the Gross-Pitaevskii equation). In the case of polaritons, which are non-equilibrium systems, c_1, c_2 and c_3 are complex, with the imaginary parts representing the process of pumping and dissipation. For a macroscopically occupied polariton state $\Psi(r,t)$, the corresponding cGLE may be expressed as follows:

$$i\hbar\partial_t\Psi = \left[E(i\nabla) + U|\Psi|^2 + V(\mathbf{r})\right]\Psi + i\left[P_{coh}(\mathbf{r},t) + \left(P_{inc}(\mathbf{r}) - \kappa - \sigma|\Psi|^2\right)\Psi\right]$$

Here $E(k)$ is the polariton energy, U denotes the strength of a δ-function interaction (pseudo)potential, $V(r)$ represents an external potential, $P_{coh}(\mathbf{r},t) = P_{coh}(\mathbf{r})\exp(i\omega_p t)$ is a coherent pump field applied to fix the phase and time dependence of the macroscopically occupied mode $\Psi(\mathbf{r},t)$, $P_{inc}(r)$ is an incoherent pump field that populates polaritons without fixing their phases, and κ and σ describe the linear and nonlinear losses, respectively. If only the low momentum modes are significantly occupied, the polariton energy $E(k)$ may be approximated by a quadratic dispersion $E(k) \approx h^2k^2/2m_{pol}$, leading to the Laplacian of Ψ in real space. In almost all experiments, only one of the P_{coh} and P_{inc} terms is present, but not both. A rigorous expansion of this framework is presented by Jonathan Keeling [12] and commonly used to model polaritonic interaction between excitons and photons in a cavity. We present this model to motivate the broader connection between nonlinear effects in various types of driven-dissipative phenomenon, as optical pumping, gain from defect centers and losses from scattering could likely have an important role in quasiparticle excitations in graphene nanomaterials.

1.6 Chapter Summary

This chapter is a brief introduction into light-matter interaction from first principles. We consider quasiparticle interactions, which are different from pure electron-electron interactions, in organic systems with defect mediated excitons strongly interacting with photons trapped in quasi-1D nanomaterials. The bosonic nature of excitons and photons may lead to collective effects like Dicke Superradiance, or polaritonic emission (using an *effective* Cavity QED toy model), which are concepts helpful for guiding future experiments. Further experimental probes with near-field scanning optical microscopy (NSOM), electron energy loss spectroscopy (EELS), light-integrated scanning tunneling microscopy (STM) and time-resolved angle resolved photoemission spectroscopy (tr-ARPES) would all help provide a more comprehensive understanding of the nanoscale light-matter interaction and the dispersion of various polaritonic excitations in the qausi-1D graphene nanomaterials. The large Purcell enhancement of emission is also proposed as a possible pathway for thinking about decay rates of emitters (like optically active topological defects) due to extremely small effective mode volumes in nanostructured graphene that result in strong light-matter interaction. Finally, we briefly present the idea of driven-dissipative systems that lead to spatio-temporal pattern formation, which maybe a useful analytical tool to explain some of the more novel light-matter effects in quasi-1D graphene.

We also note that this presentation of ideas in the introductory chapter is meant to be suggestive rather than *definitive*, as the intricate explanation for the novel effects observed in this work would require more rigorous, controlled studies for expanding this work. It is also worth mentioning that the published literature on organic microcavity light-matter interactions have reported many similar effects observed in this work, and it would be useful for future work to be inspired from results presented here. In subsequent chapters, we will mention what some of those new directions could be to help corroborate our findings.

References

[1] Schuller, J., Barnard, E., Cai, W. *et al*. Plasmonics for extreme light concentration and manipulation. *Nature Mater* **9,** 193–204 (2010).

[2] Alessandro Kovtun et al, Benchmarking of graphene-based materials: real commercial products versus ideal graphene, 2019, 2D Materials. 6, 025006.

[3] M. Hochberg et al., "Silicon Photonics: The Next Fabless Semiconductor Industry," in IEEE Solid-State Circuits Magazine, vol. 5, no. 1, pp. 48-58, winter 2013.

[4] Chrostowski, L., & Hochberg, M. (2015). Silicon Photonics Design: From Devices to Systems. Cambridge University Press.

[5] M. Green, Third Generation Photovoltaics: Advanced Solar Energy Conversion, Springer, 2003.

[6] Zongfu Yu, Aaswath Raman, Shanhui Fan, Fundamental limit of nanophotonic light trapping in solar cells, PNAS, Oct 2010, 107 (41) 17491-17496.

[7] Eli Yablonovitch, "Statistical ray optics," J. Opt. Soc. Am. 72, 899-907 (1982)

[8] F. Bonaccorso, Z. Sun, T. Hasan, and A. C. Ferrari, "Graphene photonics and optoelectronics," Nat. Photonics, vol. 4, no. 9, pp. 611–622, 2010.

[9] S A Mikhailov and K Ziegler 2008 J. Phys.: Condens. Matter 20 384204.

[10] Eli Yablonovitch and Owen D. Miller, "A great solar cell also needs to be a great LED: External fluorescence leads to new efficiency record", AIP Conference Proceedings 1519, 9-11 (2013).

[11] D. S. Dovzhenko, S. V. Ryabchuk, Yu. P. Rakovich and I. R. Nabiev, Light–matter interaction in the strong coupling regime: configurations, conditions, and applications, Nanoscale, 2018, 10, 3589.

[12] Yariv and P. Yeh, Optical Waves in Crystals (Wiley, New York, 1984).

[13] Eli Yablonovitch, Inhibited Spontaneous Emission in Solid-State Physics and Electronics, Phys. Rev. Lett. 58, 2059.

[14] Higgins, K., Benjamin, S., Stace, T. et al. Superabsorption of light via quantum engineering. Nat Communications, 5, 4705 (2014).

[15] K. D. B. Higgins, B. W. Lovett, and E. M. Gauger, Quantum-Enhanced Capture of Photons Using Optical Ratchet States, The Journal of Physical Chemistry C 2017 121 (38), 20714-20719.

[16] Ballarini, Dario and De Liberato, Simone. "Polaritonics: from microcavities to sub-wavelength confinement" Nanophotonics, vol. 8, no. 4, 2019, pp. 641-654.

[17] Jan M. Lüttgens, Felix J. Berger, and Jana Zaumseil, Population of Exciton–Polaritons via Luminescent sp3 Defects in Single-Walled Carbon Nanotubes, ACS Photonics 2021 8 (1), 182-193.

[18] S. Christopoulos, G. Baldassarri Höger von Högersthal, A. J. D. Grundy, P. G. Lagoudakis, A. V. Kavokin, J. J. Baumberg, G. Christmann, R. Butté, E. Feltin, J.-F. Carlin, and N. Grandjean, Room-Temperature Polariton Lasing in Semiconductor Microcavities, Phys. Rev. Lett. 98, 126405.

[19] C. Antón, T. C. H. Liew, G. Tosi, M. D. Martín, T. Gao, Z. Hatzopoulos, P. S. Eldridge, P. G. Savvidis, and L. Viña, Energy relaxation of exciton-polariton condensates in quasi-one-dimensional microcavities, Phys. Rev. B 88, 035313.

[20] Imamoglu, R. J. Ram, S. Pau, and Y. Yamamoto, Nonequilibrium condensates and lasers without inversion: Exciton-polariton lasers, Phys. Rev. A 53, 4250, 1996.

[21] ImamogLu, R. J. Ram, Toward polariton bose condensation and polariton lasers, Thin Films and Nanostructures, Academic Press, Volume 32, 2003, Pages 183-224.

[22] Jonathan Keeling & Natalia G. Berloff (2011) Exciton–polariton condensation, Contemporary Physics, 52:2, 131-151.

[23] L.M. Pismen, Patterns and Interfaces in Dissipative Dynamics, Springer 2006, 0172-7389.

[24] Tobias J. Kippenberg, Alexander L. Gaeta, Michal Lipson, Michael L. Gorodetsky, Dissipative Kerr Solitons In Optical Microresonators, Science, 2018, Vol. 361, Issue 6402.

[25] Aschwanden, M.J., Scholkmann, F., Béthune, W. et al. Order out of Randomness: Self-Organization Processes in Astrophysics. Space Sci Rev 214, 55 (2018).

[26] Fahhad H. Alharbi, Sabre Kais, Theoretical limits of photovoltaics efficiency and possible improvements by intuitive approaches learned from photosynthesis and quantum coherence, Renewable and Sustainable Energy Reviews, Volume 43, 2015, Pages 1073-1089

[27] W. Stręk, Cooperative energy transfer, Physics Letters A, Volume 62, Issue 5, 1977, Pages 315-316.

[28] Abasto D, Mohseni M, Lloyd S, Zanardi P. Exciton diffusion length in complex quantum systems: the effects of disorder and environmental fluctuations on symmetry-enhanced supertransfer. Philos Trans R Soc A: Math Phys Eng Sci 2012;370(1972):3750–70.

[29] Scully MO. Quantum photocell: using quantum coherence to reduce radiative recombination and increase efficiency. Phys Rev Lett 2010, 104 (20):207701.

[30] Jonathan Keeling and Stéphane Kéna-Cohen, Bose–Einstein Condensation of Exciton-Polaritons in Organic Microcavities, Annual Review of Physical Chemistry 2020 71:1, 435-459

[31] I.S. Aranson and L. Kramer, The world of the complex Ginzburg–Landau equation, Rev. Mod. Phys. 74 (2002)

Chapter 2

SYNTHESIS AND CHARACTERIZATION OF QUASI-ONE-DIMENSIONAL GRAPHENE

2.1 Background on Graphene

Monolayer graphene, originally developed by mechanical exfoliation (aka scotch tape exfoliation) by A. Geim and K. Novoselov, has been among the most exhaustively researched material in the last two decades. There are several excellent reviews available [2][13]. This chapter will introduce several key features of graphene that are helpful to build some intuitions towards understanding the interaction of defects and light in graphene.

The first bandstructure of graphene, a monolayer of carbon atoms forming a two-dimensional honey comb lattice structure, was computed in 1947 by P. R. Wallace. The bandstructure reveals that the valence band is formed by the bonding π- electrons and conduction band by the anti-bonding π* electrons. The valence and conduction bands touch at 6 points in the first Brillouin zone of the hexagonal reciprocal lattice, the so-called Dirac points. These Dirac points are associated with two inequivalent valleys at the K and K′ points. Although the gapless nature of pristine graphene is not suitable for applications in solar cells, by inducing topological defects locally during material synthesis, we can open a band gap locally while still maintain global gapless nature of graphene.

The electronic Hamiltonian describing the low-energy electronic structure of graphene within the linear dispersion regime can be expressed by a relativistic Dirac Hamiltonian H

$$H = v_F \sigma \hbar k$$

Here H is a product of the v_F Fermi velocity, σ spinor-like wavefunction and the wave-vector k of the electron. The linear low-energy dispersion relation of graphene offers the

possibility of efficient light coupling to collective electron oscillations in graphene to create graphene plasmon polaritons by significant mode volume reduction. While graphene plasmons [11] can exist over a wide range of frequencies as a function of the graphene doping level, low losses and significant confinement for plasmon frequencies below the optical phonon frequencies of ~ 0.2 eV provide unique opportunities for graphene-based infrared nano-photonic applications.

In this thesis, we study vertically grown, quasi-1D graphene nanomaterials that are stripes of multilayers with long length-to-width aspect ratios and have arbitrary rotation angles between consecutive layers (known as "turbostratic graphene") so that the layers are electronically decoupled. Since the typical thickness of these vertically grown graphene layers is on the order of ~ 10^2 nm, it easily approaches the graphitic limit in terms of the number of layers. On the other hand, the random rotation between consecutive layers preserves various unique electronic properties of monolayer graphene, including the linear energy dispersion near the Dirac point, extremely high electron mobility, and ultra-fast carrier recombination. The preservation of monolayer graphene characteristics together with the strong sub-wavelength scattering of light in these turbostratic, quasi-1D graphene nanomaterials contribute to unique light-matter interactions, which will be manifested by the experimental findings in this thesis.

2.2 Plasma Enhanced Chemical Vapor Deposition (PECVD) of Graphene

Large area graphene growth [12] [13][14] has recently been demonstrated by roll-to-roll processing with high-temperature (~1000 °C) chemical vapor deposition (CVD) systems. In spite of the success in demonstrating such industrial scale manufacturing of graphene, the overall graphene quality varies largely with area due to non-uniformities in the copper substrates. More importantly, such methods are completely incompatible with CMOS integration, as temperatures of ~ 1000 °C on a standard CMOS chip will cause migration of metal atoms and severe damages to the low-k dielectrics and CMOS devices on chip.

The need for a scalable, and CMOS compatible, low temperature synthesis method for graphene can only be realized with plasma enhanced chemical vapor deposition (PECVD).

In the Yeh group [3], we use a quartz tube chamber design (Figure 3.1) that can process multiple substrates in parallel with a 2.45 GHz microwave plasma system to synthesize graphene on various types of substrates in a single step without active heating. The choice of a 2450 MHz plasma system is mainly because the electromagnetic radiation at such microwave frequencies is able to effectively couple with the process gases (like H_2, CH_4, Ar, *etc*.) as a reactive load to the microwave circuit.

Specifically, Evanson cavities [3][4] are used to generate the plasma inside the quartz growth chamber, which allows for the microwave to be efficiently coupled to the plasma without direct physical contact from the cavities. In the original work published in 1965, H.P. Broida *et al* [4] studied 5 different types of microwave cavities to operate at 2450 MHz, that had different electrical configurations like a tapered regular design for TE_{013} mode, foreshortened ¾ wave coaxial, simple coaxial termination and foreshortened ¼ coaxial termination. The Evanson cavity used in this work is air-cooled during plasma processing, and is a foreshortened quarter-wave coaxial type cavity with an adjustable (E-mode) coupling and stub-tuning.

It is worth noting here that in the Evanson cavity design, under maximum power transfer condition between the cavity and the process chamber, some arcing can occur between the metallic tuning stub and the ceramic coupler, which will reduce the available power output for the plasma, making the plasma discharge unstable. Therefore, it is required during the growth of these materials that the ceramic tuners be adjusted to prevent the internal cavity arcing at the cost of forward power and increased reflected power. The overall synthesis quality depends on the ability to control the radical ionization energy, the mean free path of the radical and the nature of the substrate to support nucleation.

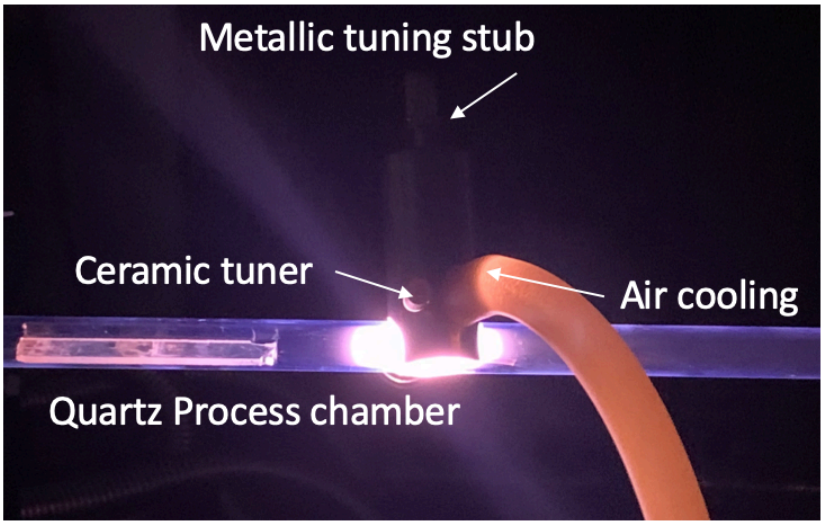

Figure 2.1: Quartz process chamber with an Evanson cavity at 2450 MHz

The synthesis of quasi-one-dimensional graphene [15-17] has been demonstrated under various process conditions of H_2/CH_4 flow rates and plasma powers, in addition to the use of organic benzene or polyacene based precursor molecules that seed the vertical growth or assist rapid growth in a preferential direction[4]. As exemplified by the SEM image in the left panel of Figure 2.2, highly directed growth of quasi-1D graphene nanomaterials could be achieved with low flow rates of 20 sccm of H_2 and 5 sccm of CH_4 and at a low plasma power < 40 Watts.

It is worth noting that the plasma power and the ratio of forward to reflected power also play an important role in determining the degree of directionality in these nanostructures, as we have seen that for reflected power greater than 2 to 5% of the forward power, the vertical nanostructured graphene show many cross-linked nanostructures, wherein multiple nucleation site quickly merge and fuse with each other to create a “coral reef” like architecture. At high plasma powers, or high flow rates, the carbon radicals undergo multiple scattering and have a lower mean free path, as the plasma mode distribution is more complex when the reflected power is non-zero, or a high forward power with enhanced microwave mode dispersion. These non-linearities cause the carbon radicals to

inter-link more rapidly. By engineering the plasma condition and flow rates, we can synthesize long aspect ratio graphene nanostructures, as depicted in Figure 2.2.

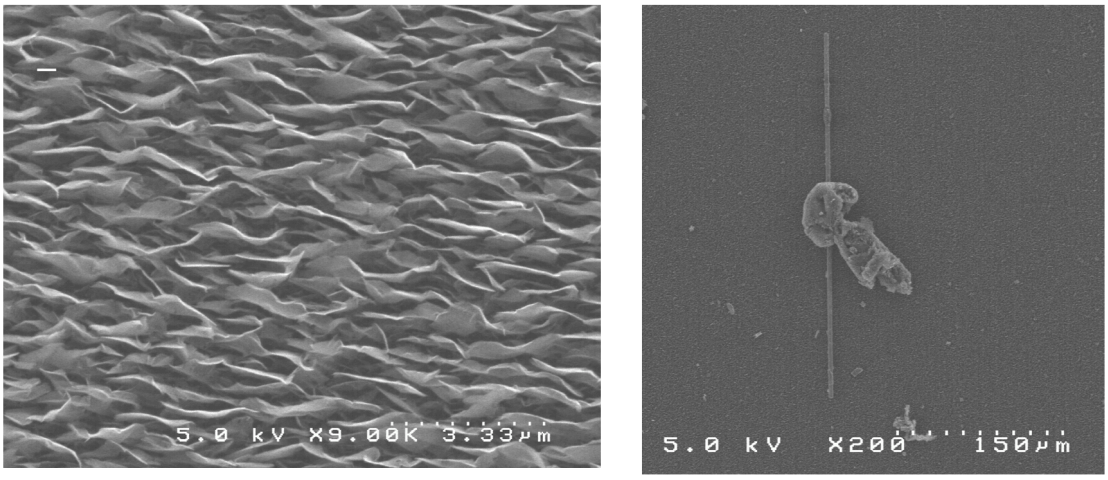

Figure 2.2: SEM images of directionally aligned growth of vertical quasi-1D graphene nanostructures before (left panel) and after (right panel) liquid phase exfoliation.

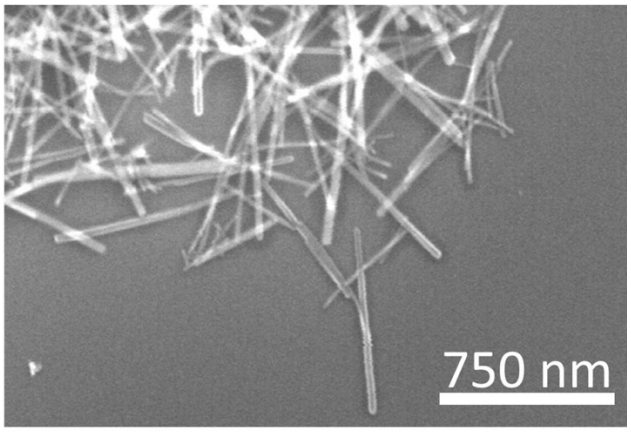

Figure 2.3: Exfoliated vertically grown quasi-1D graphene with long aspect ratios

Feedstock gases [18] apart from methane (CH_4) have been widely studied to also produce vertically aligned graphene nanostructures. Hydrocarbons like C_2H_2, or fluorocarbons like CF_4, CHF_3, C_2F_6 have been popular options of carbon sources to feed the growth of graphene. Growth without organic C_6-containing precursors is much harder to control, unless a higher hydrocarbon that can produce C_2 radicals are used. Many experimental studies have found

that the presence of C_2 radicals to assist in vertical orientation better than horizontal orientation because C_2 (or C=C) radicals experience steric hindrance when aligned horizontally, and thus condense vertically. This prevents the growth of multilayers of sheet graphene oriented horizontally. The C_6 radical also has a similar effect. Other mechanisms and reasons for vertical growth cited in literature are often harder to verify, due to the complex nature of plasma chemistry, and it is easier to rely on the thermodynamics and stereochemistry of radical bond formation.

Once a vertical growth is seeded from a nucleation site on the substrate -- typically a site is activated by plasma bombardment and radicals can condense at the site to form stable sp^3 or sp^2 bonds, further vertical growth can be supplemented by carbon radicals from the dissociation of CH_4 or the precursor.

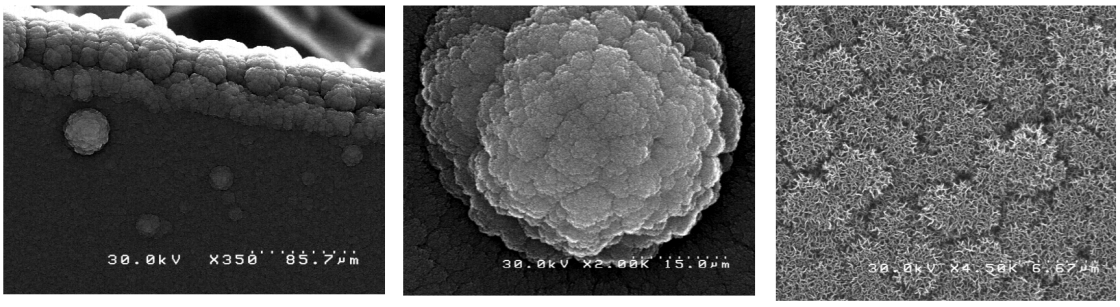

Figure 2.4: SEM images of the morphology of graphene synthesized under conditions of rapid growth at high plasma powers (> 50 Watts) and large gas flow rates (> 45/5 sccm H_2/CH_4), showing that the resulting graphene nanomaterials exhibit micro-domains, which destroy the long aspect ratios for quasi-one-dimensionality.

From our experimental investigation, we have also noticed that sharp corners and edges in a copper foil substrate can amplify the plasma field strength through roughness. Such sharp corners receive maximum ion bombardment from the process gas ionization and also tend to concentrate the electromagnetic fields, leading to the most likely first growth nucleation sites. Similarly, copper foils that are too large tend to prevent the growth of graphene due to effective dissipation of the plasma field, as the copper itself acts like an absorber for the E-field produced by the microwave plasma discharge. This is perhaps the biggest limitation

of using the Evanson microwave plasma cavities as the size of the substrate is largely limited to less than (1 cm × 1 cm) copper foils.

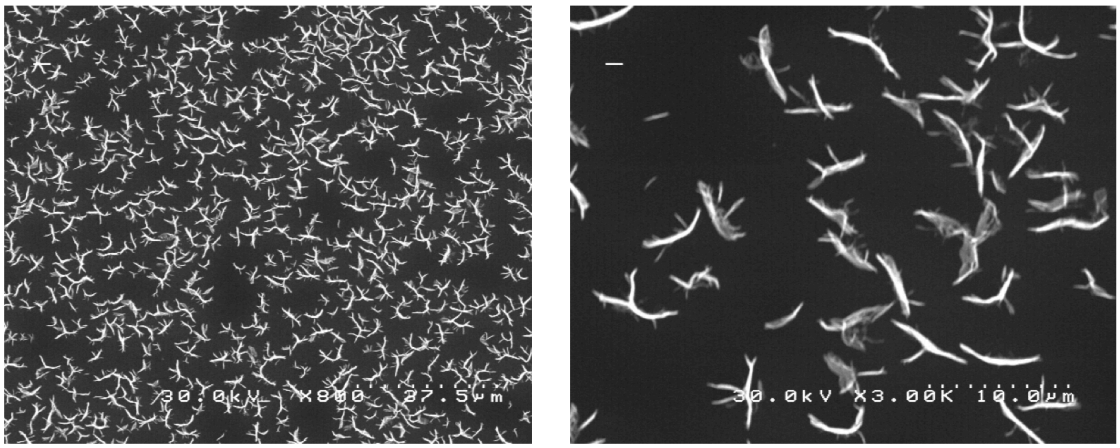

Figure 2.5: SEM images of the early stages of PECVD synthesis, showing vertically aligned quasi-1D graphene domain formation

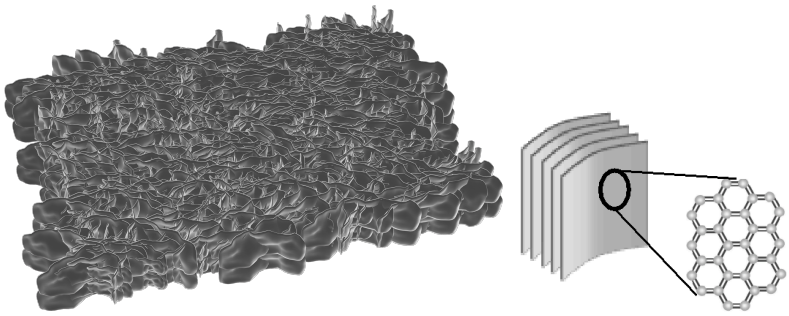

Figure 2.6: The vertically aligned growth depicting few layers (< 20 layers) of graphene

In order to achieve industry scale production of vertically oriented graphene, or multilayer horizontal sheet graphene, one needs to incorporate roll-to-roll processing with NO contact to the plasma cavity / plasma source. Current industrial standard plasma cavities use alumina ceramic coating, which are meant only for inert plasma chemistry and not suitable for harsh organic plasmas. It is therefore necessary to use a thin dielectric spacer like glass, to act as a sacrificial layer, or to explore other plasma generation sources like inductively coupled plasma (ICP) or capacitively coupled plasma (CCP) configurations. The future of

manufacturing vertically aligned quasi-1D graphene nanomaterials will depend on which application drives the demand for these novel materials. In a setting where selective growth of quasi-1D graphene is needed, it becomes important to have controlled and repeatable plasma dynamics and chemistry to meet the application needs. Current efforts with Evanson cavity will be limited to chips smaller than (1 cm × 1 cm) in size.

2.3 Raman Characterization of Graphene Nanomaterials

Raman spectroscopy [6] is an integral characterization technique to assess the quality of graphene based on the vibrational fingerprint of graphene and graphene related materials (GRM). From the Raman spectra one could estimate the number of graphene layers, the orientation angle between the layers, edge defects and the nature of edges (zig-zag or arm chair), presence of dopants, *etc*. For instance, Cancado et al. [5] established a relationship among the in-plane sp^2 crystallite size L_a, the excitation energy E_L of the laser source used for Raman spectroscopy (in eV), and the intensity ratio I(D)/ I(G) for the D and G Raman modes:

$$L_a = \frac{560}{E_L^4} \left(\frac{I_D}{I_G}\right)^{-1}$$

The signature vibrational modes of graphene include the D-, G- and 2D (*a.k.a.* G′)-bands [6]. The G-band is a first order scattering process that comprises of two degenerate phonon modes – the in-plane transverse optical mode (iTO) and the in-plane longitudinal mode (iLO) and is observed between 1582 to 1585 cm^{-1}. This G band can be seen in 1-layer, 2-layer, few-layers and multilayer graphene as well. Doping the material will sensitively affect the position and linewidth of the G band. The fermi level dependence also modulates the density of electrons and holes due to phonon self-energy correction. The G′-band (or 2D-band) is a harmonic of the D-band, which is a symmetry allowed inter-valley Raman mode that is comprised of two iTO phonon modes around the K-K′ point. The G′ frequency is a function of the excitation laser energy. A major use of the G′-band is to identify the number of layers in graphene, because the G′-band is sensitive to the stacking order and

inter-layer interactions in graphene materials with 2 or more layers. Perhaps the most relevant to device engineering is the disorder induced D-band, which is a symmetry-breaking Raman mode that only appears in the presence of defects or edges.

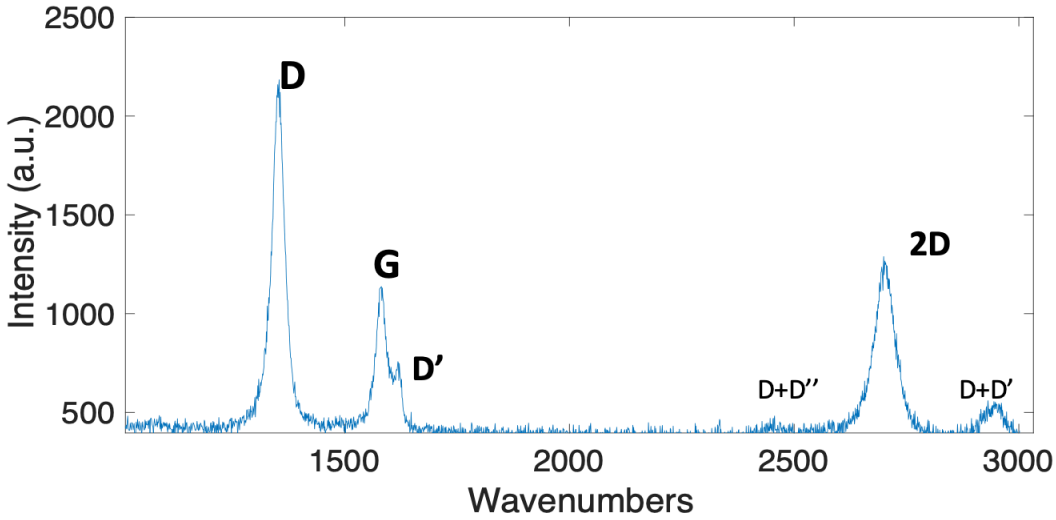

Figure 2.7: A representative Raman spectrum of PECVD-grown graphene nanomaterials, showing various Raman modes

Defects in the honeycomb lattice breaks the translational symmetry and the amounts of defects is reflected in the intensity of the D peak. More details for group theoretic derivation of various symmetry groups associated with the Raman modes in graphene can be found in Dresselhaus *et al.* [6].

2.4 Defect Engineering in Graphene Nanomaterials

In this thesis we will discuss two classes of defects that we will refer to for the remainder of the thesis. The first type of defects are 0D-like defects that are directly induced from the plasma synthesis process itself when different domains stitch together imperfectly and thus result in topological defects, or due to reactive edge termination after growth that captures ambient oxygen, to form C=O bonds, or other ring defects creating C-5, C-7, C-8 ring structures, or the isolation of such ring structures creating domains of “polyacene” type defects. These defects are sparse and delocalized throughout the material.

The second class of defects, which we can refer as type-2 defects, are engineered in the material by intentional exposure to Ar^{+} ion bombardment of O_2 plasma exposure to activate certain edge defects. These defects tend to cluster around the regions of plasma exposure, and their optical response is entirely different from the type-1 defects that are delocalized. These type-2 defects cause material damages that deteriorate the pristine electronic properties of graphene, but they also reveal interesting light-matter interaction dynamics due to the damage caused to the quasi-one-dimensionality of the nanomaterials. Both type-1 and type-2 defects provide useful information about the carrier dynamics of excitons lifetimes, and photoluminescence emission properties, *etc*.

TEM imaging (done at KNI, Caltech jointly by M. Teague and C-C. Hsu) of these quasi-one-dimensional graphene nanostructures upon liquid exfoliation with N-methyl pyrolidone type organic solvents shows the distinct hexagonal honeycomb arrangement of carbon atoms, along with some point defects. Vertically grown quasi-one-dimensional graphene, after exfoliated and placed on a TEM grid, reveals the atomistic morphology. From the figure below, we notice clear periodic arrangements of carbon atoms that are seen in high contrast. These periodic arrays are parallel to the TEM incident electrons and show the interlinking pattern where different graphene growth from different nucleation sites stitch together forming vacancy defects, point defects and Stone-Wales type ring defects where the number of carbon atoms is less than 6 or more than 6 per ring structure of the honeycomb. Such point defects also arise when the process plasma itself bombards and knocks out carbon atoms, such as hydrogen plasma (weak effect) or the carbon CN radicals in the plasma. From the TEM image we can see the nature of type-1 defects directly, as these materials were not subjected to any intentional Ar+ bombardment, but still reveal atomic defects. Upon closer examination in Figure 3.8 (b) we can see the zig-zag termination of the edges of the exfoliated graphene.

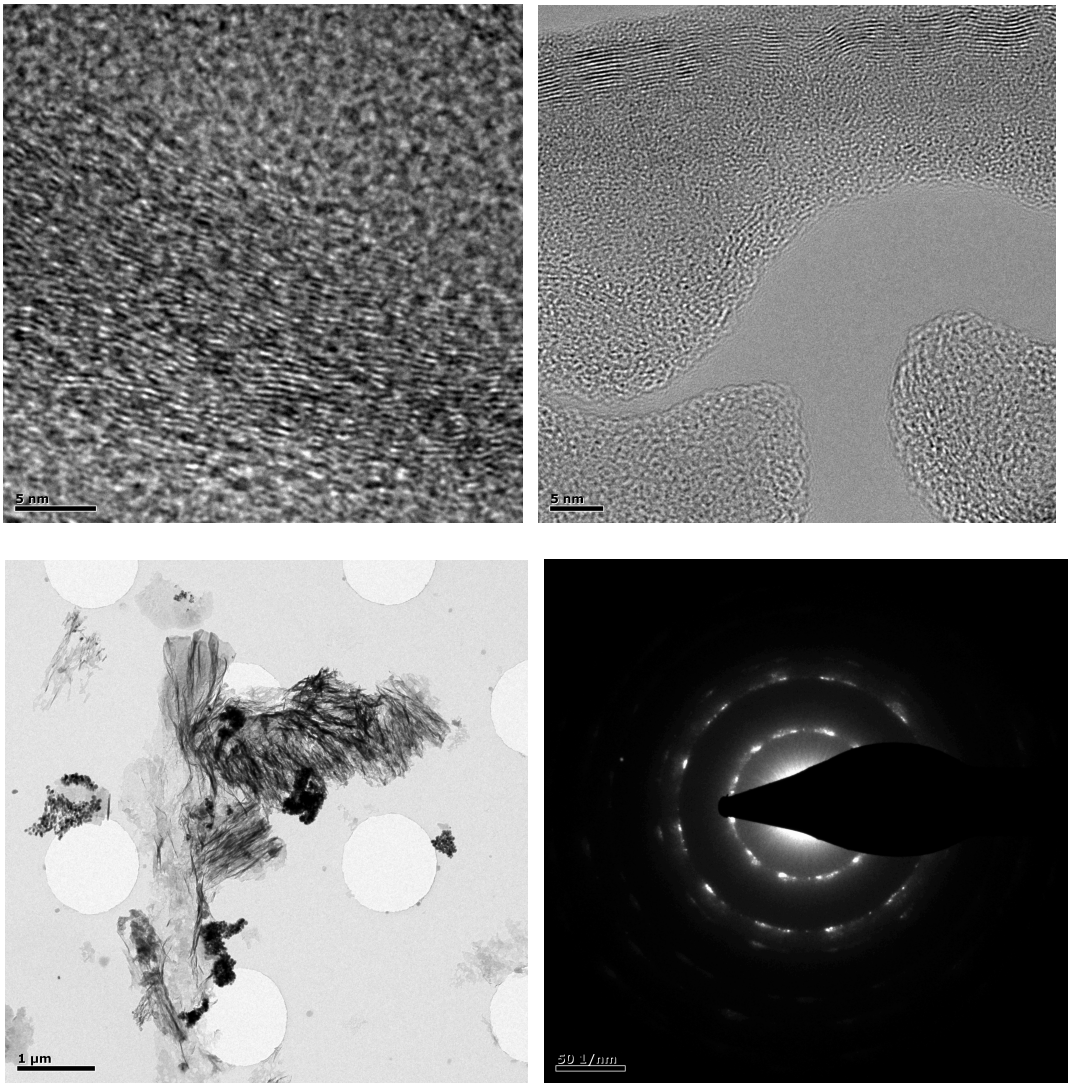

Figure 2.8: Electron microscopy with atomic resolution (a-b) High resolution TEM images. (c)TEM grid with exfoliated graphene nanomaterial. (d) Selected area electron diffraction (SAED)showing arbitrary rotation angles in the turbostratic multilayers of quasi-1D graphene (obtained jointly by Marcus and Chen-Chih Hsu)

2.5 Liquid Phase Exfoliation of Graphene

Large scale technology adoption of 2D materials and nanomaterials requires emerging 2D materials, like graphene, transition metal dichalcogenides (TMDs), "MXene" (M: transition metal, X: carbide, nitride or carbon nitride), *etc*. to be produced in large quantities, and also be manufactured with methods that can be quickly integrated with

existing foundry technology to be CMOS process compatible. Many research efforts to understand the physics of electronic, photonic, phononic and plasmonic interactions has been focused on materials synthesized from methods that are still at very early stages of scalability or technology readiness. Starting from the "scotch tape" mechanical exfoliation to polymer free transfer methods, the current methods of transferring 2D nanomaterials is extremely cumbersome and non-reproducible. Roll-to-roll synthesis has emerged as a promising candidate for large area continuous synthesis, but again transfer to standard 8 inch or 12 inch wafers leads to defects like wrinkles, cracks and adatom impurities. High-temperature CVD method used currently for vast majority of 2D materials is also not viable for CMOS integration, as temperatures in excess of 1000 °C cause diffusion and inter-layer migration of metal atoms at the nano- and micro scales as well as detrimental damages to delicate low-k dielectrics and nanoscale devices. We have developed two industrially compatible methods for material synthesis and handling: low-temperature PECVD synthesis and vacuum assisted deposition by spin-coating or drop-coating through inkjet dispersing mechanisms.

The ability to deposit 2D materials, whether monolayer or multi-layer, on lithographically patterned regions with 2D materials dissolved in organic volatile solvents, provides the control of the targeted material thickness and the exact position and geometry of the deposition. The work by V. Nickolosi *et al* [7] examined 20 different organic solvents for various 2D materials based on the solvent surface tension or the solvents Hildebrand solubility parameter. An essential condition is that the process of solvent vaporization should not cause the various 2D layers to aggregate, which is met when the solvent satisfies Trouton's rule (requiring high boiling point or a high solubility parameter). In spite of nearly 20 solvents identified by V. Nickolski *et al*, we restrict our experiments to toluene, ethylene cellulose, cyclohexanone and terpineol, as these are also used in making graphene ink dispersion for printed electronics. The work by J. Coleman *et al* [8] has also suggested cyclohexanone, N-methyl pyrrolidone (NMP), dimethylformamide (DMF), which have relatively low boiling points (with NMP boiling point being 200 °C). Airbrush coating technique was performed with little success due to the diffuse coating and sparse material

deposition. Airbrush coating however can be optimized by repeated coatings in same area, but would become time intensive. The use of surfactants to stabilize the liquid exfoliated 2D materials often degrades the material quality when removing such surfactants [9] (like sodium dodecyl sulfate, lignin molecules, porphyrins, *etc*.). Spin-coating of such liquid exfoliated solvents containing graphene nanomaterial also does not yield promising results as the process of spin coating acts like a mass centrifuge system and separates the exfoliated layers of graphene differently as a function of mass and radial velocity during the spin coating process. Drop coating followed by heat assisted vacuum desiccation expedites the process of deposition, as described in the Figure 2.9 below. The Raman spectroscopic studies of an exfoliated sample at different locations are shown in Figure 2.10, and the SEM image of an exfoliated sample that was further crushed is shown in Figure 2.11.

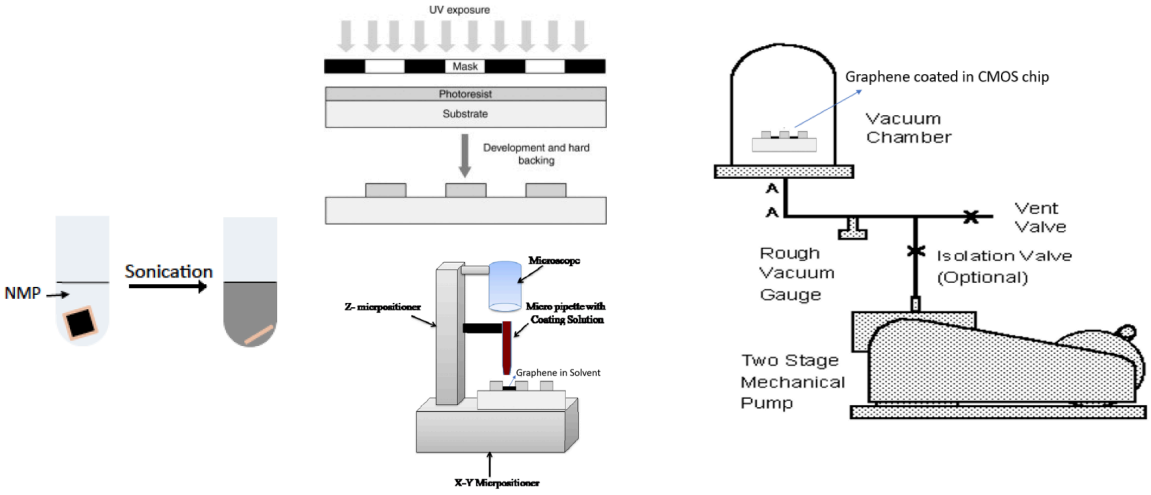

Figure 2.9: Heat assisted vacuum deposition of liquid exfoliated graphene

Using solvents like NMP or cyclohexanone, we first sonicated the quasi-1D graphene nanomaterials and then deposited the material into regions defined by optical lithography. This approach is generally unsuitable for applications in photoconductive photodetectors, or other optoelectronic applications requiring integrated graphene devices. Next, we used an inkjet deposition tool, or an airbrush to deposit the graphene material dispersed in the solvent. Finally, we used a vacuum chamber to keep samples at sufficiently low pressure

to slowly vaporize the solvent. Good choice of solvents is critical, as the ability of the solvent to solvate and separate the interconnected materials is important and less toxic solvents are also important consideration for sustainability. Water is also a suitable alternative but it quickly vaporizes because of a lower boiling point, which can cause aggregation of layers and chunks faster than NMP. Detailed molecular dynamic simulations were done by Daniel Blankschtein *et al* [9] to study the solvation effects of NMP, DMSO, DMF and water.

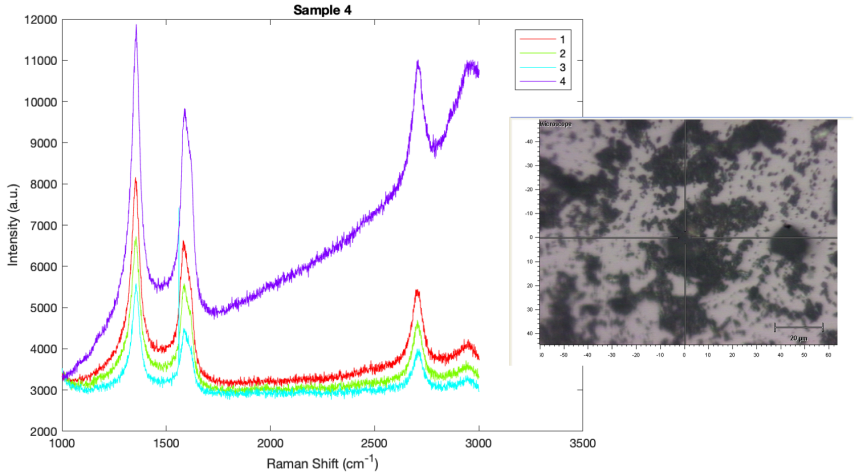

Figure 2.10: Raman characterization at four different locations after spin-coating the exfoliated graphene. Work with Stella, SURF 2019

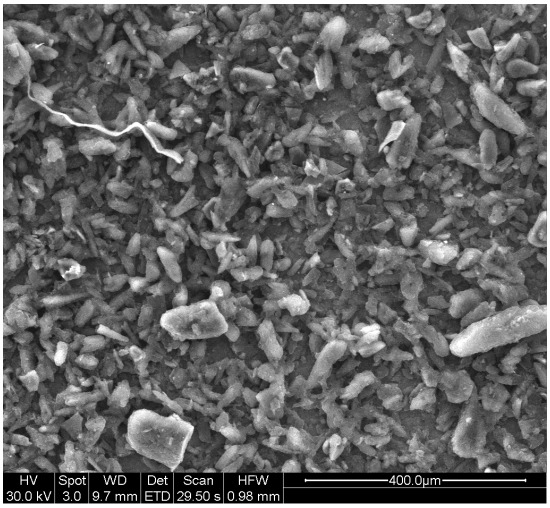

Figure 2.11: SEM image of liquid exfoliated graphene after crushing the as-grown quasi-1-D nanomaterial to induce defects

2.6 Chapter Summary

The use of low-temperature PECVD synthesis of quasi-1D graphene has been demonstrated on substrates like copper, silicon and oxides like quartz, and the materials have been characterized with Raman and TEM studies. The morphology of these quasi-1D graphene are highly sensitive to plasma powers and flow rates of the feedstock gases like hydrogen gas and methane gas as the free radicals created within the microwave plasma scattering time or mean free path is affected by changing the flow rates and plasma power density. Raman spectroscopy combined with TEM imaging allows for atomic scale characterization and vibrational fingerprint studies of varies defects and disorder in these nanomaterials. We also developed a scalable method for exfoliating and coating multi-layer graphene for applications that may not need as-grown nanostructures, like flexible electronics. This solution processing will also allow for large scale growth of high quality turbostratic graphene for applications ranging from composite materials to flexible electronics in the future.

Further work may be explored to achieve growth of these graphene nanomaterials on polymer substrates, transition metal dichalcogenides (TMDs) and other 2D materials for investigating light-matter interaction at interfaces of heterostructures. Other synthesis ideas like growth of graphene on nonlinear crystals like lithium niobate, or diamond, may hold interesting application in quantum optics. Microwave and RF plasma synthesis at low-temperatures on thin-film metals like Cu or Au can also be useful for applications in low contact resistance interfaces with 2D heterostructures, and would be crucial to expand the adoption of 2D materials for integrated nanophotonics and nanoelectronics.

References

[1] P. R. Wallace, The Band Theory of Graphite, Phys. Rev. 71, 622, 1947.

[2] Geim, A., Novoselov, K. The rise of graphene. *Nature Mater* **6,** 183–191 (2007).

[3] Nai-Chang Yeh *et al* 2019 *Nanotechnology,* **30** 162001.

[4] Chen-Chih Hsu, Jacob D. Bagley, Marcus L. Teague, Wei-Shiuan Tseng, Kathleen L. Yang, Yiran Zhang, Yiliang Li, Yilun Li, James M. Tour, N.-C. Yeh, High-yield single-step catalytic growth of graphene nanostripes by plasma enhanced chemical vapor deposition, Carbon, Volume 129, 2018.

[5] F. C. Fehsenfeld, K. M. Evenson, and H. P. Broida , "Microwave Discharge Cavities Operating at 2450 MHz", Review of Scientific Instruments 36, 294-298 (1965)

[6] Bruce McCarroll , "An Improved Microwave Discharge Cavity for 2450 MHz", Review of Scientific Instruments 41, 279-280 (1970)

[7] L. G. Cançado, A. Jorio, E. H. Martins Ferreira, F. Stavale, C. A. Achete, R. B. Capaz, M. V. O. Moutinho, A. Lombardo, T. S. Kulmala, and A. C. Ferrari, Quantifying Defects in Graphene via Raman Spectroscopy at Different Excitation Energies, Nano Letters 2011.

[8] L.M. Malard, M.A. Pimenta, G. Dresselhaus, M.S. Dresselhaus, Raman spectroscopy in graphene, Physics Reports, Volume 473, Issues 5–6, 2009, Pages 51-87

[9] Jonathan N. Coleman, Mustafa Lotya, Arlene O'neill, Shane D. Bergin, Paul J. King, Umar Khan, Karen Young, Alexandre Gaucher, Sukanta De, Ronan J. Smith, Igor V. Shvets, Sunil K. Arora, George Stanton, Hye-Young Kim, Kangho Lee, Gyu Tae Kim, Georg S. Duesberg, Toby Hallam, John J. Boland, Jing Jing Wang, John F. Donegan, Jaime C. Grunlan, Gregory Moriarty, Aleksey Shmeliov, Rebecca J. Nicholls, James M. Perkins, Eleanor M. Grieveson, Koenraad Theuwissen, David W. Mccomb, Peter D. Nellist, Valeria Nicolosi, Two-Dimensional Nanosheets Produced By Liquid Exfoliation Of Layered Materials, Science, 2011.

[10] Arlene O'Neill, Umar Khan, and Jonathan N Coleman, Preparation of High Concentration Dispersions of Exfoliated MoS2 with Increased Flake Size, Chemistry of Materials 2012 24 (12), 2414-2421

[11] Shih CJ, Lin S, Strano MS, Blankschtein D. Understanding the stabilization of liquid-phase-exfoliated graphene in polar solvents: molecular dynamics simulations and kinetic theory of colloid aggregation. J Am Chem Soc. 2010 Oct 20;132(41):14638-48. PMID: 20879739.

[12] M. Jablan, H. Buljan and M. Soljačić, *Phys. Rev. B* **80**, 245435 (2009).

[13] Polat, E., Balci, O., Kakenov, N. *et al.* Synthesis of Large Area Graphene for High Performance in Flexible Optoelectronic Devices. *Sci Rep* **5,** 16744 (2015).

[14] Li, X. S. et al. Large-Area Synthesis of High-Quality and Uniform Graphene Films on Copper Foils. Science 324, 1312–1314, (2009).

[15] Novoselov, K. S. et al. A roadmap for graphene. Nature 490, 192–200 (2012).

[16] Shahzad Hussain *et al,* Low-temperature low-power PECVD synthesis of vertically aligned graphene, 2020 *Nanotechnology* **31** 395604

[17] Wu Y, Qiao P, Chong T and Shen Z 2002 Carbon nanowalls grown by microwave plasma enhanced chemical vapor deposition *Adv. Mater.* **14** 64–67

[18] Zhang, Z. Y., Lee, C.-S., Zhang, Vertically Aligned Graphene Nanosheet Arrays: Synthesis, Properties and Applications in Electrochemical Energy Conversion and Storage, W. J., *Adv. Energy Mater.* 2017.

[19] Kefan Cen et al, Plasma-enhanced chemical vapor deposition synthesis of vertically oriented graphene nanosheets, Nanoscale, 2013.

[20] K. J. Tielrooij *et al.*, "Photoexcitation cascade and multiple hot-carrier generation in graphene," *Nat. Phys.*, vol. 9, no. 4, pp. 248–252, 2013.

[21] S. Kim, M. S. Jang, V. W. Brar, K. W. Mauser, L. Kim, and H. A. Atwater, "Electronically Tunable Perfect Absorption in Graphene," *Nano Lett.*, vol. 18, no. 2, pp. 971–979, 2018.

[22] M. Acik and Y. J. Chabal, "Nature of graphene edges: A review," *Jpn. J. Appl. Phys.*, vol. 50, no. 7 PART 1, pp. 0–16, 2011.

[23] Y. W. Tan *et al.*, "Graphene at the Edge," *Science (80-.).*, vol. 666, no. March, pp. 1705–1708, 2009.

[24] A. Cortijo, F. Guinea, and M. A. H. Vozmediano, "Geometrical and topological aspects of graphene and related materials," *J. Phys. A Math. Theor.*, vol. 45, no. 38, 2012.

[25] G. Reina, J. M. González-Domínguez, A. Criado, E. Vázquez, A. Bianco, and M. Prato, "Promises, facts and challenges for graphene in biomedical applications," *Chem. Soc. Rev.*, vol. 46, no. 15, pp. 4400–4416, 2017.

[26] A. H. C. Neto, F. Guinea, N. M. R. Peres, K. S. Novoselov, and A. K. Geim, "The electronic properties of graphene," vol. 81, no. March, 2007.

[27] F. Bonaccorso, Z. Sun, T. Hasan, and A. C. Ferrari, "Graphene photonics and optoelectronics," *Nat. Photonics*, vol. 4, no. 9, pp. 611–622, 2010.

[28] M. F. El-kady, Y. Shao, and R. B. Kaner, "Graphene for batteries, supercapacitors and beyond," pp. 1–14.

[29] Y. Arao, F. Mori, and M. Kubouchi, "Efficient solvent systems for improving production of few-layer graphene in liquid phase exfoliation," *Carbon N. Y.*, vol. 118, pp. 18–24, 2017.

[30] E. L. Lim, C. C. Yap, M. H. H. Jumali, M. A. M. Teridi, and C. H. Teh, "A Mini Review: Can Graphene Be a Novel Material for Perovskite Solar Cell Applications," *Nano-Micro Lett.*, vol. 10, no. 2, pp. 1–12, 2018.

[31] K. Karimi, "The Characterization of Graphene Paper for Flexible Electronics Application," 2016.

[32] A. De Sanctis, J. D. Mehew, M. F. Craciun, and S. Russo, "Graphene-based light sensing: Fabrication, characterisation, physical properties and performance," *Materials (Basel).*, vol. 11, no. 9, 2018.

[33] M. Casalino *et al.*, "Vertically Illuminated, Resonant Cavity Enhanced, Graphene-Silicon Schottky Photodetectors," *ACS Nano*, vol. 11, no. 11, pp. 10955–10963, 2017.

[34] Z. Bo, Y. Yang, J. Chen, K. Yu, J. Yan, and K. Cen, "Plasma-enhanced chemical vapor deposition synthesis of vertically oriented graphene nanosheets," *Nanoscale*, vol. 5, no. 12, pp. 5180–5204, 2013.

[35] H. Buljan, M. Jablan, and M. Soljacic, "Plasmons in Graphene: Fundamental Properties and Potential Applications," *Proc. IEEE*, vol. 101, no. 7, pp. 1689–1704, 2013.

[36] X. Miao *et al.*, "High efficiency graphene solar cells by chemical doping," *Nano Lett.*, vol. 12, no. 6, pp. 2745–2750, 2012.

[37] G. Nandamuri, S. Roumimov, R. Solanki, G. Nandamuri, S. Roumimov, and R. Solanki, "Remote plasma assisted growth of graphene films Remote plasma assisted growth of graphene films," vol. 154101, no. 2010, pp. 2008–2011, 2014.

[38] Y. Lu, X. Liu, and D. Kuzum, "Graphene-based neurotechnologies for advanced neural interfaces," *Curr. Opin. Biomed. Eng.*, vol. 6, pp. 138–147, 2018.

[39] C. A. Howsare, X. Weng, V. Bojan, and D. Snyder, "Substrate considerations for graphene synthesis on thin copper films," 2012.

S. Bae *et al.*, "Roll-to-roll production of 30-inch graphene films for transparent electrodes," *Nat. Nanotechnol.*, vol. 5, no. 8, pp. 574–578, 2010.

[40] L. Cao, M. J. Meziani, S. Sahu, and Y.-P. Sun, "Photoluminescence Properties of Graphene versus Other Carbon Nanomaterials," *Acc. Chem. Res.*, 2013.

[41] K. S. Novoselov, V. I. Fal, L. Colombo, P. R. Gellert, M. G. Schwab, and K. Kim, "REVIEW A roadmap for graphene," *Nature*, vol. 490, no. 7419, pp. 192–200, 2012.

[42] X. Zhang, J. Xin, and F. Ding, "The edges of graphene," *Nanoscale*, vol. 5, no. 7, pp. 2556–2569, 2013.

[43] M. R. Rezapour *et al.*, "Graphene and Graphene Analogs toward Optical, Electronic, Spintronic, Green-Chemical, Energy-Material, Sensing, and Medical Applications," *ACS Appl. Mater. Interfaces*, vol. 9, no. 29, pp. 24393–24406, 2017.

[44] P. Ajayan, P. Kim, and K. Banerjee, "Two-dimensional van der Waals materials," *Phys. Today*, vol. 69, no. 9, pp. 38–44, 2016.

[45] O. Kozák, M. Sudolská, G. Pramanik, P. Cígler, M. Otyepka, and R. Zbořil, "Photoluminescent Carbon Nanostructures," *Chemistry of Materials*. 2016.

[46] G. Yang, L. Li, W. B. Lee, and M. C. Ng, "Structure of graphene and its disorders: a review," *Sci. Technol. Adv. Mater.*, vol. 19, no. 1, pp. 613–648, 2018.

[47] O. Neill, U. Khan, P. N. Nirmalraj, J. Boland, and J. N. Coleman, "Graphene Dispersion and Exfoliation in Low Boiling Point Solvents," pp. 5422–5428, 2011.

Chapter 3

EXPERIMENTS ON NOVEL LIGHT-MATTER INTERACTION

3.1 Photoluminescence Investigation of Defects

The ability of graphene or other gapless material to be useful for solar photon conversion requires the presence of color centers that have well defined or tunable band-gaps. Confocal photoluminescence (PL) spectroscopy offers a direct insight into various defects that have radiative decay pathways. Among the various techniques for measuring carrier recombination lifetimes without physical contact to the material such as: time resolved PL (TRPL), transient photoconductivity by microwave reflection (uPCD), quasi-steady state photoconductivity (QSSPC), resonant coupled photoconductive decay (RCPCD), transmission modulated photoconductive decay, and pump-probe measurement of free carrier absorption. Our studies will focus primarily on PL and TRPL. Combined with temperature dependent photoluminescence we can identify whether such luminescent modes are coupled with phonon interactions.

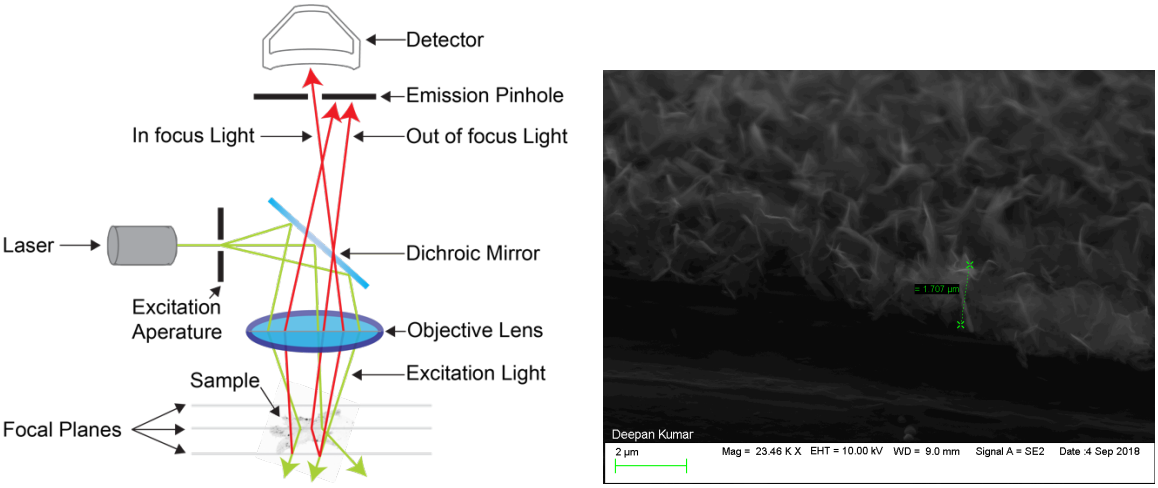

Figure 3.1: Basic layout of confocal microscopy for photoluminescence characterization and SEM image of pristine quasi-1D graphene. Credit: Nikon Microscopy U, Nikon Instruments © 2021

In order to examine the PL emission from pristine or modified quasi-one-dimensional graphene, we use the Zeiss LSM 880 Confocal Microscope at the Beckman Institute, which is sensitive to emissions from 400 nm to 750 nm, and is equipped with laser sources at 405, 458, 488, 514, 561, 594 & 633 nm, Tunable 2-photon Coherent Ultra Laser 720-1020 nm. This system is equipped with a 32 channel GaAsP PMT detector, along with 34 channel QUASAR detector for spectral imaging. The ZEISS QUASAR multichannel photomultiplier detection is based on a filter-free system that guides the desired wavelength range to the target detector using adjustable optical wedges and slider light stops

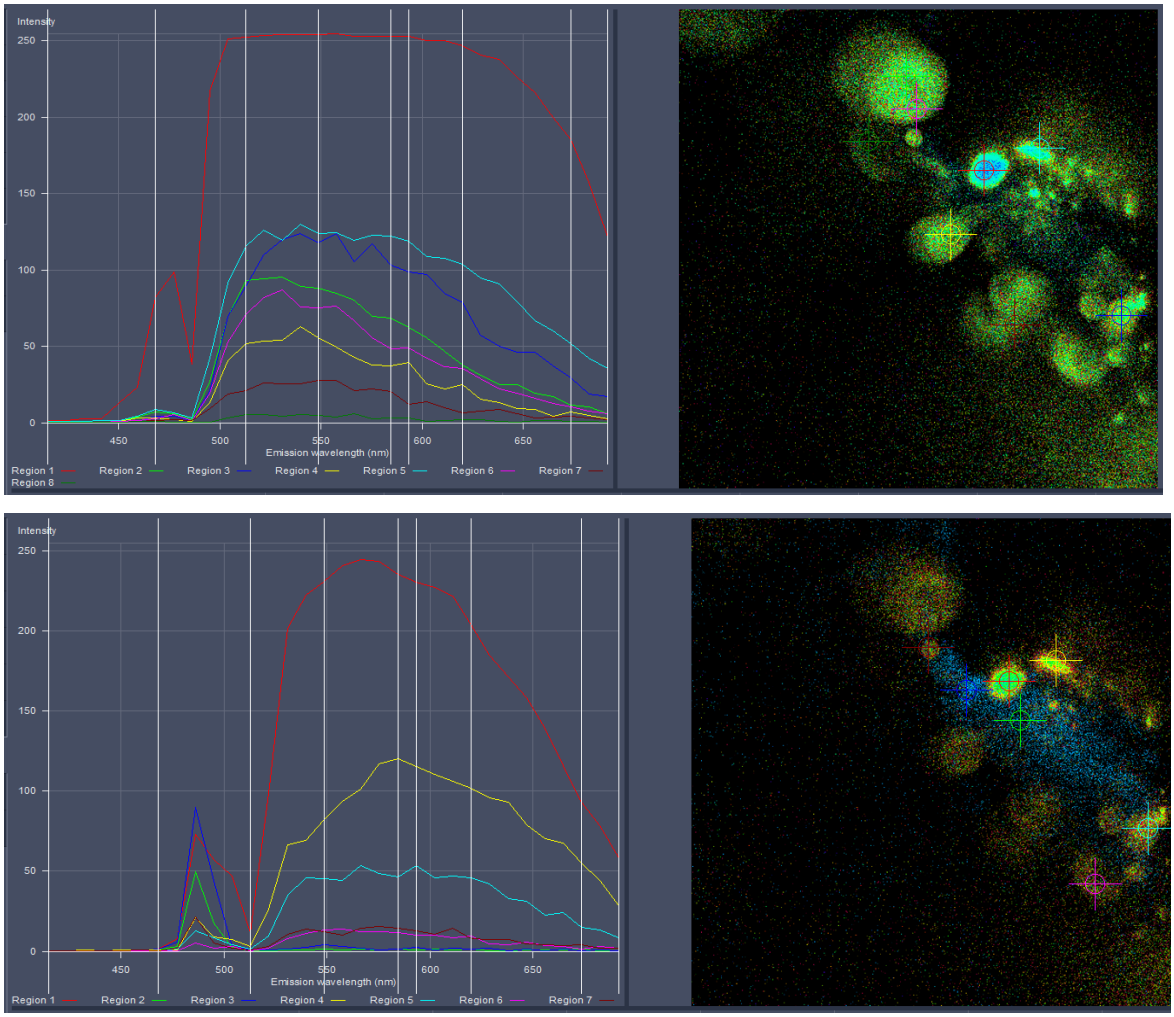

Figure 3.2: 488 nm and 514 nm excitation dependent emission of as-grown quasi-1D graphene with less than 5 mW laser pump power

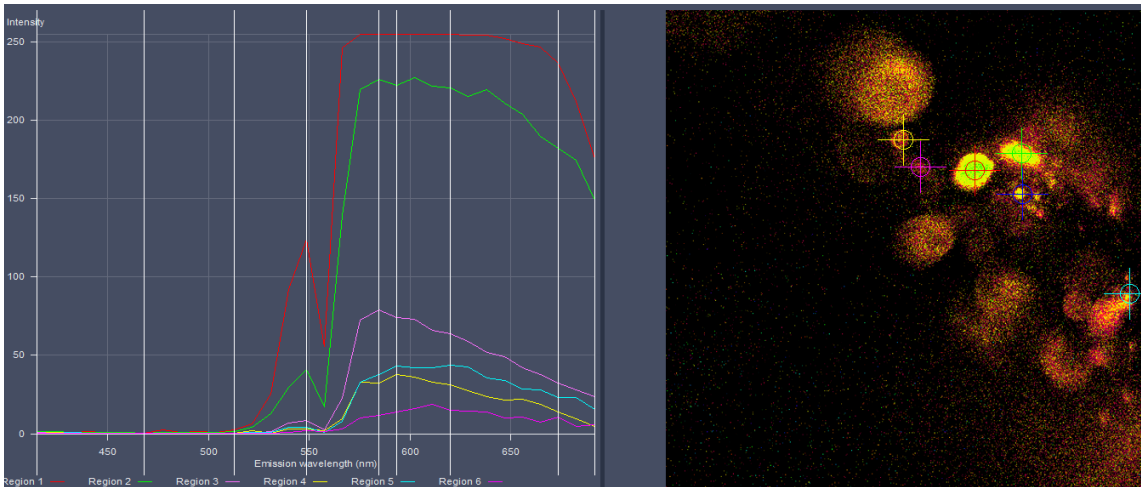

Figure 3.3: 566 nm excitation dependent emission of as-grown quasi-1D graphene with less than 5 mW laser pump power

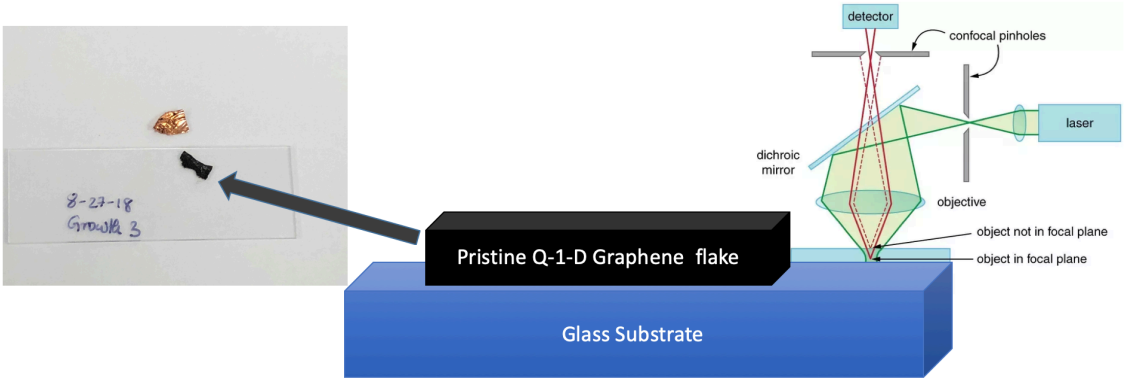

Figure 3.4: As-grown quasi-1D graphene is transferred from the copper foil and placed on a quartz slide for confocal microscopy. Spot diameter is nearly 100 μm.

In Figures 3.2 – 3.3, the use of MBS filters suppresses the excitation beam and thus creates a tail on the blue shifted emission. Our very first photoluminescence measurements on as-grown quasi-1D graphene displayed a surprising broad distribution of wavelengths and sparse point like emissions and some clustered emission centers. At this stage, the cause of this light emission was not immediately obvious because our materials synthesized from PECVD only use CH_4 and H_2 with organic C_6 precursors, and that our x-ray photoelectron spectroscopy had confirmed that these samples were pure graphene nanomaterials. We hoped that by exfoliating the material further we could understand the depth distribution of the color centers. The use of N-methyl-Pyrolidone (NMP) in the exfoliation process was

able to induce more color centers by attaching some functional groups with the graphene, as shown in Figures 3.5 – 3.6. This process introduced two unknown variables in trying to deconvolve the origin of light emission: First, the exfoliation process breaks the material down during sonication and ultracentrifugation, which introduces many edges, and unsatisfied bonds when the material is broken. Second, the use of NMP chemical also adds unknown chemical functionalization. For the PL studies of exfoliated graphene nanomaterial, we tried drop coating the material (Right panel of Figure 3.6) to control the thickness and then studied the PL as a function of the thickness or the amount of material.

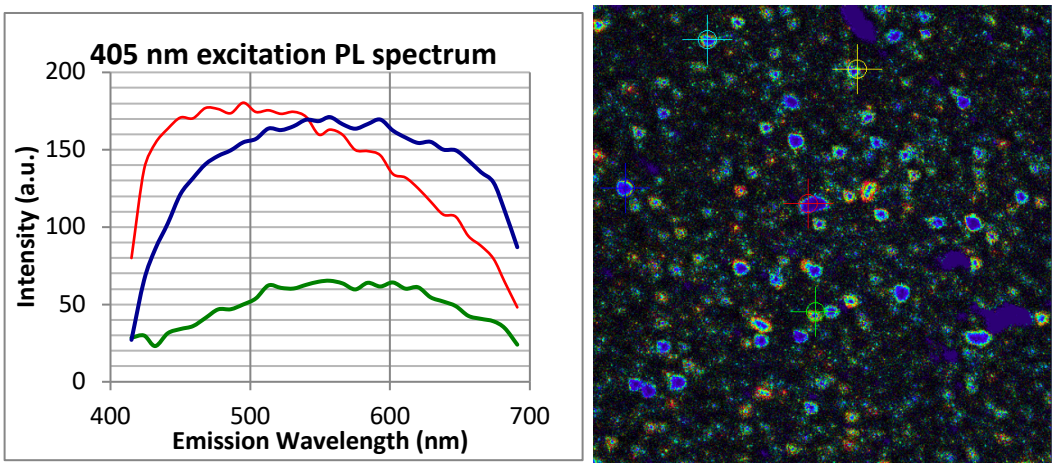

Figure 3.5: PL spectra from liquid exfoliated graphene coated on a silicon substrate by means of spin coating. (Laser pump power < 5mW)

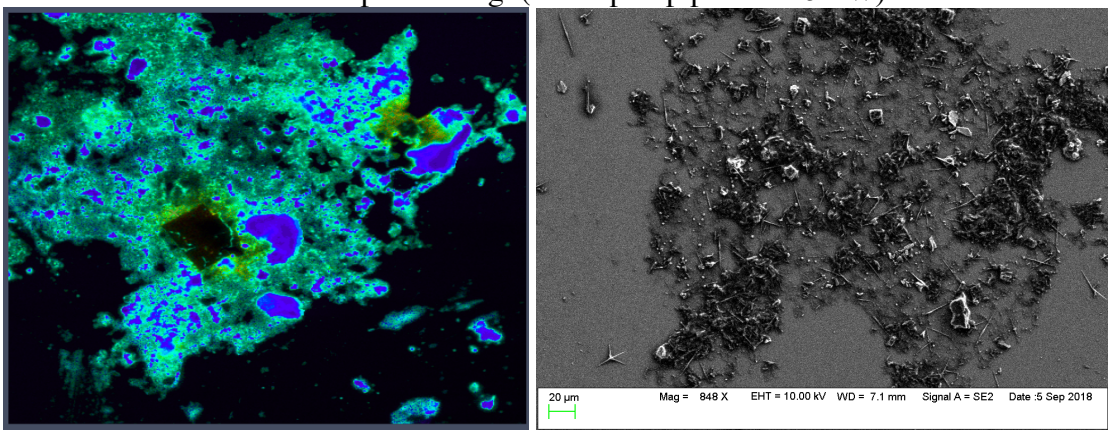

Figure 3.6: PL emission from liquid phase exfoliated quasi-1D graphene nanomaterial with SEM image on a drop coated sample

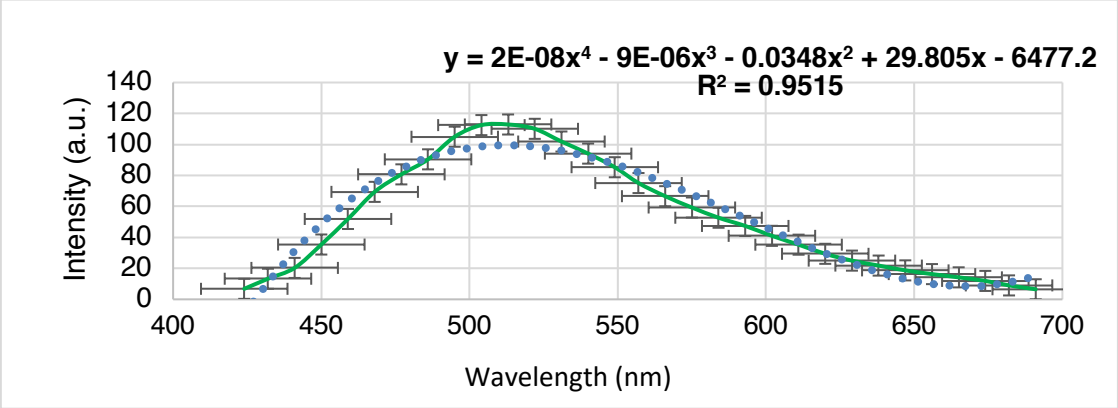

Figure 3.7: PL emission spectrum from liquid phase exfoliated quasi-1D graphene nanomaterial excited at 405 nm

The excitation wavelength dependent emission has a strong emission peak always centered near 560-565 nm window. To understand its origin, we note that sp^3 defects are well known to be quantum light sources in carbon nanotubes, but the exact nature of these defects required controlled experiments. For more details on polariton dynamics of sp^3 defects in carbon nanotube (CNT) systems, see [21]. It is well known in the literature that graphene oxide has emission centered ~ 560 nm. However, the lack of direct oxygen in our PECVD process led us to rule out the possibility of C=O related emission earlier. Subsequently, by studying Ar plasma induced damages, we found that we could activate different color centers in graphene nanomaterials by creating reactive sites to localize sp^3 defects or to form C-X or C=X bonds with ambient atmosphere, where X represented some atomic element.

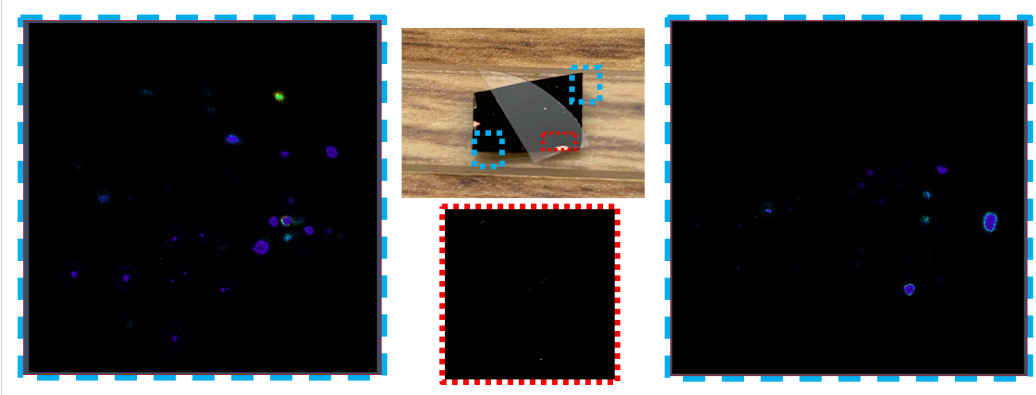

Figure 3.8: As-grown quasi-1D graphene nanomaterial on copper for examining the effect of Ar plasma induced luminescent defect centers. Red region shows no PL when masked from Ar plasma, while blue boxes reveal enhanced PL after exposure to Ar plasma.

By using two samples grown on copper and silicon substrates, we applied a thin quartz slide to mask some portion of the graphene and then investigated the PL emission before and after subjecting the material to Ar plasma, as shown in Figure 3.8 for sample on copper and in Figures 3.9 and 3.10 for sample on silicon.

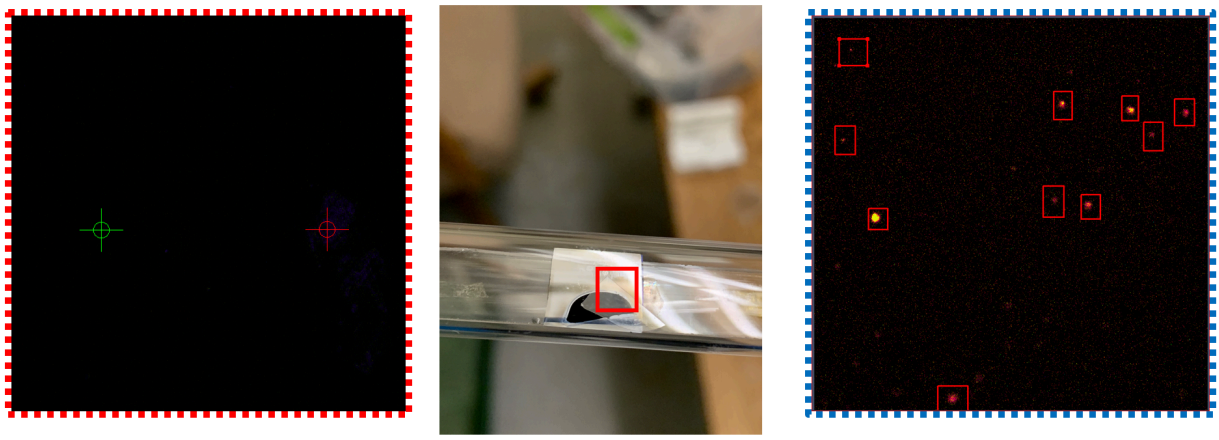

Figure 3.9: The red box shows PL spectrum on the graphene-on-silicon sample before being Ar+ plasma bombardment and the red boxes on the right show many more luminescent color centers that appear after plasma exposure. (Ar plasma at 10 Watts for 5 minutes)

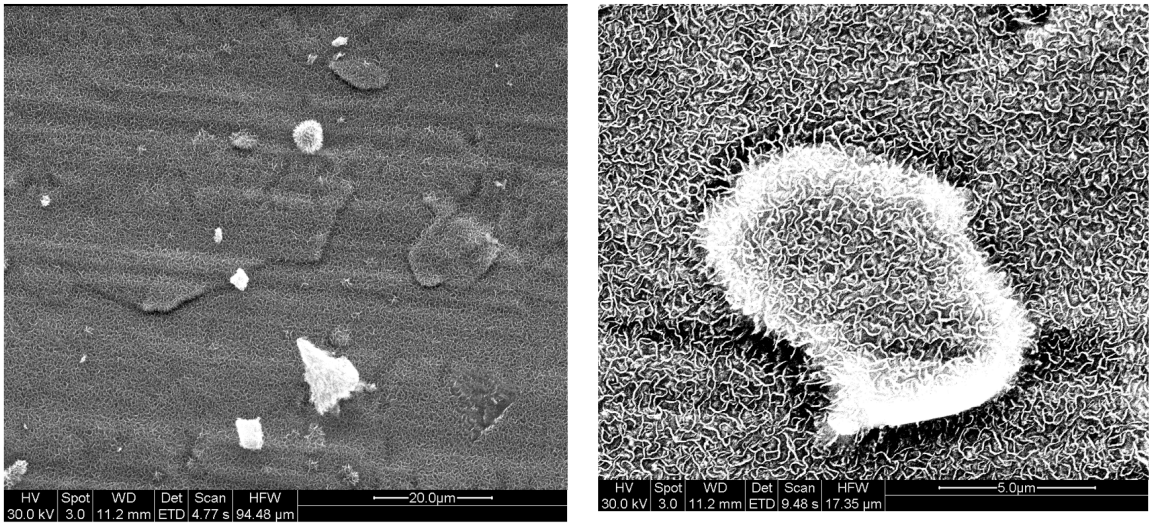

Figure 3.10: SEM images showing the microscopic nature of defect morphology of graphene nanomaterial on Si substrate after Ar plasma irradiation. Here the same sample has been mapped by PL spectroscopic studies, revealing enhanced PL.

The experimental results shown in Figures 3.8 – 3.10 confirm that defects induced by Ar plasma resulted in localized color centers in quasi-1D graphene nanomaterials, and a spectral peak at 561 nm appeared in many samples after Ar plasma irradiation, as exemplified in Figure 3.11. To confirm the conjecture that these PL emissions were indeed from oxygen bonding locally, we exposed pristine quasi-1D graphene to oxygen plasma to verify the nature of the peak at 560 nm.

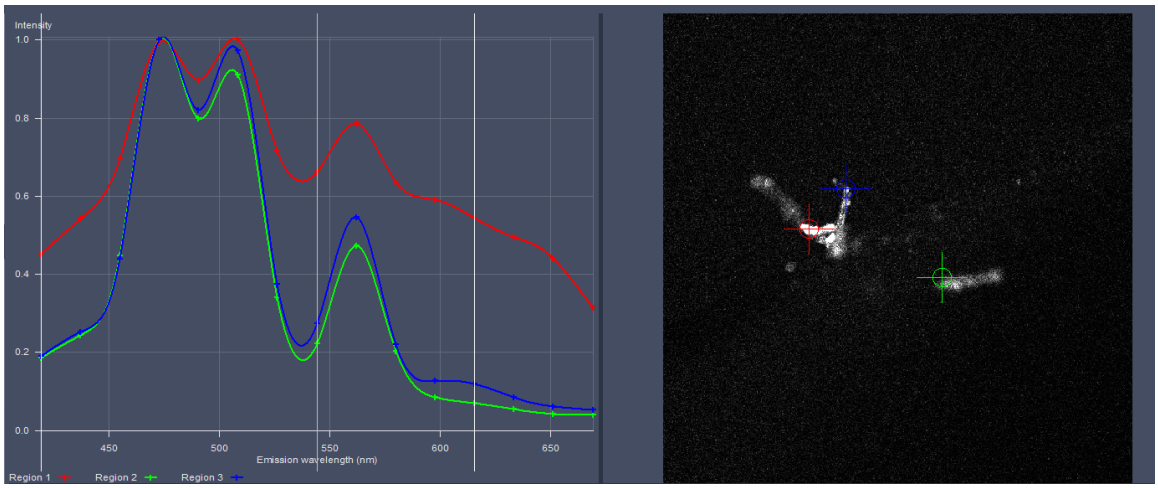

Figure 3.11: 488 nm excitation PL spectra taken on different locations of a graphene sample after Ar plasma irradiation, showing a distinct peak at 560 nm that indicated the likelihood of PL emission from the C=O bond.

In the next set of experiments, we used an aluminum foil with 1 mm holes as Ar plasma etch windows that would selectively expose graphene to Ar plasma (Figure 3.12) and added some trace amounts of oxygen. We selected this approach to verify that the strong PL emission clusters are definitively from regions exposed to the plasma, as the previous experiments with covered quartz piece may have be incomplete masking; this is the rationale for complete masking with Al foil and selective etch windows made with holes from 1 mm syringe needles. The PL spectra of these plasma irradiated graphene under different excitation wavelengths are shown in Figures 3.13 – 3.15. The strong PL emission from graphene nanomaterials with high concentrations of type-2 defects that we induced by Ar plasma irradiation (Figures 3.13 – 3.15) renders a direct proof that the PL emission properties of qausi-1D graphene nanomaterials can be engineered by inducing defects to make the material strongly luminescent.

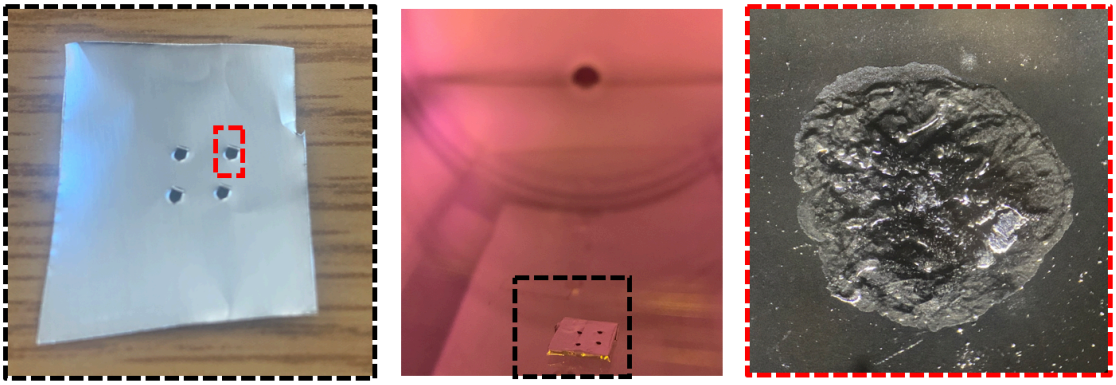

Figure 3.12: Graphene nanomaterials on a (1 cm × 1 cm) silicon substrate covered with an Al foil with 4 etch windows of 1 mm in diameter (left panel), which were subjected to Ar plasma and some trace amounts of oxygen plasma subsequently (middle panel). The graphene sample after Ar plasma irradiation is shown in the right panel.

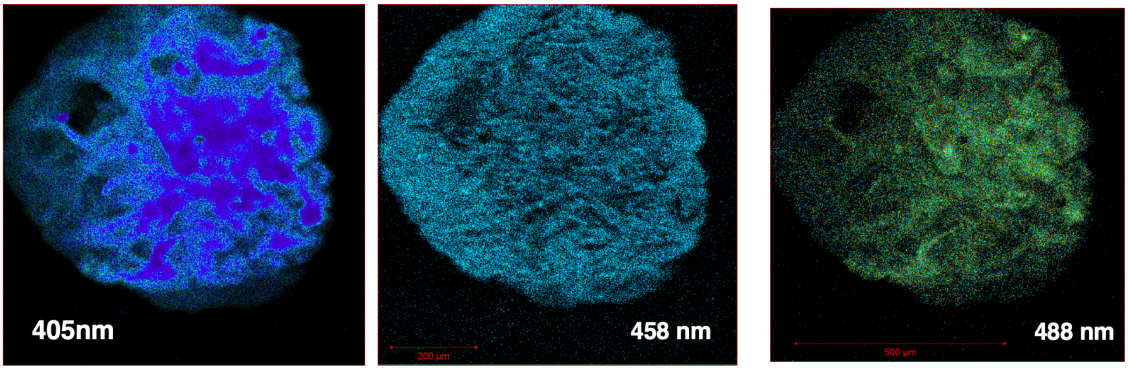

Figure 3.13: PL emission from defect engineered graphene with 405 nm, 458 nm and 488 nm excitation showing broadband emission dependent on the excitation wavelength.

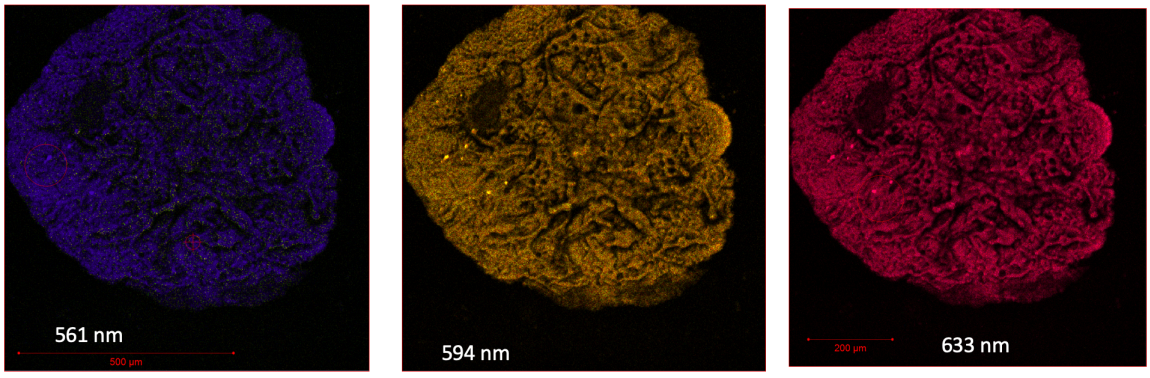

Figure 3.14: PL emission from defect engineered graphene with 561 nm, 594 nm and 633 nm excitation, showing broadband emission dependent on the excitation wavelength.

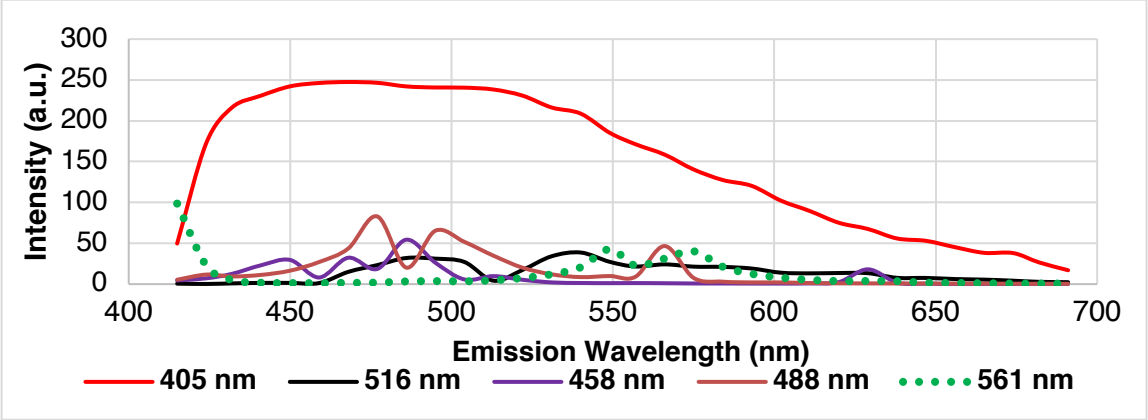

Figure 3.15: Representative PL emission spectra for different excitation wavelengths (405 nm, 458 nm, 488 nm, 516 nm and 561 nm) in Ar/O plasma induced defects in graphene nanomaterials from Figure 3.13-3.14

For samples shown in Figure 3.12, that were irradiated with Ar/O plasma, we show the spectra collectively on Figure 3.15 for different excitation wavelengths, where the different intensities are related to different peak power various laser used in LSM 880. The 405 nm is a pigtailed c.w. laser diode with peak power of 15 mW, we use an Ar laser for emission at 458 nm, 488 nm, with peak powers of 25 mW. The pump at 561 nm is from a Diode Pumped Solid State laser which has a peak power of 20 mW, while the 594 nm laser pump is from a HeNe laser with peak power of 2 mW, and 633 nm pump has a peak power of 5 mW. Refer Zeiss LSM 880 manual [23] for detailed laser specifications. All the laser lines are attenuated with a VIS-AOTF (Acousto-Optical Tunable Filter). The difference in intensities for each emission peak is related to using lasers with different peak powers, keeping similar attenuation factor. It is not immediately evident if the emission has different quantum yield for emission as a function of excitation wavelength. The colors of the PL emissions shown in Figure 3.13 and 3.14 reflect true colors of the emissions. Since we used a T80/R20 mirror to suppress the laser peak emission, some spectra represent the dominant color of the pump if the red/blue emission were weaker than the peak color around the laser pump after suppression by the T80/R20 mirror. It should also be mentioned that the detector (GaAsP-PMT) spectral sensitivity was not uniform and the detector quantum yield rolled off at longer wavelengths, as described in [23].

Excitation dependent photoluminescence from graphene oxide has been a subject with many proposed mechanisms without a firm consensus due to the diversity in materials and methods to create graphene oxide in solid or liquid phase techniques. The review by Yanling Hao *et al* [14] has indicated, among others, mechanisms involving giant red edge effect, surface traps model, edge estate model, quantum confinement effect, and electronegativity of heteroatom model, and also suggests some synergistic model combining these effects. The existence of type-1 or type-2 defects in quasi-1D graphene invariably created domains of sp^2 clusters separated by defect grain boundaries, and some sp^3 clusters from hydrogen termination, which reduces the carbon aromaticity as the relative concentration of π electrons diminishes. The degrees of heteroatoms (like N, O, Cl, *etc*.) also play a role in determining the dipole strength as the C=X bond becomes an effective dipole due to the difference in electronegativities, leading to small charge accumulation on the carbon and heteroatoms. From a phenomenological stand point, the experimental data suggest that these defects are able to create stable energy states that can be tunes by the optical excitation, which are findings different from typical two-level systems in semiconductors, as the photoluminescence of the latter obeys Kasha's rule so that emission is always from the band edge, irrespective of the PL excitation wavelength.

For potential photonic device applications, the strong wavelength-dependent PL spectra implied that there were strong interactions among the excited states, leading to exciton-exciton and polariton-polariton interactions due to the continuous spread of energy levels in the visible and IR (shown in next sub-sections). This cooperative effect, which has also been reported by others [14,15], would play a crucial role in facilitating strong light-matter interactions.

3.2 Blue-Shifted Emission from Defects

From the above measurements, a unique nonlinear effect that is often seen in the two-photon or multi-photon absorption processes is noted, for the 561 nm excitation. The appearance of a distinct blue shifted peak (Figure 3.15), commonly called an anti-Stoke

fluorescence peak, was investigated further. As shown in Figure 3.16, the blue-shifted emission became strongly enhanced when we further treated the sample with trace amounts of O_2 plasma. The absence of such a blue shifted peak at other excitation energies, despite broad blue shifted tails, also suggested that a resonant pumping of the 2.2 eV energy gap of the defects, which is very close to the C=O bonding energy, was able to manifest some coherent energy exchange, similar to cavity QED in the creation of an upper polariton branch.

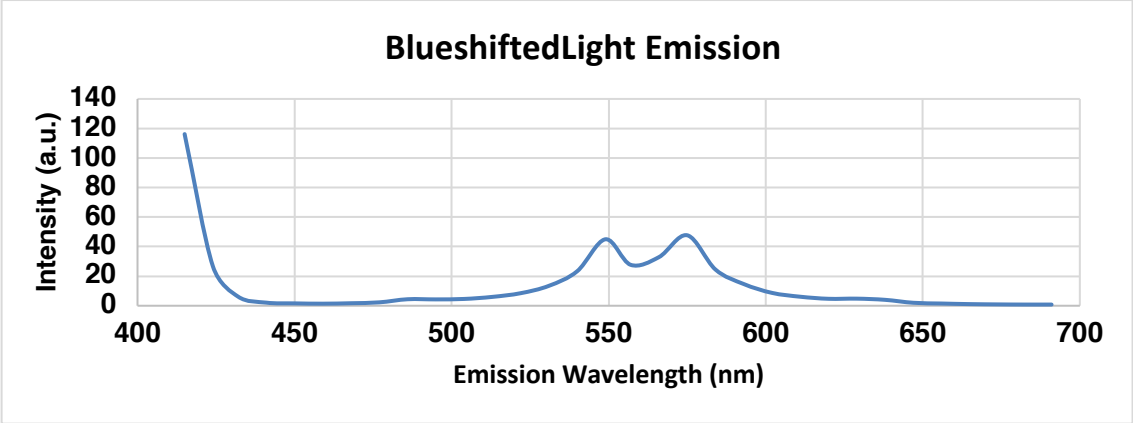

Figure 3.16: The blue-shifted emission is strongly enhanced when we further treated the sample with trace amounts of O_2 plasma. The pump wavelength used here is 561 nm, which is suppressed using a T80/20 mirror, no other optical filter is used.

The existence of this blue shifted peak in pristine quasi-1D graphene nanomaterial with sparse 0D defects from the growths (type-1 defects, by our terminology), as exemplified in Figure 3.17, is also indicative that the PECVD synthesis process allows for some reactive oxygen bonding. The creation of C=O bond may have taken place in the PECVD process chamber as the base pressure of the system is typically 1 torr, which has traces of oxygen; or during the venting process after growth, when the material can become locally oxidized in regions with reactive defect sites post plasma reaction.

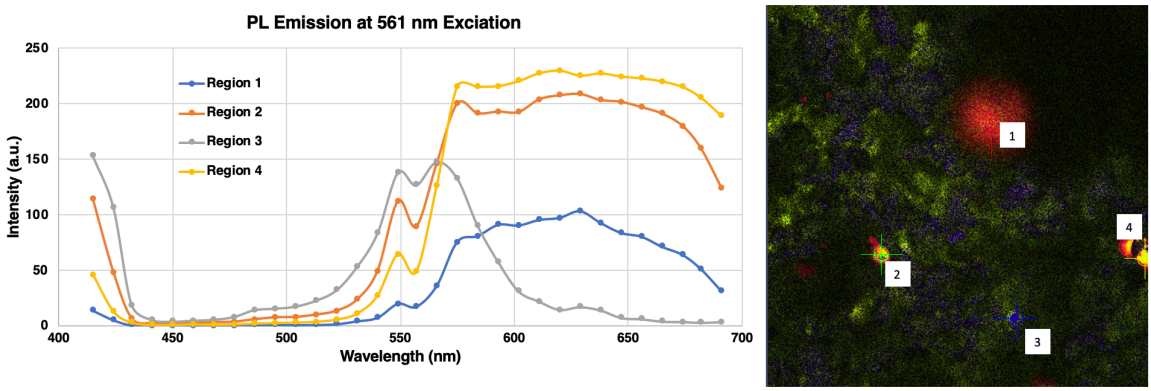

Figure 3.17: Blue shifted emission from as-grown quasi-1D graphene with only type-1 defects. The pump wavelength is at 561 nm, which is resonant with the 2.2 eV defect energy.

One possible interpretation for the blue shift is attributed to contributions from phonons to the ground state, and the suppression of the Stokes fluorescence is because the red shifted or Stokes emission is below the "cut-off" frequency of the cavity, suggested by D. G. Lidzey *et al* [1]. Such blue-shifted light emission has also been commonly reported in graphene quantum dots systems [2]. This may be consistent with our findings, as the narrow widths (on the order of ~ 10- 10^2 nm) of graphene nanomaterials can support quantum confinement of light, similar to the optical cavity analogy. The work by C. Li *et al*. [2] on graphene quantum dots have speculated that the up-conversion comes from the energy difference between the π and σ orbitals around 1.1 eV. When a bunch of low energy photons excite electrons in the π orbitals, they would transition to a high energy state such as the LUMO state and then fall back to the ground state. This mechanism also points to examining the electronic structure of the C=O bond energies to explain why the energy difference is consistently around 1 eV from 420 nm to 625 nm, which is very close to the 1.1 eV noted by others studying graphene quantum dots, the latter contain significant C=O functional groups. From a solar energy harvesting perspective, this natural up conversion could allow for harnessing higher energy excited states without the need for direct band-gap opening. It is also worth noting that our current data are limited by the GaAsP detector sensitivity. A better UV detector will be necessary to measure the full extent of the blue-shifted photons.

Other alternative explanations for the observation of blue shift in organic polaritonic systems include: the saturation of the ground state that necessitates populating the upper polaritonic states (P. Lagaoudakis *et al*. [3]); potential pathways like the intracavity optical Kerr effect; gain-induced frequency pulling; and coherent polariton interactions. It is easier to think about these blue shifted light emissions from a coherent scattering process between different hybridized energy states (or orbitals) as discussed above. Further studies could potentially reveal some additional factors contributing towards this blue shifted photon emission from CW pump.

3.3 Time Resolved Photoluminescence (TRPL) Investigation

Now that we have identified the nature of these sparse type-1 defects and engineered type-2 defects, we proceed to investigate the lifetimes of these color centers as a function of temperature and sample thickness, as the carrier lifetime in these metastable states is key to designing metal contacts and verifying the feasibility of hot electron extraction. Pristine graphene has carrier lifetime << 1 ps, and for this reason, excited hot electrons rapidly recombine within a few 100 nm in length, which makes it impossible to place metal contacts sufficiently close to capture them.

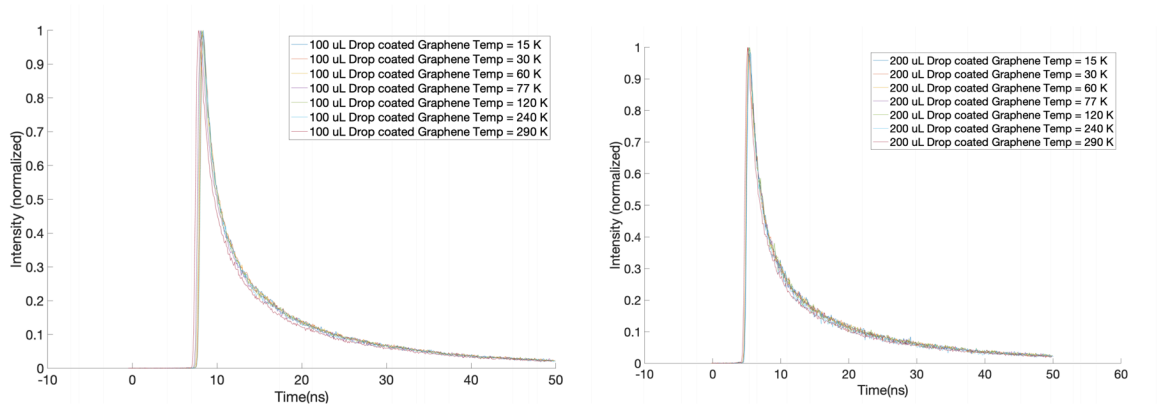

Figure 3.18: 355 nm excitation of exfoliated graphene sample as a function of temperature. The initial results indicated a clear double exponential nature of the emission. The left panel has 5 μm of exfoliated Graphene and right panel has 10μm of exfoliated Graphene.

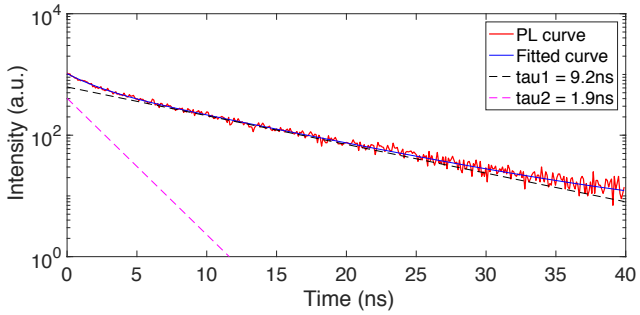

Figure 3.19: Double exponential fitting of lifetimes of pristine quasi-1D graphene under 355 nm excitation.

We used two different measurement setups to investigate the lifetime in the visible light with a Streak camera connected to a Nd:YAG laser at 355 nm pulsed excitation @ 10 Hz repetition rate at Beckman Laser Resource center, and 450-800 nm tunable laser with a time correlated single photon correlator (TCSPC) in a confocal Leica SP8 microscope.

As shown in Figure 3.18, the TRPL spectra of taken on as-grown quasi-1D graphene nanomaterials of different thicknesses and over a wide range of temperatures (from 15 K to 300 K) exhibited no discernible temperature dependence. By fitting the time dependence to a double exponential decay function (as exemplified in Figure 3.19), the resulting temperature dependence lifetimes τ_1 and τ_2 for three different samples thicknesses (5 μm, 10 μm and 20 μm) are shown in Figure 3.20. Both lifetimes exhibited very slight decrease with decreasing sample thickness and nearly no temperature dependence. These results strongly suggest that the lifetimes associated with the PL signals are not mediated by phonons. The second observation, which needs to be examined closely, is whether the width of the quasi-1d-garphene affects the lifetime or do the carrier lifetime depend just on the distribution of defects within a given width of pristine quasi-1d-graphene.

Beckman Institute laser Resource Center provided the Nd:YAG picosecond measurement facilities for these TRPL studies. The instrumentation for these measurements were Acton Research Corporation ARC SpectraPro-275 with a 0.275 m triple grating monochromator / spectrograph, Hamamtsu Blanking unit, Hammatsu Fast sweep unit, Hamamtsu Digital camera C4742-95, Hamamatsu C5680 Streak Camera, continuous wave Mode-Locked

Nd:YAG laser, and Regenerative oscillator. The Nd:YAG can emit at 1064 nm, 532 nm, 355 nm and 266 nm. We use a Pellin-Broca prism to steer the beam onto the excitation path. A Quantum Composer 9615 is used for the pulse generation.

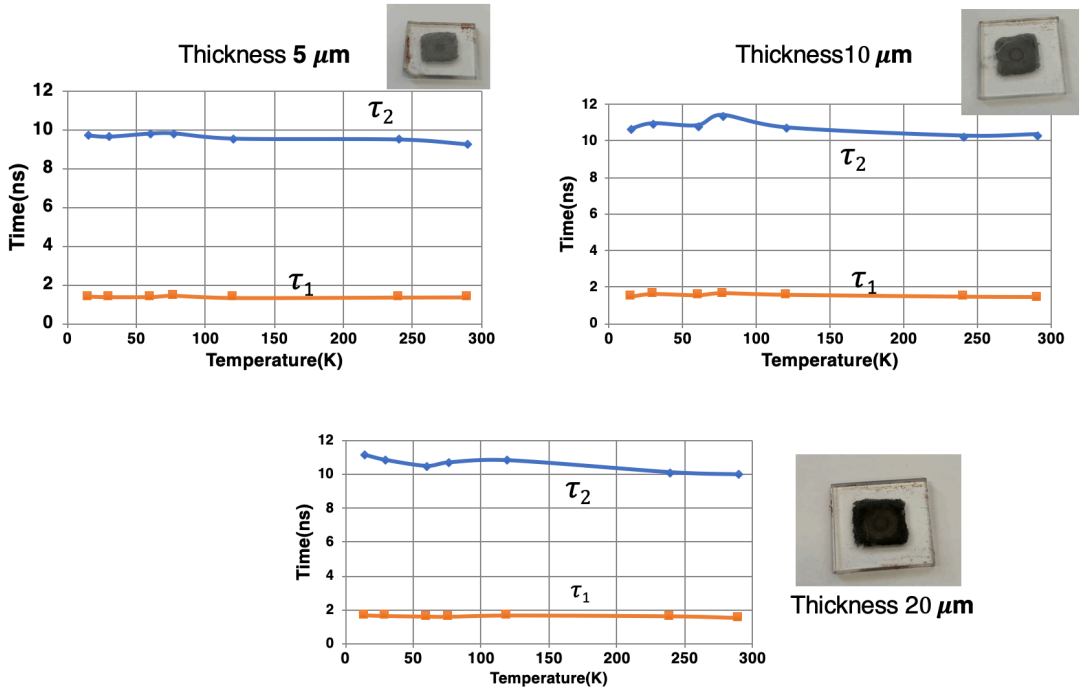

Figure 3.20: Thickness and temperature dependence of carrier lifetimes of exfoliated as-grown graphene on quartz for different amounts of exfoliated graphene. Two relaxation times τ_1 and τ_2 are identified from fitting the TRPL data for 355 nm excitations.

The physical origin of the double exponential curve was not entirely clear, apart from a phenomenological explanation of ultrafast carrier decay initially, and some long lived meta-stable states that have a lifetime up to 10 ns. Lifetime imaging done with the Nd:YAG / Streak camera system provides insights into a lifetime from a spot size about 1 cm in diameter, and hence to get a local mapping of lifetime, we use a Leica SP8 confocal microscope with a PicoQuant TCSPC for lifetime imaging in the visible. This additional measurement can provide the local lifetime of quasi-1D graphene nanomaterials with sparse and local color centers. A schematic illustration of the operation principle for the lifetime measurements is shown in Figure 3.21.

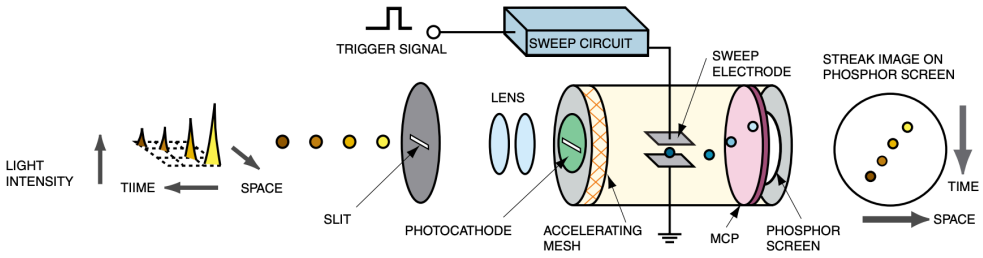

Figure 3.21: Operating principle of Streak camera-based lifetime measurement. Credit: hofstragroup.com

The lifetime data shown in Figure 3.23 with 478 nm excitation taken from Leica SP8 microscope shows carrier lifetime measured within the gray region of interest depicted in Figure 3.22 left panel image. The lifetime of the sample using the Nd:YAG set-up at 355 nm pump however shows longer lifetime because of two reasons: the spot size on the Beckman Nd:YAG can be as large as 0.5 to 1 cm with pulse energy of 0.1mJ per pulse, or 1 mW power (since rep rate is 10Hz), the white light laser used in Leica SP8 has peak power of < 50mW (refer Leica Product manual [24]) with repetition rate of 10kHz, which makes energy per pulse 500 μJ, with a spot size of ~100 μm. This difference in power density turns out to be large; the Nd:YAG being nearly **10^{-4} J/cm^2/pulse** (@ 10Hz, 1mW, spot diameter 1 cm), and the Leica ~ **0.5 J/cm^2/pulse** (@10kHz rate, 50mW, spot diameter 100 μm). This difference in energy density per pulse for unit area (in **cm^2),** and can actually be explained from polariton decay being sensitive to pump intensity, and shows that larger pump causes rapid decay of excited states, due to large population build up. The first hint at power dependence of lifetime of polariton is studied further in section 3.5.

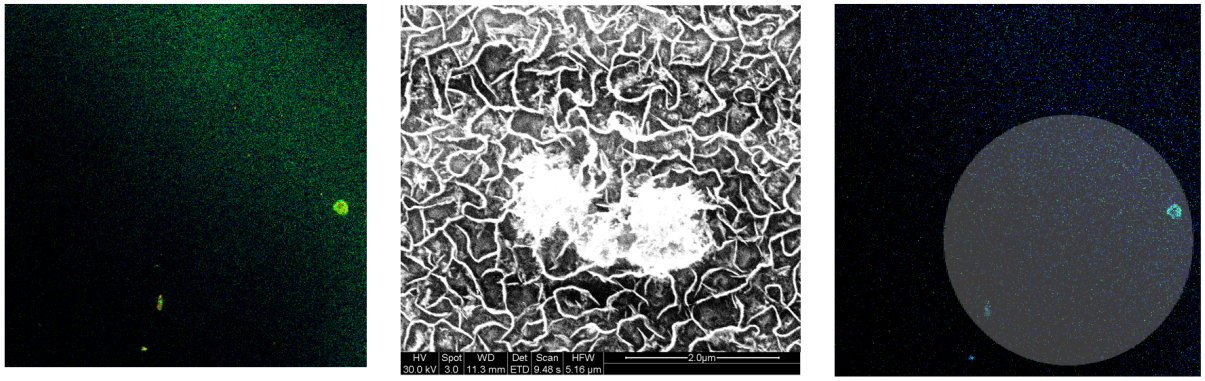

Figure 3.22: SEM image of a defect from Ar plasma damage and the PL emission with 478 nm excitation and emission from 560 nm to 737 nm with 10 MHz NKT laser. The right panel shows selection of the region of interest for estimating lifetimes.

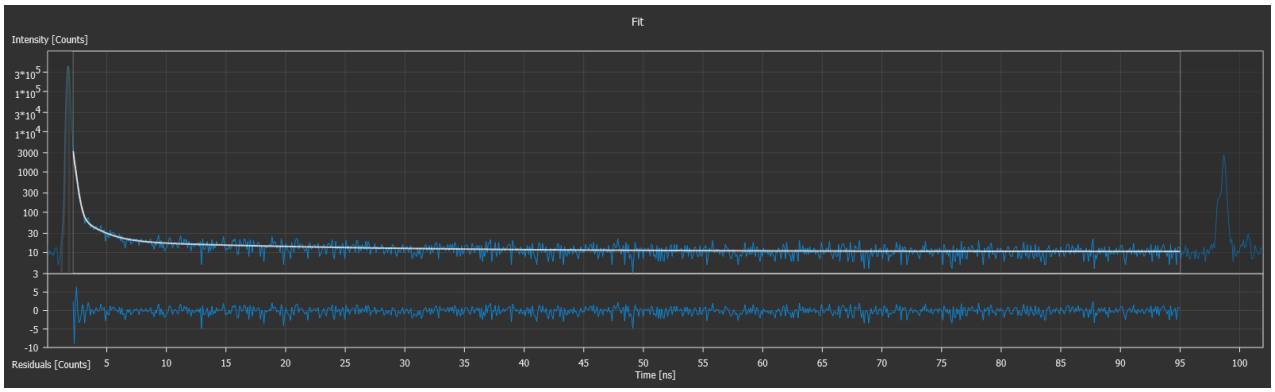

Figure 3.23: Emission relaxation by 478 nm excitation from graphene sample irradiated by Ar plasma shows much shorter lifetimes from the gray region of interest selected to measure the lifetime of type-2 defects engineered by Ar plasma irradiation.

To further understand the lifetimes, we carried out additional lifetime measurements on samples irradiated by Ar plasma, where the PL emission from a defect and the SEM image of the sample are shown in Figure 3.22, and the TRPL data are shown in Figure 3.23. When the curve in Figure 3.23 was fitted to an exponential decay function, we obtained a lifetime of 182 picoseconds, with an amplitude (indicating the number of photon events fitted) of 36,000 counts (or equivalent intensity of 70,000 counts/a.u.) and a much weaker long lifetime of 1 ns with amplitude of 100 photon count events (or 1500 counts / a.u.). These

fitting results suggested that the strongly defected regions with type-2 defects exhibited relaxation closer to a mono-exponential decay with ultra-fast lifetimes. Here we note that we only estimated the fit after 2.17 ns to account for the initial instrument response. On the other hand, the same sample with a localized high defect density from Ar plasma, when excited with a large area, high power density 355 nm Nd:YAG, still shows a long lifetime (~ 9 ns), as depicted in the spectrum shown in Figure 3.24.

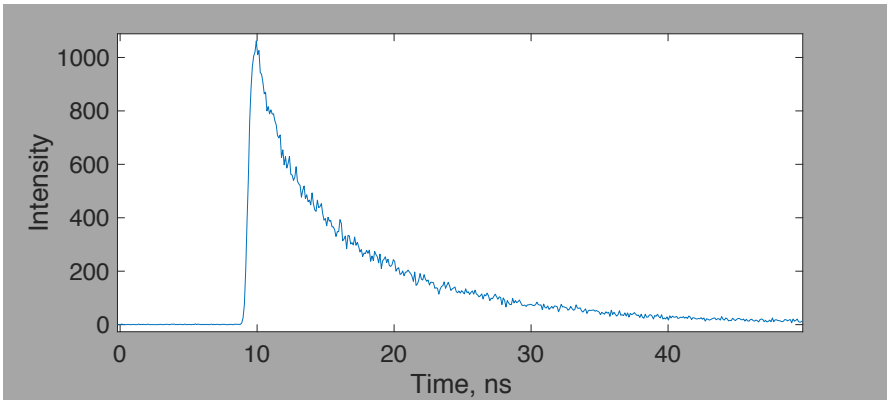

Figure 3.24: Emission relaxation by 355 nm Nd:YAG pump at 10 Hz on type-2 defect induced sample with preserved quasi-1D geometry, with $\tau 2 \sim 9$ ns

From the above corroborative experiments, it becomes clear that the double exponential decay shows that the initial ultrafast decay is dominated by defects that are lumped on edges of the material or defects that are clustered, whereas the longer lifetime light emission is predominantly from the sparse metastable topological defects (the type-1 defects). This conclusion is further bolstered by studying defective quasi-1D graphene with doping, such as nitrogen atoms introduced from N-based precursors. As further corroborated by the helium-ion beam microscope (HIM) images in Figure 3.25, large holes and microscopic tears are apparent in as-grown, N-doped graphene nanomaterials, in contrast to the smooth edges of undoped graphene. These perforations in N-doped graphene nanomaterials were developed as the result of imperfect stitching of different domains during the PECVD synthesis, which resulted in significantly reduced lifetimes (Figure 3.26). Thus, large areas of defect free graphene nanomaterials with sparse C=O or point defects are important for realizing metastable states with long lifetimes. This notion can be

further corroborated by recent *Ab initio* calculations of exciton radiative lifetimes by H.-Y. Chen *et al* [26], which demonstrated that the lifetimes of radiative recombination of 0D excitons are temperature independent and are linearly proportional to the exciton binding energy. Moreover, the exciton lifetimes for some representative 0D molecules with benzene or pentagon rings were found to be in the range of $10^1 \sim 10^2$ ns, comparable to the 10 ~ 11 ns lifetime associated with type-1 defects.

Note: All components of an instrument have a limited time resolution and contribute to the output response of the instrument. The Instrument Response Function (IRF) is a convolution of all of these contributions from the laser, detector, electronics, and optics.

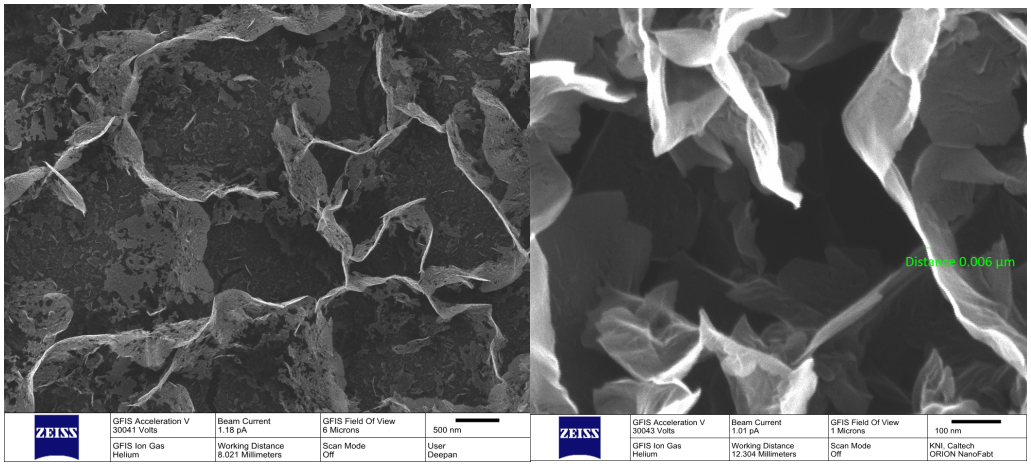

Figure 3.25: HIM images of quasi-1D graphene nanomaterials. The left panel is a HIM image taken on defective, N-doped graphene nanomaterials with sub 1 ns lifetime, and the right panel is a HIM image taken on undoped graphene nanomaterials with ~ 10 ns lifetime.

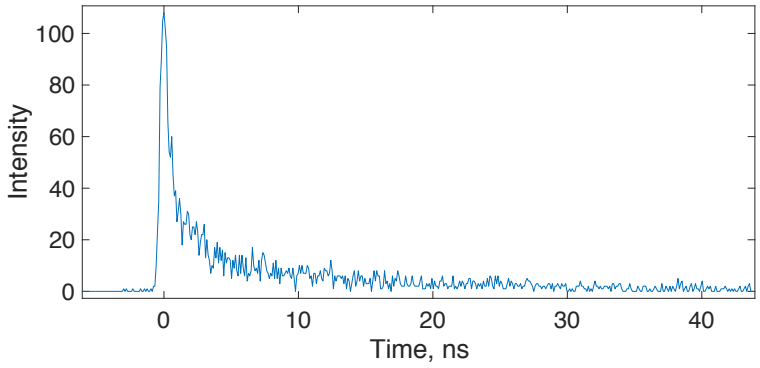

Figure 3.26: TRPL of N-doped graphene nanomaterials, showing τ2 lifetime < 2 ns.

In conclusion, we have seen that the carrier dynamics of quasi-1D graphene nanomaterials in the visible spectrum consist of contributions from two types of defects, and the low-density of localized 0D defects as well as the quasi-1D features of graphene appear to play an important role for the graphene nanomaterials to support long emission lifetimes. Further studies need to be done by tuning the excitation wavelength and the power of the excitation laser to observe if there are any deviations from the general trend reported here.

3.4 Power Dependence of Light Emission

Standard photon lasers operate under the weak coupling regime, whereas the polariton lasers require strong coupling between the exciton and photon in the cavity as well as interactions among polaritons before radiative relaxation. The polariton, built from two distinct bosons, has a low mass. The excitonic nature of the polariton wavefunction introduces interaction in the polariton gas. Threshold power in these types of laser [8] is 50 times smaller than those of a typical VCSEL, and the threshold is not directly dependent on the number of excitons/ quantum wells. Rather, the threshold behavior is due to increased interaction between the polaritons. However, a polariton laser can transition to a photon laser at the saturation density of excitons, which is similar to a gain medium with excessive defects. Thus, we can potentially convert the quasi-1D graphene with sparse C=O / other topological defects to a more band-gap like material (*e.g.*, graphene oxide) entirely, making it a regular photon lasing gain medium.

Conventional photon lasers are characterized by a sharp increase in output power beyond the threshold, when the gain from stimulated emission exceeds losses. However, in the lack of a well-defined gain medium, the presence of metastable excitonic states also supports the possibility of polariton lasing, when the light emission output scales with the pump power from a sub-linear regime to a super-linear regime at some “threshold”, as exemplified in Figure 3.27. Coherent light emission (or “lasing”) does not need population

inversion and stimulated emission as the only mechanism. Polariton lasers are seen as the bridge between two rich domains of physics, the photon lasing regime and condensation of bosonic particles in thermal equilibrium. (Refer Y. Yamamato et al. [5]). Many-body coherence allows for excitons interactions, where the thermal de Broglie wavelength of excitons exceeds the Bohr radius of the excitons, giving rise of "exciton lasers" without the need for electronic population inversion. Room temperature polariton lasing has been reported by many groups in microcavity systems with well define semiconductors like perovskites, or CdTe, GaAs, ZnO, etc (Refer Rui Sui *et al*. [6]). The threshold needed for polariton lasing happens at much lower energy than needed for typical photon lasers. The high binding energy of organic excitons (~ 1 eV) or the Frenkel excitons allows for lasing at room temperatures rather than cryogenic temperatures, as first reported by Forrest and Cohen [25].

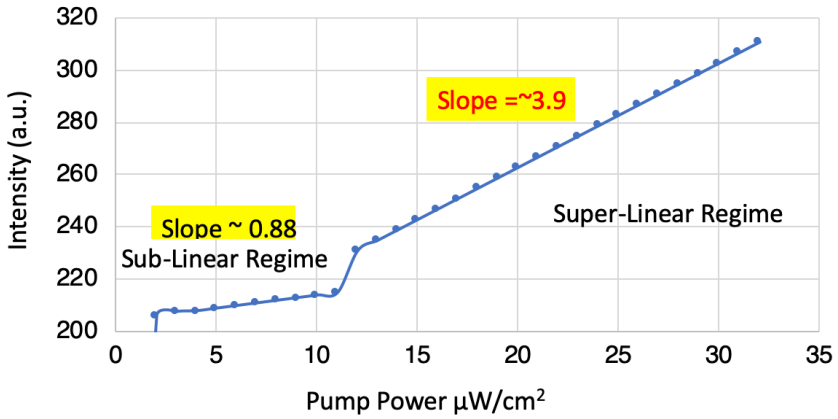

Figure 3.27: Power dependence of blue-shifted 450 nm emission intensity for excitation at 561 nm, showing variations from a sublinear regime to a super-linear regime at a threshold power ~ 12 µW/cm^2 as a signature of polariton lasing in quasi-1D graphene.

Typical polariton lasers are built with microcavities that are fabricated to be resonant at some wavelength to support a single-mode "lasing". In such systems, when the excitation intensity or pump fluence is increased, there is a sharp super-linear increase of the ground state population. At such a crossover, there is a clear reduction in linewidth, indicating increased phase coherence. In our system, the lack of any "single-mode cavity" possibly allows for a broader coherent state associated with strong interactions among the

population of excited states, leading to the transition from a sub-linear regime to a super-linear regime at a threshold power. Further experiments with Michelson interferometers and CW excitation need to be done to measure the exact linewidth and coherence time of light emission from quasi-1D graphene, but the signature of polariton lasing seen from this threshold behavior of emission is a hint towards using these materials directly in optical Fabry-Perot cavities or distributed Bragg reflectors for higher coherence polariton lasing.

The work by Hui Deng et al [7] has also suggested that the increase in blue-shift intensity beyond the threshold power may be attributed to phase-space filling from polariton interactions, which is in line with the experimental observation of the quasi-1D graphene nanomaterial. The realization of practical polariton lasers, as suggested by Paolo Lugili *et al* [8] requires that the polariton decay time is resistant to temperature variation. Our earlier results of temperature dependent PL studies indeed revealed that the emission relaxation of pristine quasi-1D graphene nanomaterials was nearly temperature independent from 15 K to 300 K (Figure 3.20). Thus, these quasi-1D graphene nanomaterials in a single-mode optical cavity can be a promising route towards visible low-threshold coherent light sources. Further studies on the coherence length and coherence time are needed for each emission wavelength to conclude which emission lines are actually coherent, if at all.

3.5 Signatures of Higher Harmonic Effects

When we excited our quasi-1D graphene nanomaterial by a multi-photon femtosecond laser (Tunable Coherent Chameleon Ultra Laser Inc.), we observed a spectral signature that resembled some possible nonlinear effects from two photon absorption. The laser power used was 164.8 mW with a pulse repetition rate at 80 MHz. Our initial results provided hints on the possibility of coherent emission from some collective low energy states, and possibly nonlinear effects like second harmonic generation maybe expected as quasi-1D graphene has broken inversion symmetry, thus allowing for both χ^2 and χ^3 effects. We also repeated the PL emission measurements on samples with engineered defects (Figure

3.29) and then compared with the results taken on pristine graphene sample shown in Figure 3.28.

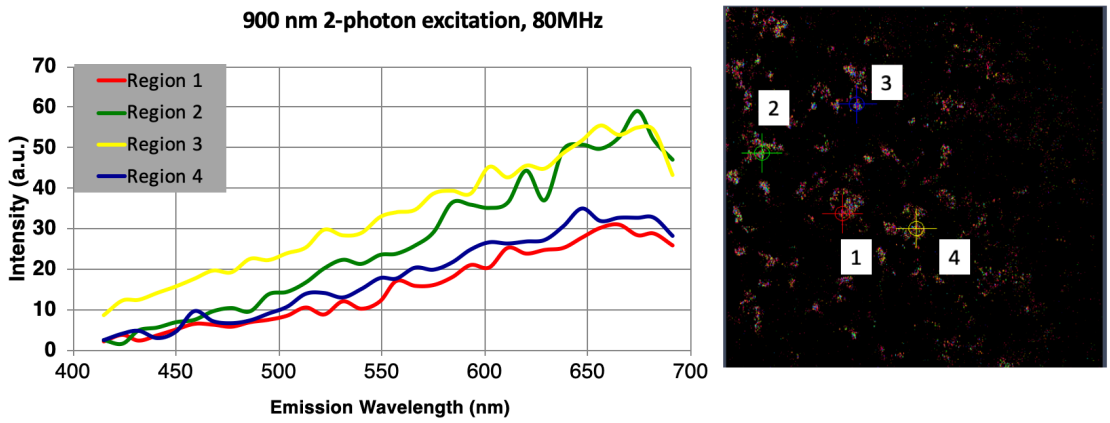

Figure 3.28: Light emission spectra from the lower energy states of pristine quasi-1D graphene when excited at 900 nm with a two-photon pulsed femtosecond light source at 80 MHz.

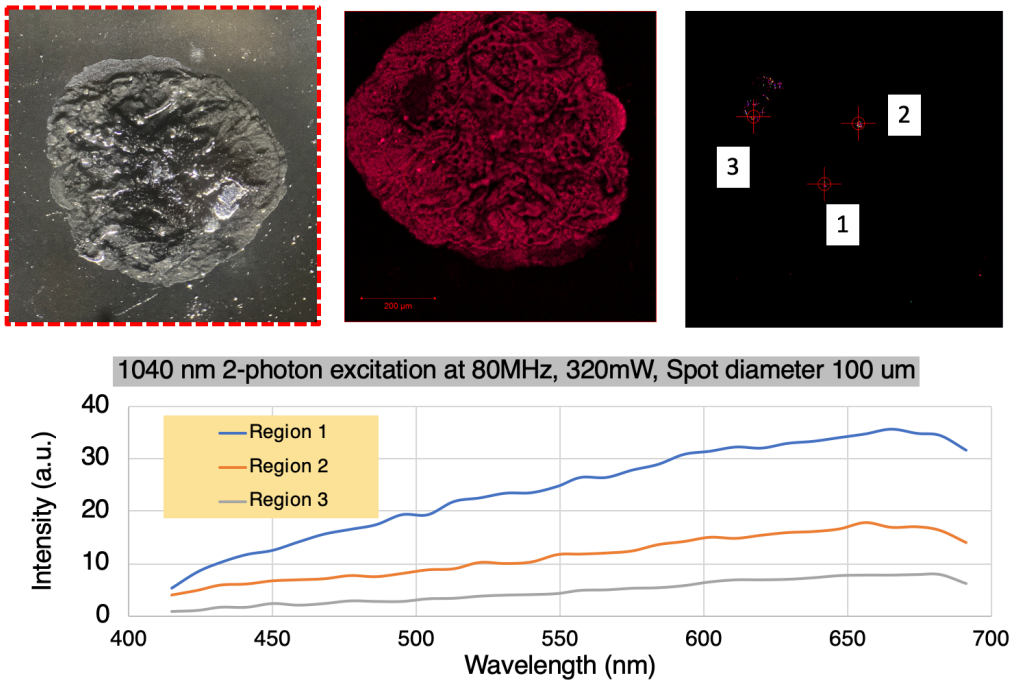

Figure 3.29: Light emission spectra from the lower energy states of defect engineered quasi-1D graphene nanomaterial.

Moreover, we note that higher emission intensities may be associated with both shorter polariton lifetimes and larger counts of polaritons, and so cannot be solely attributed to a larger population of polaritons in the lower energy states. Interestingly, however, this behavior was not just limited to the visible spectrum, but was also observed when we excited as-grown graphene with a 532 nm CW laser and detected the emission spectrum using an InGaP infrared detector, as shown in Figure 3.30.

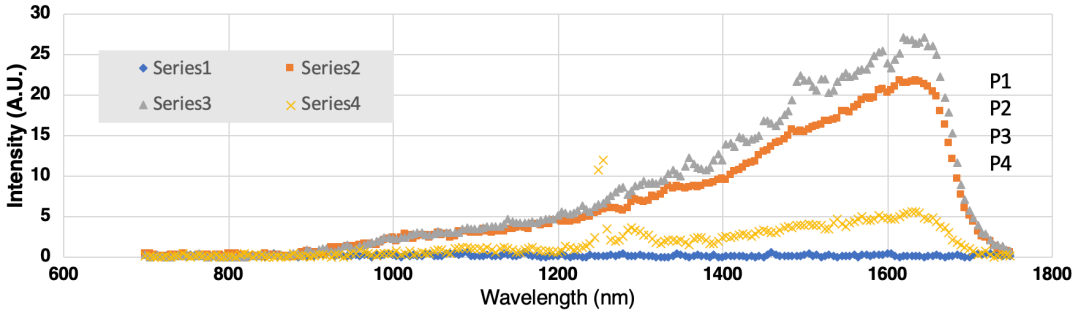

Figure 3.30; PL emission spectra of as-grown quasi-1D graphene when excited with 532 nm CW pump at different peak powers: P1 = 15 mW, P2 = 12 mW, P3 = 6 mW, and P4 = 3 mW.

The peak power was modulated using a variable attenuator, such that P2 = 0.8 P1 (orange trace on graph), P3 = 0.4 P1 (yellow trace), P4 = 0.2 P1 (blue trace). The PL emission spectra again exhibit the same behavior as a collective decay towards the lowest excited state, similar to a previous report that conjectured photon-BEC [9]. Without proper control on the concentration of emitters / defects, which would have been easier in dye-based laser by deterministic control on molar concentration, we are unable to verify whether the observed PL emission characteristics may be related to condensation of photons. The observation of PL emission spectra (Figure 3.28-3.30), wherein the intensity is higher from longer wavelengths maybe attributed to different physical origins, but from a device fabrication perspective, it becomes useful to understand how to engineer such defects that will produce PL that is not broadband but more coherent, or vice-versa based on the application.

Graphene being a Centro-symmetric crystal does not show any Second Harmonic generation (SHG). However, local defect clusters can break local inversion-symmetry,

causing the defects sites to be sensitive to second harmonic effects. This symmetry property of graphene and local broken symmetry of defects can explain why we see light emission only from highly localized regions on the quasi-1D graphene. It is however not completely known why we see a broad emission spectrum, rather than emission from 2ω when we pump at ω. To explain the existence of other meta stable energy states, one may need to account of strong-interaction between excited polaritonic quasi-particles that are scattered from higher or lower potential traps, leading a spread in emission spectrum. Even from a χ^2 framework, phase matching becomes important and whether the material has some quasi-phase matching (QPM) is not entirely clear and will need more detailed investigation as a function of the width of the quasi-1D graphene, which can be controlled by the PECVD synthesis time. The amount and type of defects that show these higher harmonic effects also needs to be studied for useful applications in bioimaging, in-vivo nonlinear light emission for biomedical applications, to name a few possible uses.

3.6 Infrared Photoluminescence

So far, we have studied the light-matter interaction in quasi-1D graphene nanomaterials in the visible, and have able to characterize the exciton-polaritonic effects associated with either type-1 or type-2 defects. It is therefore only a matter of curiosity to examine the energy landscape below the visible spectrum to see if any other carrier dynamics can be teased out from experimental data. We used the CNSI Integrated Nanomaterial Laboratory facilities at UCLA for these measurements. In the instrumentation setup shown in Figure 3.31, we used the Acton SP2300 spectrometer with wavelength range from visible to ~ 2.5 μm. The excitation source was a 20 mW, 532 nm laser. The signal was measured using SR830 Lock-in amplifier + femto-Watt detector and the cryo measurements were made with an ARS closed-cycle cryostat with a base temperature at 7K.

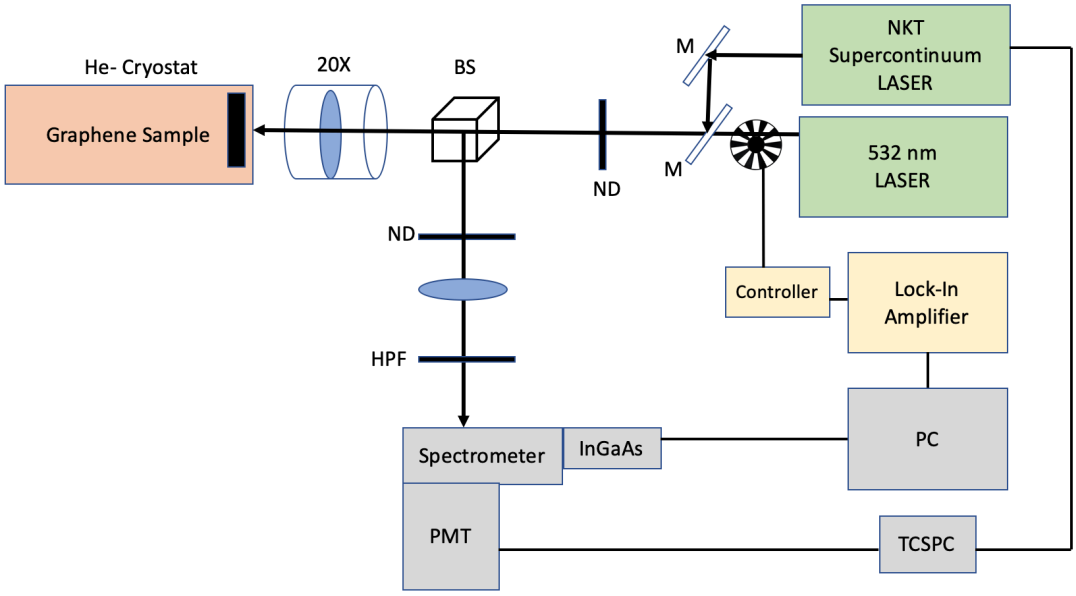

Figure 3.31: Integrated optical setup used for various spectroscopy experiments in the Visible-IR.

The linear energy-momentum dispersion relation of graphene persists up to ~ 1 eV, or about 1240 nm in wavelength. Many of the optical effects in this energy regime are mediated by strongly -coupled optical phonons (within 0.2 eV) and other low energy excitonic defects. Here we investigated two variations of quasi-1D graphene. One was as-grown samples in their pristine form, the other was liquid exfoliated samples deposited on quartz. Both these variations show remarkably unique optical signatures when probed with CW 532 nm and pulsed light sources, confirming some early conjectures and also revealing additional pleasant surprises. When we excited a liquid phase exfoliated graphene sample with 532 nm CW pump, we observed broad PL emission from 650 nm to 1800 nm. As shown in Figure 3.32, which is a representative spectra obtained from the sample, showing a weak background emission, with a sech^2 type envelope. The spectra in Figure 3.32 can be obtained in other parts of the sample indicating the presence of a random distribution of defects states where the intensity and envelope of the PL emission helps us to identify any particular type of defect.

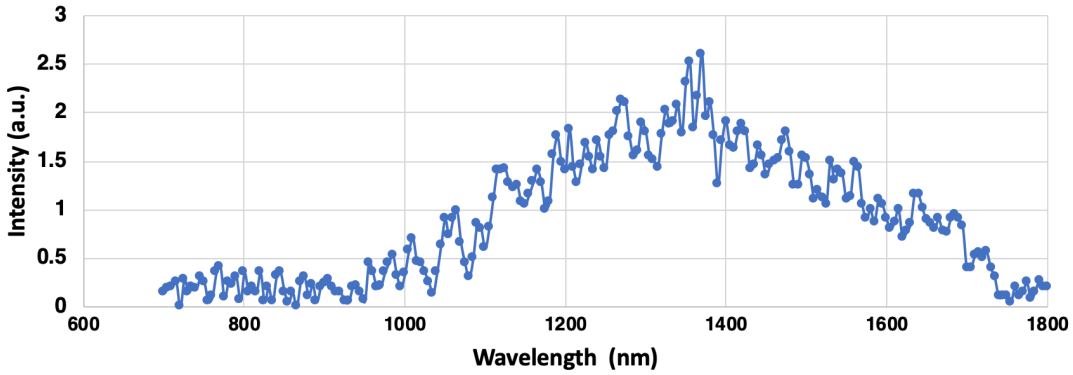

Figure 3.32: Infrared PL emission spectrum of liquid-phase exfoliated graphene nanomaterials, showing a broadband PL emission envelop with some distinct peaks that are above the noise threshold.

To better understand the physical origin of the small peaks, we investigated the power dependence of these peaks by using a variable attenuator to modulate the maximum 20 mW peak power of the 532 nm pump. As shown in Figure 3.33 for spectra taken on the same location of the exfoliated graphene sample, where the peak power is indicated in the legend as P1 > P2 > P3 > P4, we found that although the envelope PL emission intensity decreased with decreasing peak power, the small peaks above the envelope spectrum persisted with decreasing peak power.

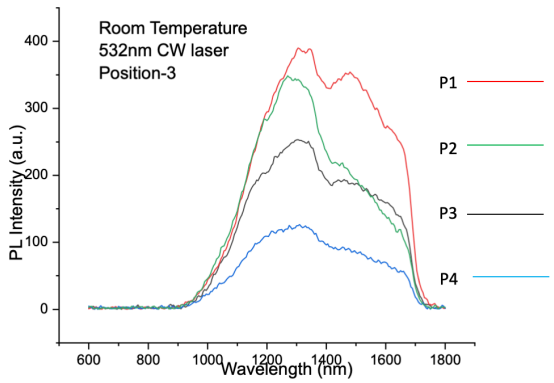

Figure 3.33: Power dependent PL spectra taken with excitation at 532 nm on an arbitrary location (called Position-3) of an exfoliated graphene sample on quartz by varying the peak power arbitrarily using a variable attenuator.

Next, we moved to different locations on the same exfoliated sample to further verify the power dependence of the small peaks. In most other locations, we found the same trend of a broad PL emission with some minor intensity fluctuations on top, and so we do not include the multitude of raw/ similar data here. However, at one position called Position-1, we observed a very unique and unexpected PL emission behavior that resembles some type of standing-modes in a Fabry-Perot cavity, as shown in Figure 3.34. Since we did not expect any new trend, we repeated the measurement such that P4 > P3 > P2 > P1. For this experiment we did not perform a detailed power dependent emission measurement, but used a variable attenuator to reduce the pump intensity and obtained emission spectra for various excitation power.

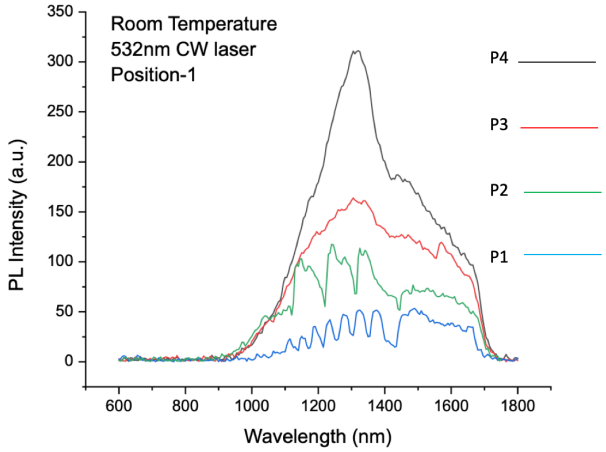

Figure 3.34: PL emission spectra taken with excitation at 532 nm on Position-1 of an exfoliated sample, showing signatures of leaky cavity modes.

It is worth noting that the PL emission from this sample only showed such a well-defined cavity mode in one location, which reflects the random / chaotic structure of the exfoliated samples. It is indeed too early to deduce anything beyond observing that the emission has some patterns of Fabry-Perot modes. However, in the absence of well-defined structures, it would be useful to examine the PL emission from as-grown, pristine, quasi-1D graphene under similar excitation conditions, as they were well-ordered nanostructures with controlled sample dimensions. Using the optical setup described in Figure 3.31, we performed temperature-dependent PL studies of the exfoliated samples from 0.67 eV (1860 nm) to 1.9 eV (650nm) to compare with the temperature dependent behavior of defects in

the visible, where we concluded that there was no observable change in carrier lifetimes with either temperature or sample thickness. For future work, time-resolved PL (with pulsed 532 nm pump and IR detector) needs to be studied by modifying the experimental setup to reduce the optical path length from the sample to the detector. It is believed that the difficulties in obtaining TRPL data in the infra-red could be attributed to the emission being more directive, and thus aperture alignment sensitive, unlike broadband PL emission without any signatures of coherence or directivity.

In the infrared PL spectra, we would expect to see some contributions from phonon interactions that would affect the PL characteristics.

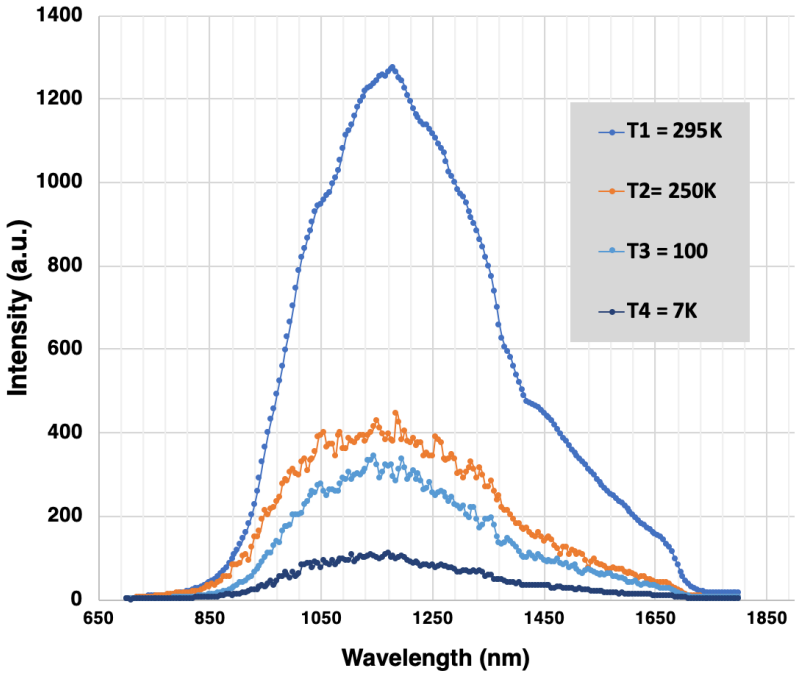

Figure 3.35: Temperature dependent PL emission characterization with CW 532 nm excitation under peak power illumination of 20 mW.

Using a helium-cryostat, we cycled the sample temperature from 295 K down to 7 K and measure the PL emission at different temperatures. For most band-gap semiconductors the PL emission intensity would be higher at lower temperatures because of the suppression in phonon mediated scattering pathways. Radiative decay is often quenched in phonons exchange energy / momentum with an excited “bright state” to dark states that relax

without photon emission due to a momentum preserving relaxation process in the dark states, similar to the indirect band-gap transition. In exfoliated graphene, we observed the inverse effect (Figure 3.35), wherein at high temperatures the PL intensity is higher than those at cryogenic temperatures. It is also worth noting that there is no clear trend in the decrease of PL intensity as we reduced the sample temperature. This trend rules out the possibility of PL emission amplified by sample heating. The reduction in PL intensity from ~ 300 K to 250 K showed a sharpest drop in PL intensity for a 50 K temperature change, whereas from 250 K to 100 K, we only observed a marginal drop in the PL intensity with temperature. One possible explanation for this nonlinear temperature dependence of PL intensity could be the mechanism of thermally activated delayed fluorescence (TADF). TDAF energy relaxation exploits the thermal bath of the sample to couple with dark states, thus creating more "bright states" for radiative decay. This mechanism could qualitatively explain the overall temperature dependence, but the non-linearity is a peculiar feature that needs more investigation

3.7 Second Order Correlation Measurement

In optical interferometers such as the Michelson interferometer, Mach–Zehnder interferometer, or Sagnac interferometer, one splits an electromagnetic field into two components, introduces a time delay to one of the components, and then recombines them. The intensity of the resulting field is measured as a function of the time delay. In this specific case involving two equal input intensities, the visibility of the resulting interference pattern is given by:

$$\nu = |g^{(1)}(\tau)|$$
$$\nu = \left|g^{(1)}(\mathbf{r}_1, t_1; \mathbf{r}_2, t_2)\right|$$

where the second expression involves combining two space-time points from a field. The visibility ranges from zero, for incoherent electromagnetic fields, to one, for coherent electromagnetic fields. Anything in between is described as partially coherent. Generally, the first-order correlation function $g^{(1)}(0) = 1$ and $g^{(1)}(\tau) = g^{(1)}(-\tau)*$, and the

first-order and second-order correlation functions are defined by the following expressions and also exemplified in Figure 3.36:

$$g^{(1)}(\tau) = \frac{\langle E^*(t)E(t+\tau)\rangle}{\left\langle |E(t)|^2 \right\rangle}; \qquad g^{(2)}(\tau) = \frac{\langle I(t)I(t+\tau)\rangle}{\langle I(t)\rangle^2}$$

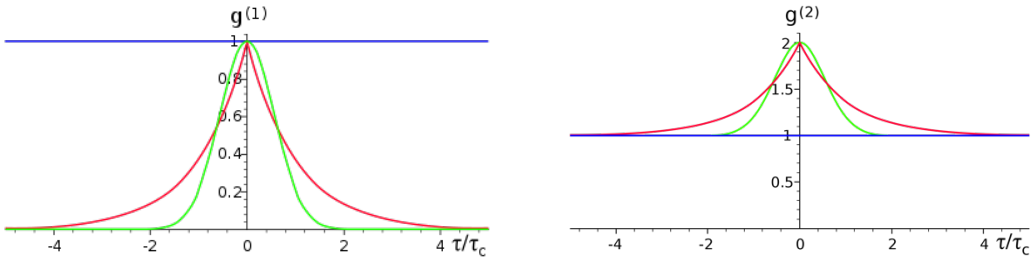

Figure: 3.36: Typical behavior of the first-order correlation (left) and the second-order correlation (right) for laser light (blue) as a function of the time delay τ normalized to the coherence time τ_c. The blue curve is for a coherent state (an ideal laser or a single frequency). In contrast, the red curve represents a Lorentzian chaotic light (*e.g.*, collision broadened), and the green curve is for a Gaussian chaotic light (*e.g.*, Doppler broadened).

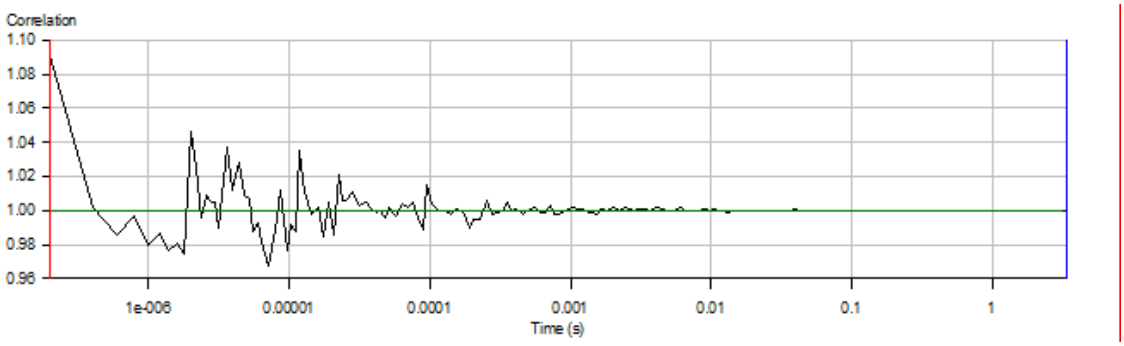

Figure 3.37: Measured second order correlation of quasi-1D graphene grown on silicon substrate, indicating nearly coherent nature of light emission when excited with CW 561 nm (power 5 mW) for up to 0.01 s.

By taking the quasi-1D graphene grown on silicon substrate, we studied the emission of light when pumped with c.w. 561 nm laser and correlated the intensity from two detectors by splitting the emitted light with a beamsplitter. The resulting measurements of the second order correlation is shown in Figure 3.37. Here we note that the plot in Figure 3.37 was not normalized to the coherence time, as that would require a more rigorous measurement in

an interferometer. Further studies are needed to measure $g^2(0)$ for various emission lines, and to identify whether we can tune the degree of spatial and temporal coherence of scattered light by engineering material properties (*e.g.*, the aspect ratio of the quasi-1D graphene or defect engineering) to allow for three-level lasing like situation to be conducive. The correlation fluctuations can indicate the presence of some thermal light in addition to purely coherent states. These initial results are promising to investigate whether PL emission from coherent processes can lead to tunable coherent emission.

3.8 Signature of Spatial Coherence: Interference Fringes

Among many ways of characterizing the coherence of light, a Michelson interferometer is usually the best technique to identify the characteristic coherence time from correlations measurements. To identify the coherence length, the observation of interference fringe patterns is a unique signature of coherent light. In this context, it would be useful to investigate spatially resolved PL maps of the quasi-1D graphene nanomaterials for any possible interference fringe patterns.

As shown in Figure 3.38, we observed clear signature of interference fringe patterns in an as-grown quasi-1D graphene sample over multiple areas when the sample was excited by 470 nm light at 80 MHz and a peak power 10 mW, where the lifetimes of this sample (0.58 ns and 2.0 ns, see Figure 3.39) were consistent with the presence of large edge defects. Typical interference fringes with a high coefficient of finesse (on the order of 10^3) will have sharp bright and dark bands. However, when the coefficient of finesse is less than 1, smeared fringe patterns will appear. From the intensities of the patterns shown in Figure 3.38, we found that the ratio of the peak intensity to the lowest intensity was 4/2 or 1/ 0.5, which indicated a good estimate for the coefficient of finesse F = 1 when we considered the multiple beam interference calculation.

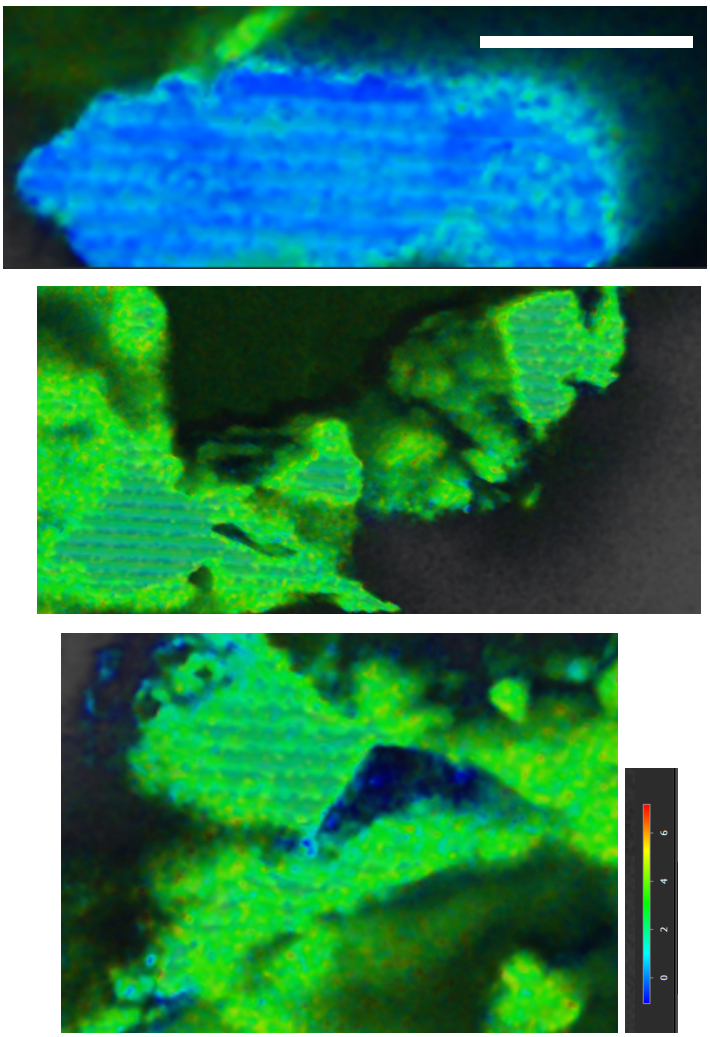

Figure 3.38: False color intensity fringe patterns taken on different areas of as-grown quasi-1D graphene when excited at 470 nm light at 80 MHz, peak power 10 mW, spot diameter 80 μm. Scale bar is 5 μm.

These observations indicate the presence of strong coherent optical effects in quasi-1D graphene that have not been reported so far. It would be important to study whether the graphene nanomaterial can produce such spatial patterns at other wavelengths by tuning the degree of interlinking which may lead to better finesse in the fringe pattern. The degree to which the graphene nanomaterial crosslink, from plasma synthesis, could perhaps be modulating the spatial length scale where scattered light retains spatial coherence. This conjecture would need controlled PECVD synthesis at various growth conditions to map the dependence of material quality.

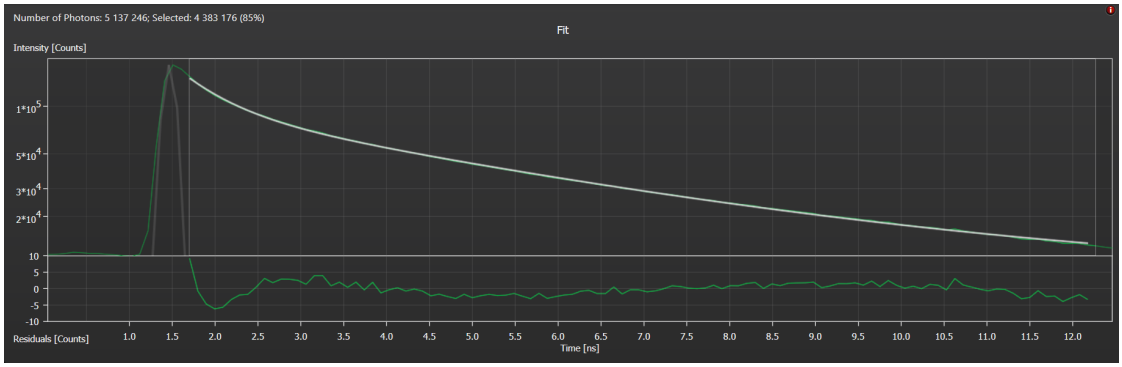

Figure 3.39: Time-resolved PL emission from the material shown in Figure 3.38, confirming sample with lifetimes of 0.58 ns and 2 ns, which indicates that the PL emission is dominated by defects from the edges when the pristine sample is broken.

3.9 Signatures of Coherent Emission

Given the unexpected PL emission spectra from exfoliated graphene nanomaterials showing *signatures* of thermally activated delayed fluorescence and PL emission of a leaky multi-mode Fabry-Perot like emission in some random locations, we were motivated to further investigate the PL emission from pristine, quasi-1D graphene nanomaterial grown on Silicon substrate, with plasma power 30W, within 10 minutes, with a total width of ~ 3 μm.

At this stage, we can only speculate about the exact mechanism of lasing like emission being related to defect induced amplified spontaneous emission or Anderson Localization, among other possible mechanisms. It becomes useful to understand the PL emission from pristine sample so as to guide future material synthesis and material engineering to introduce effective three-level systems within quasi-1d-graphene for more pronounced coherent emission.

Figure 3.40 illustrates the power-dependent PL spectra taken on the as-grown sample, where P1 indicated the power with a 66% ND filter, which yielded 33% of the 20 mW peak

power (P2). When the full CW laser power was applied without any ND filter, we observed the first signature of a lasing-like peak at 995 nm together with some small peaks at other frequencies.

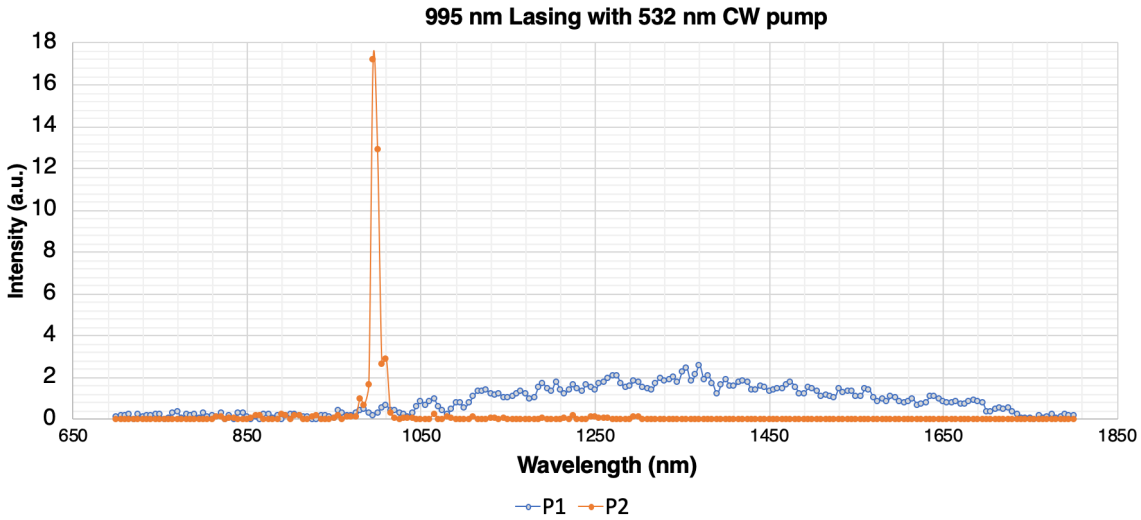

Figure 3.40: PL emission spectra taken on one location of an as-grown quasi-1D graphene nanomaterial excited by CW pump at 532 nm with 20 mW (P2) and 66% (13.2 mW) of the peak power (P1), with spot size of 100 μm diameter, showing a lasing-like peak at 995 nm with 20 mW excitation.

By comparing the intensities of the 995 nm peak with and without the ND (neutral density) filter, we found that the intensity had increased by a factor of 86, from 0.2 to 17.4. The spectral narrowness of this peak also eliminated the possibility of amplified spontaneous emission (ASE), as such a process would have required a separate gain medium and the resultant PL emission would have been much broader. The uniqueness of this lasing-like transition was that the PL emission was mostly suppressed in all other wavelengths, showing a clean single-mode lasing preference. As much as this was an exciting observation that had not been anticipated, we moved to further investigate other locations of the sample for reproducibility of the 995 nm peak.

The existence of a broad distribution of metastable energy levels from defects and the strong quasiparticle(polaritonic) interaction may account for this coherent emission peak.

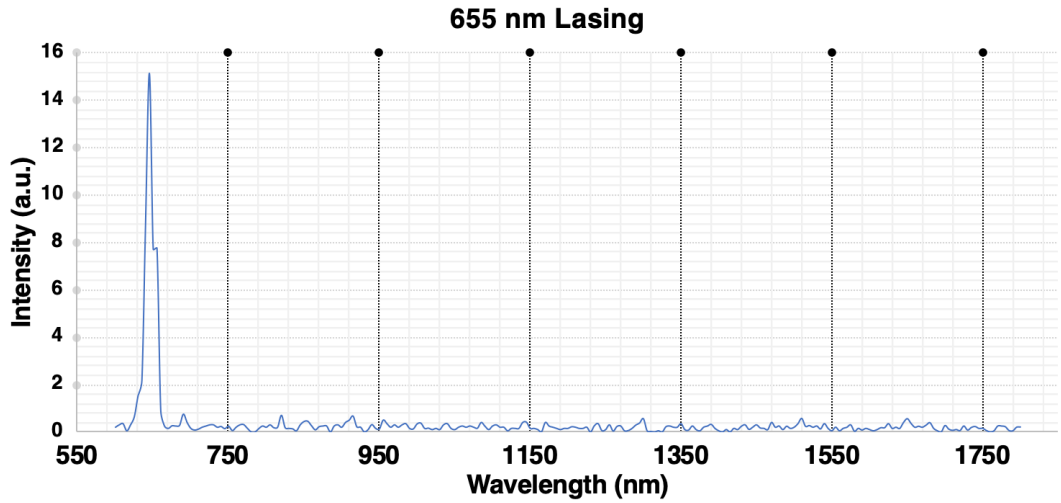

Figure 3.41: PL emission spectrum taken on a second location of the same as-grown quasi-1D graphene nanomaterial as in Figure 3.40, excited by CW pump at 532 nm with 20 mW, with spot size of 100 μm diameter. The spectrum shows a lasing-like peak at 655 nm.

Similar to our previous observation, we also observed another single-mode lasing peak at 655 nm in a different location of the sample (see Figure 3.41), this time almost in the visible spectra, which we did not see before using the confocal microscope arrangement with the LSM 880. In order to better understand the light-matter interaction in this material, we continued to use the CW laser at 532 nm to excite various parts of the sample. In another arbitrary location on the pristine, quasi-1D graphene, we found a strong lasing peak at 1570 nm with a few other amplifying peaks at many other wavelengths, as shown in Figure 3.42.

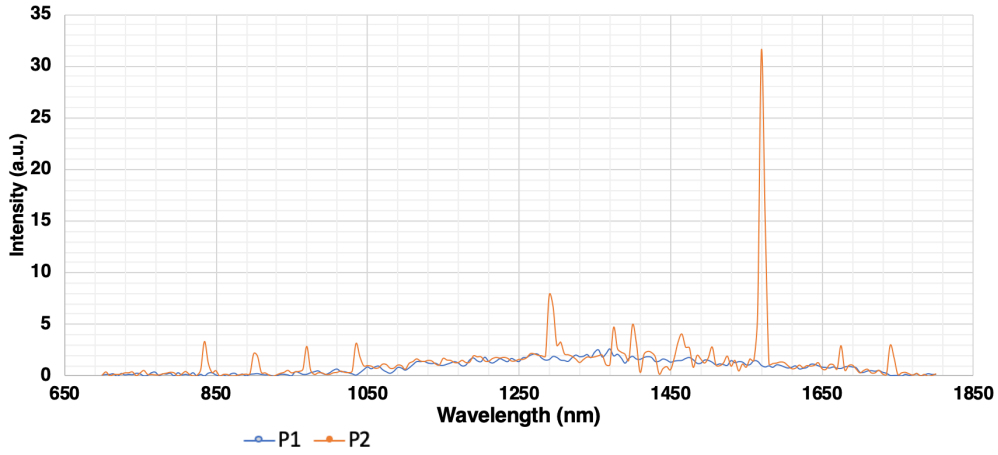

Figure 3.42: PL emission spectra taken on a third spot of the same as-grown quasi-1D graphene nanomaterial as in Figures 3.40 and 3.41, excited by CW laser at 532 nm with 20

mW (P2) and 66% (13.2 mW) peak power (P1), with spot size of 100 μm diameter. A lasing-like peak at 1570 nm and several other small peaks are apparent for the spectrum taken at P2.

The appearance of other peaks is certainly a new hint that there is a possibility of lasing (or amplified spontaneous emission) at multiple wavelengths. The geometry of the quasi-1D material being interconnected at many locations during the PECVD synthesis *may* be treated like coupled resonators where the defect is distributed randomly (in the case of type-1 defects) or selectively induced.

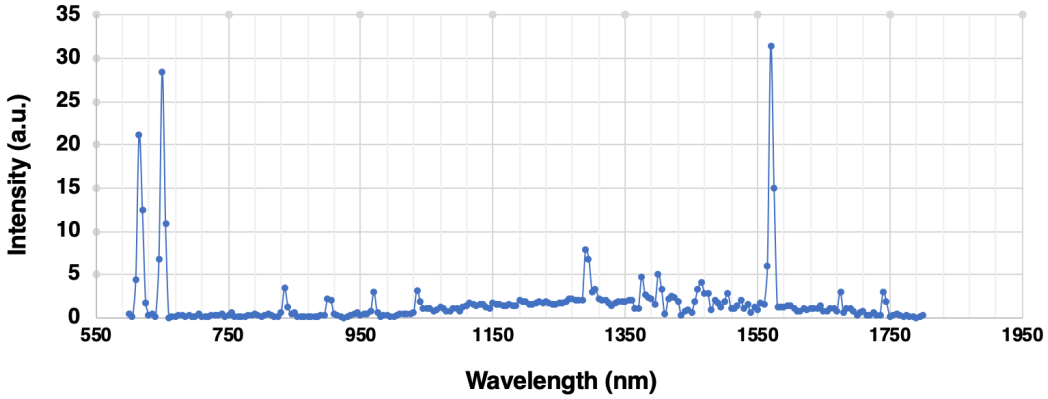

Figure 3.43: PL emission spectrum from a fourth area of the same as-grown graphene sample, showing multi-mode emission from 615 nm, 650 nm and 1570 nm with CW 532 nm excitation at 20 mW.

The PL emission spectrum in Figure 3.43, taken at another different location of the same sample as for Figures 3.40 – 3.42, revealed a departure from a single mode emission to a multi-mode emission. With many other peaks emerging with some amplified peaks, the lasing phenomena exhibited a mode distribution, and thus indicating the availability of various cavities modes within the 100 μm spot. The measurements being done at room temperature, where the PL intensity was expected to be the highest based on our temperature dependent studies shown in Figure 3.35, also indicates that these nanomaterials could be ideal candidates for high temperature lasing, which is in contrast to most conventional lasers requiring cryogenic cooling. The objective of this thesis is grounded on realizing our initial thought-experiment where photon trapped in a cavity should exhibit some degrees of coherent long-range interaction process, and the observed

signatures of lasing is certainly a confirmation that quasi-1D graphene is a perfect candidate to create collective excited states that can be amplified through cavity-photon interaction.

Lastly, we observed, yet another signature of nonlinear optical processes while pumping a different part of the sample with CW 532 nm, when we found a lasing peak at 1290 nm as well as some signature of a damped optical comb or a well defined multimode lasing- like emissions, as shown in Figure 3.44.

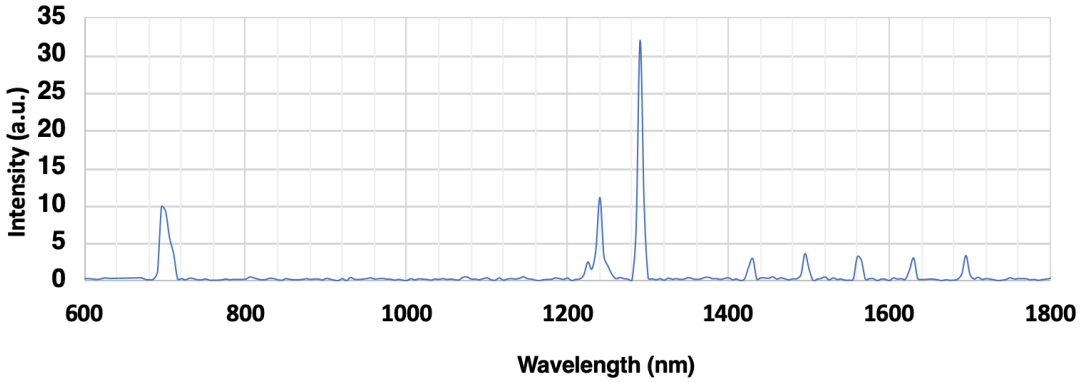

Figure 3.44: PL emission spectrum from a fifth area of the same as-grown graphene sample with CW pump at 532 nm, 15 mW peak power, and laser spot size of 100 μm diameter. The spectrum shows a dominant lasing-like peak at 1290 nm as well as periodic, comb-likes peaks at 1430 nm, 1495 nm, 1565 nm, 1630 nm, and 1695 nm.

The spectrum shown in Figure 3.44 is the first observation of a nearly periodic PL emission peaks, with peak positions at 1430 nm, 1495 nm, 1565 nm, 1630 nm and 1695 nm and the intensities well above the noise floor, indicating the possibility of weak optical frequency comb, or multimode lasing.

During the experiments designed to measure the infrared photoluminescence and the corresponding lifetimes, we accidentally found “frequency comb” like spectra from our as-grown quasi-1D graphene nanomaterial. Conventional optical frequency combs are a phase-stabilized mode locked laser. However, such a signature can also be a simple multi-mode laser oscillation in a cavity. By using 21 THz as the mode spacing (from the measured spectra), we can compute the cavity length L only if we know the refractive index of graphene for plasmon wavelengths accurately. If we assume L to be related to the width of

the quasi-1d-graphene, we need to corroborate the FSR for different width of material (which depends on growth time) and estimate true cavity length, as the index would be the same for plasmons.

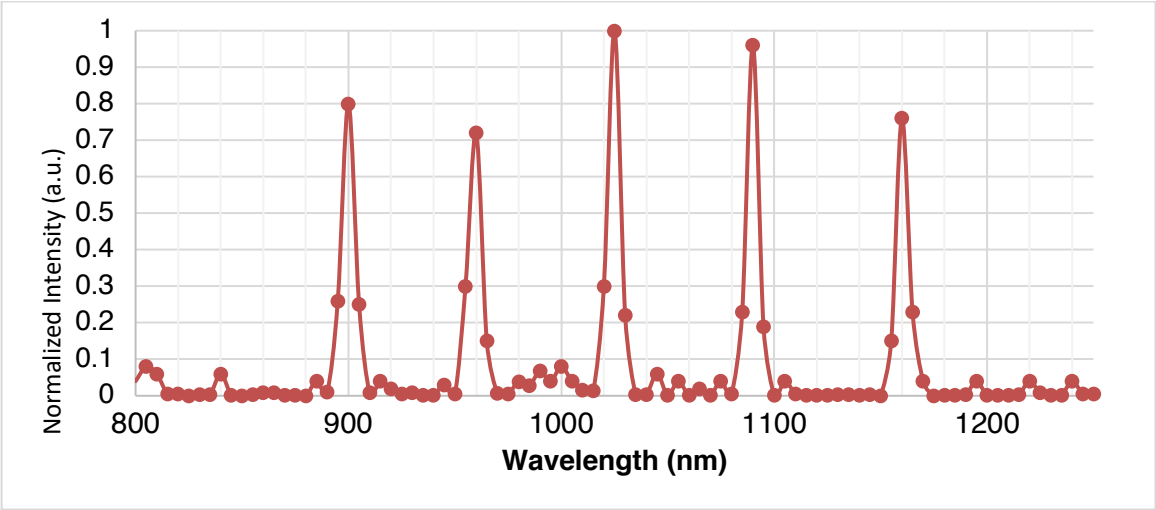

Figure 3.45: The output from CW 532 nm excitation at 20 mW with spot size diameter of 100 μm. Emission peaks at 900 nm, 960 nm, 1025 nm, 1090 nm, 1160 nm.

The distance between two consecutive modes, the Free spectral range (FSR), is about 21 THz on average for modes between 333 THz (900 nm) and 312 THz (960 nm).

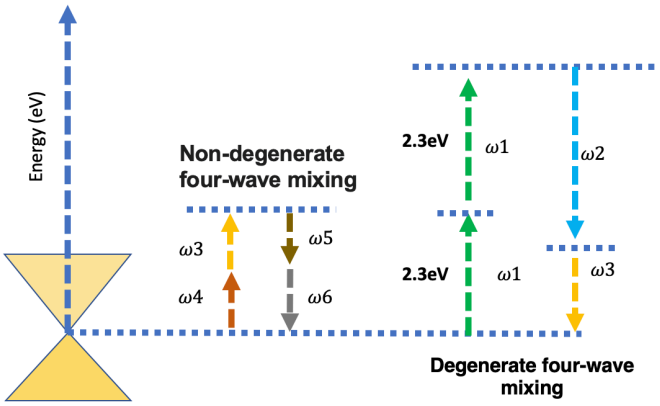

Figure 3.46: Third order non-linear process in graphene at energy beyond the linear-dispersion.

The Kerr nonlinearity is meditated by the refractive index change upon interaction with light, given by $n = n_o + I.n_2$ where n_2 is the Kerr coefficient (also called nonlinear index of refraction) and n_o is the refractive index at frequency v_o of light and *I* is the irradiance of the field. It would be important to verify whether this emission pattern was a result of multimode amplification of light or some other nonlinearity of the material facilitating optical comb generation from degenerate and non-degenerate four-wave mixing. We still need to experimentally measure the value of n_2 from pump-probe Z-scan measurements (PPZM). The work done in Scientific Reports (2019) 9:10540 by A.M. Majedi *et al.* serves as a useful primer.

For a mode-locked laser with FSR ~ 21 THz, with N = 6, we get time domain pulse width ~ **7 fs** (computed as 1/N*FSR = 1/6*21THz) and repetition rate (1/FSR = 1/21THz) as 0.05 ps or **50 fs.** Further analysis and measurements are needed to understand the spectral phase and temporal shape of the measured spectrum. The ultrafast carrier dynamics of graphene combined with broadband absorption and Pauli blocking effect has attributed graphene as an ultrafast saturable absorber. Unlike semiconductor saturable absorber mirrors (SESAM), graphene saturable absorbers have been studied as ultrafast pulse generation by tuning the fermi level in graphene. Further studies are needed to understand the effect of functionalization, layer thickness and defect density on the ultrafast carrier relaxation upon intense CW pumping.

The principle of ultrafast lasers from graphene can also be explained from a graphene saturable absorber (GSA) without invoking Kerr lens mode locking, as suggested by F. Canbaz *et al* [27]. They reported 19 fs pulses from GSA using ~ 275 mW laser pump with tunable output from 836 nm to 897 nm. Further studies need to be done to verify the mechanism of such periodic frequency domain emission.

3.10 Chapter Summary

In this chapter we have demonstrated the excitation wavelength dependent photoluminescence from quasi-1D graphene nanomaterials and were able to attribute the emission at 560 nm to be perhaps from the presence of C=O. We have presented initial results that suggest oxygen plasma treatment can selectively induce these C=O defects. The precise mechanism of excitation wavelength dependent emission is a subject with many suggestive mechanisms, and further studies are needed to identify the origin or PL broadening, with detailed TEM assisted mapping of defects and their PL properties. We also noted some interesting blue shifted photoemission, which is also reported by other organic dye systems, and hence we could study if such blue shift emission can be seen by tuning the pump laser carefully for resonantly exciting other defect modes. From our time resolved photoluminescence studies we established the temperature insensitivity of visible emission and strong dependence on defect density and pump power used. The temperature independent lifetimes are consistent with *ab initio* calculations of 0D exciton radiative lifetimes, suggesting that our notion of PL emissions originating from point defects in quasi-1D graphene nanomaterials is theoretically justifiable. We also found indications that the width of quasi-1D graphene nanomaterials determines the lifetime of excitonic / polaritonic emission from the material. The resonant pump at 561 nm also showed signatures of polaritonic lasing threshold, but more studies are needed to attribute the cause of power dependence of the emission on the pump power. Our initial experiments on using multi-photon femtosecond laser pump had a novel light emission that can be explained from second order nonlinearities, but with regard to SHG detailed studies on thickness dependence on phase matching would be needed to understand the spectral characteristics. Additional measurements of the second order correlation and observation of interference fringe patterns from the PL studies of as-grown quasi-1D graphene nanomaterials in the visible range further indicated coherent light-matter interaction.

Novel light emission, whether through three-level lasing, or polaritonic lasing, is certainly a phenomenon that was not expected when we began these experiments. Such finding

strongly supports our conjecture that these quasi-1D nanostructures have intricate light-matter interactions worth further exploration. One possible direction to pursue is to see if the lasing like peaks may be tuned by material synthesis parameters or defect engineering. Multimode amplified spontaneous emission with nearly equally spaced emission lines also calls for more studies on varying the growth time to change quasi-1D graphene width to see if mode spacing can be tuned. By directly synthesizing quasi-1D graphene on optical fibers, or silicon waveguide coupled to optical fibers, future experiments can be done to verify mode-locked ultrafast lasing from saturable absorption, similar to the work reported by others.

References

[1] Kyriacos Georgiou, Rahul Jayaprakash, Alexis Askitopoulos, David M. Coles, Pavlos G. Lagoudakis, and David G. Lidzey, Generation of Anti-Stokes Fluorescence in a Strongly Coupled Organic Semiconductor Microcavity, ACS Photonics 2018 5 (11), 4343-4351

[2] Jianhua Shen, Yihua Zhu, Cheng Chen, Xiaoling Yang, Chunzhong Li, Facile preparation and upconversion luminescence of graphene quantum dots, Chem. Commun., 2011,47, 2580-2582

[3] Yagafarov, T., Sannikov, D., Zasedatelev, A. et al. Mechanisms of blueshifts in organic polariton condensates. Commun Phys 3, 18 (2020).

[4] Jürgen Mony, Manuel Hertzog, Khushbu Kushwaha, and Karl Börjesson, Angle-Independent Polariton Emission Lifetime Shown by Perylene Hybridized to the Vacuum Field Inside a Fabry–Pérot Cavity, The Journal of Physical Chemistry C 2018 122 (43), 24917-24923

[5] A. Imamoglu, R. J. Ram, S. Pau, and Y. Yamamoto, Nonequilibrium condensates and lasers without inversion: Exciton-polariton lasers, Phys. Rev. A 53, 4250

[6] Rui Su, Carole Diederichs, Jun Wang, Timothy C. H. Liew, Jiaxin Zhao, Sheng Liu, Weigao Xu, Zhanghai Chen, and Qihua Xiong, Room-Temperature Polariton

Lasing in All-Inorganic Perovskite Nanoplatelets, Nano Letters 2017 17 (6), 3982-3988

[7] Seonghoon Kim, Bo Zhang, Zhaorong Wang, Julian Fischer, Sebastian Brodbeck, Martin Kamp, Christian Schneider, Sven Höfling, and Hui Deng, Coherent Polariton Laser, Phys. Rev. X 6, 011026

[8] Guillaume Malpuech, Aldo Di Carlo, Alexey Kavokin, Jeremy J. Baumberg, Marian Zamfirescu, Paolo Lugli, *Room-temperature polariton lasers based on GaN microcavities*, Applied Physics Letters 81, 412-414 (2002)

[9] Klaers J, Schmitt J, Vewinger F, Weitz M. Bose-Einstein condensation of photons in an optical microcavity. Nature. 2010 Nov 25;468(7323):545-8. doi: 10.1038/nature09567. PMID: 21107426

[10] Matković, A. Beltaos, M. Milićević, U. Ralević, B. Vasić, D. Jovanović, R. Gajić, Spectroscopic imaging ellipsometry and Fano resonance modeling of graphene, J. Appl. Phys. 112, p. 123523, 2012.

[11] Thakur, S., Semnani, B., Safavi-Naeini, S. et al. Experimental Characterization of the Ultrafast, Tunable and Broadband Optical Kerr Nonlinearity in Graphene. Sci Rep 9, 10540 (2019). https://doi.org/10.1038/s41598-019-46710-x

[12] Zhixing Gan, Hao Xub and Yanling Haoc, Mechanism for excitation-dependent photoluminescence from graphene quantum dots and other graphene oxide derivates: consensus, debates and challenges, Nanoscale, 2016,8, 7794-7807

[13] Y. Q. Dong, J. W. Shao, C. Q. Chen, H. Li, R. X. Wang, Y. W. Chi, X. M. Lin and G. N. Chen, Carbon, 2012, 50, 4738–4743

[14] Ryan S. Bennink, Vincent Wong, Alberto M. Marino, David L. Aronstein, Robert W. Boyd, C. R. Stroud, Jr., Svetlana Lukishova, and Daniel J. Gauthier, Honeycomb Pattern Formation by Laser-Beam Filamentation in Atomic Sodium Vapor, Phys. Rev. Lett. 88, 113901

[15] H. Zhang, S. Virally, Q. Bao, et al., "Z-scan measurement of the nonlinear refractive index of graphene," Optics Letters, Vol. 37, pp. 1856–1858 (2012).

[16] E. Hendry, P. J. Hale, J. Moger, A. K. Savchenko, and S. A. Mikhailov, "Coherent nonlinear optical response of graphene," Physical Review Letters, Vol. 105, 097401 (2010).

[17] R. Wu, Y. Zhang, S. Yan, et al, "Purely coherent nonlinear optical response in solution dispersions of graphene sheets," Nano Letters, Vol. 11, pp. 5159–5164 (2011).

[18] T. Gu, N. Petrone, J. F. McMillan, et al., "Regenerative oscillation and four-wave mixing in graphene optoelectronics," Nature Photonics, Vol. 6, pp. 554–559 (2012).

[19] Lüttgens JM, Berger FJ, Zaumseil J. Population of Exciton-Polaritons *via*Luminescent sp^3 Defects in Single-Walled Carbon Nanotubes. ACS Photonics. 2021 Jan 20;8(1):182-193.

[20] Yagafarov, T., Sannikov, D., Zasedatelev, A. et al. Mechanisms of blueshifts in organic polariton condensates. Commun Phys 3, 18 (2020).

[21] LSM 880 Zeiss Product Manual: https://www.zeiss.com/microscopy/us/products/confocal-microscopes.html

[22] Leica SP8 microscope product manual: https://www.well.ox.ac.uk/files-library/lecia-sp8-confocal-user-manual.pdf

[23] Kéna-Cohen, S., Forrest, S. Room-temperature polariton lasing in an organic single-crystal microcavity. Nature Photon 4, 371–375 (2010). https://doi.org/10.1038/nphoton.2010.86

[24] W. D. Tan, C. Y. Su, R. J. Knize, G. Q. Xie, L. J. Li, and D. Y. Tang , "Mode locking of ceramic Nd:yttrium aluminum garnet with graphene as a saturable absorber", Applied Physics Letters 96, 031106 (2010).

[25] Ferda Canbaz, Nurbek Kakenov, Coskun Kocabas, Umıt Demırbas, and Alphan Sennaroglu, "Generation of sub-20-fs pulses from a graphene mode-locked laser," Opt. Express 25, 2834-2839 (2017).

Hsiao-Yi Chen, Vatsal A. Jhalani, Maurizia Palummo, and Marco Bernardi, Ab initio calculations of exciton radiative lifetimes in bulk crystals, nanostructures, and molecules", Phys. Rev. B 100, 075135 (2019).

C h a p t e r 4

Experiments in Solar Energy Harvesting

4.1 Conventional Photovoltaic Device Characterization

In a landmark paper published by the Panasonic Group [1] in 2014 "Achievement of More Than 25% Conversion Efficiency with Crystalline Silicon Heterojunction Solar Cell", the current record for heterojunction with intrinsic thin layer (HIT) devices was reported (Figure 4.1).

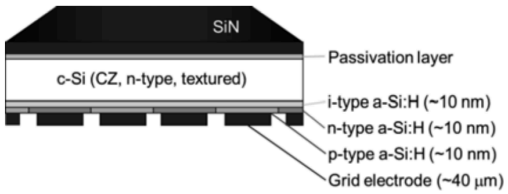

PROGRESS IN CELL PARAMETERS

Year	2013	2014	Improvement
Area [cm^2]	101.8	143.7	
Thickness [μm]	98	150	
V_{oc} [V]	0.750	0.740	−1.3%
J_{sc} [mA/cm^2]	39.5	41.8	+5.8%
F.F. [%]	83.2	82.7	−0.6%
E_{ff} [%]	24.7	25.6	+3.6%

Figure 4.1: Design and characteristics of the Panasonic record Si cell with greater than 25% efficiency (IEEE © 2014, S. Okamoto *et al.*)

Although other materials have shown better solar conversion efficiency [2], the market today is dominated by silicon, and for this reason, we will consider factors that can improve efficiency for all materials. Concentrating sunlight by large mirrors can focus the photon density to a small area. This method helps to go beyond the detailed balance limit (refer Appendix for the formalism of Shockley-Queisser limit, or the SQ limit) as the current in a short-circuited device increases linearly with increasing photon flux, while the open-circuit voltage increases logarithmically, thus resulting in a superlinear increase in the power output. The acceptance half-angle determines the amount of concentration of sunlight as $1/\sin^2$(half-angle). The sun, with its mean distance from earth, subtends a half-angle of 0.2665^o at the Earth's surface. This value translates to a maximum solar

concentration of 46,200 suns (or a photon flux that is 46,200 times more than 1-sun photon flux). Concentrators also need to track the position of the sun to keep the sunlight in focus, and it has been argued that implementing such concentrators is a small material or infrastructure cost. However, the real downside of this idea is that at such high concentrations, the heating in semiconductors would require substantial cooling. Contrary to this issue encountered in typical semiconductor-based solar cells, the findings presented in previous chapters of this thesis suggest that solar devices based on our quasi-1D graphene nanomaterial can overcome the requirement of cooling. (Refer to the article "Energy conversion approaches and materials for high-efficiency photovoltaics" by Martin A. Green* and Stephen P. Bremner [2] for a review of current state-of-art in bandgap materials for solar energy harvesting.)

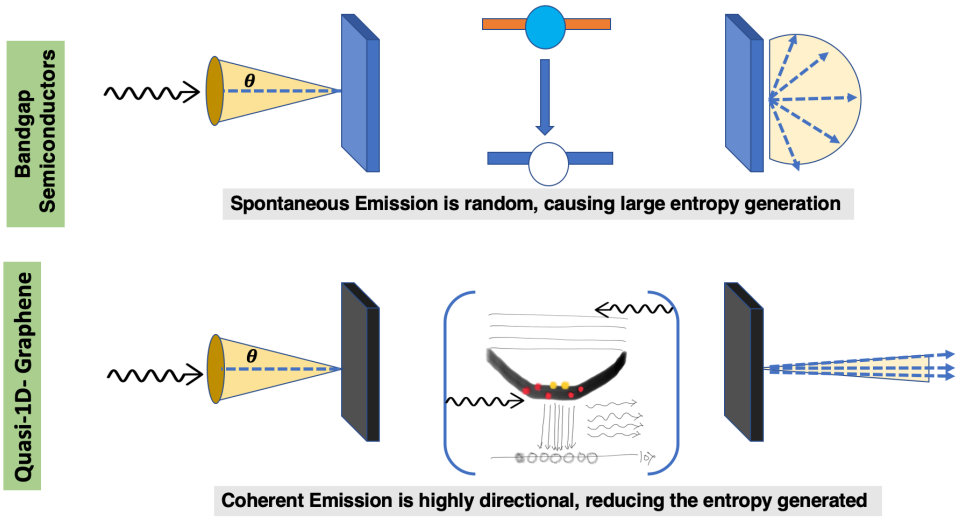

Figure 4.2: Definition of the acceptance half-angle (θ) for concentrated sunlight and the effect of entropy production in spontaneous emission *vs.* coherent emission.

Some efforts on eliminating the need for using large solar concentrators have been focused on designing light collecting nanostructures or microstructures that would limit the light collection angle within the acceptance angle (Figure 4.2). Within the acceptance angle, the cell would convert only direct sunlight and not the diffuse sunlight that can be selectively reflected from the solar cell, as only direct sun can be effectively concentrated. A solar cell may also surpass the SQ limit if the emission of photons is suppressed. However, it

has been shown that energy conservation prohibits this possibility in systems where emission angle is not restricted. In this context, we anticipate the occurrence of multiple absorption events in a solar cell to overcome the SQ limit. Such time asymmetric systems needs light trapping structures to prevent any emission from escaping the material and to be re-absorbed within the material. As clearly demonstrated in previous chapters of this thesis, our quasi-1D graphene nanomaterial is uniquely positioned to achieve this objective by its broadband absorption and selective coherent emission at specific wavelengths. In this chapter, we will show the effect of light concentration in power output.

4.2 Bifacial Graphene Solar Photon Conversion

The first-generation design of our solar energy conversion devices was built under the assumption that we needed different Bragg grating to act as frequency selective surfaces so that white light could be selected at various wavelength bands and be transmitted to the graphene for energy harvesting, as schematically shown in Figure 4.3. We also exploited the design of asymmetric metal electrodes by using gold and aluminum metals for the Bragg metal contacts on the top and bottom of the device. The initial assumption was that the work function difference between graphene and the metallic electrodes [3] would set up a built-in electric field at the interfaces, as there would be a spontaneous charge transfer across the graphene-metal junction to normalize the Fermi level, thus allowing for hot photoelectrons to be collected. The work function of pristine graphene is around 4.6 eV, whereas those for gold and aluminum are around 5 eV and 4.2 eV, respectively. Therefore, the graphene-gold interface would be n-doped and the graphene-Al junction would be p-doped. Without any prior work in the literature on graphene based active solar absorbers, the initial design was inspired from first-principles results obtained by other groups in building optoelectronic devices with graphene.

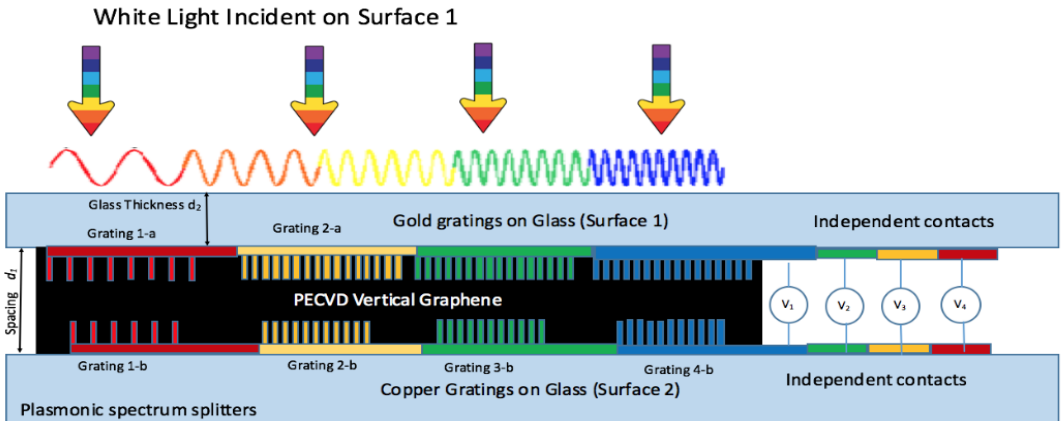

Figure 4.3: Original design of a bifacial solar energy harvesting system with quasi-1D graphene.

The fabrication of the Bragg metal contacts was done directly on quartz (500 micron thickness) from University Wafer *Inc.*. Before electron beam lithography, we deposited a thin layer of chrome (30 nm) to act as a charge dissipation layer for the insulating quartz substrate.

Next, we spin-coated PMMA 950 A9 / PMMA 495 A4 for 1 minute with a thickness of 200 nm, followed by 60 s baking at 180 °C, and then exposed the resist to the designed pattern using the Quanta NPGS E-beam lithography system at the Kavli Nanoscience institute. Once the pattern was written, we developed the pattern in MIBK:IPA (1:3) for 30 seconds. After developing the positive tone resist, we directly deposited 50 nm of Al on one device and 10 nm Ti / 40 nm Au on the second device to act as the two metal contact layers on two identically patterned quartz substrates. The fabrication procedures are summarized in Figure 4.4.

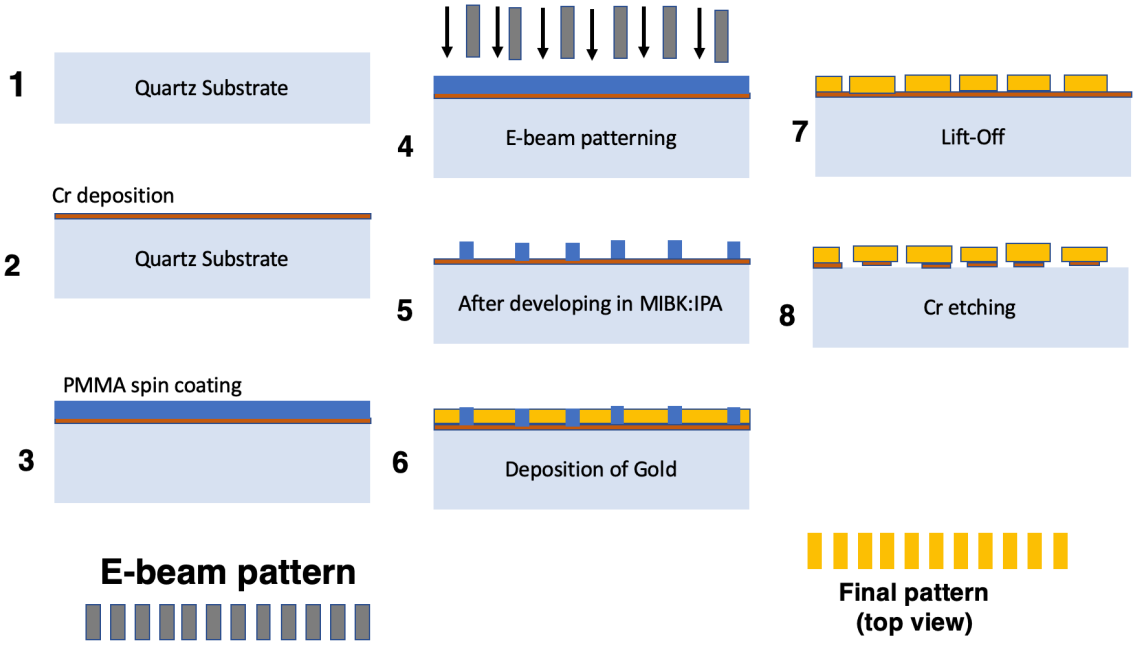

Figure 4.4: Fabrication sequence for nanoscale Bragg metal contacts with gold.

After performing electron beam evaporation, we lifted-off the metal deposited on the resist using a combination of acetone and heated Remover-PG at 60 °C. After lift-off, we etched the base Cr layer with a chrome etchant for 10 s. Examples of the resulting metal contacts are shown in Figure 4.5. This fabrication sequence allows for quick prototyping for different designs and is CMOS scalable for large scale manufacturing. The optimum dose for e-beam was identified by performing a dose array on the pattern to be around 80 uC/cm^2. The assembly of the original device did not allow for wire bonding, given the three-dimensional nature of the final device and the thin brittle film of graphene nanomaterial. A schematic setup of the metal contacts and graphene with Keithley 2450 source meter are depicted in Figure 4.6. Instead of direct sun, we use an Abet Solar simulator that has a nearly identical solar spectrum and power density.

Each Bragg grating was 10 micron long with 500 nm spacing (Figure 4.5) to select light in the green wavelength band of the solar spectrum, as green light has the maximum solar irradiance. The Abet solar simulator produces about 1000W/m^2 and is capable of

performing testing under standard testing conditions, which involves a liquid cooled substrate to keep the device at 25 °C.

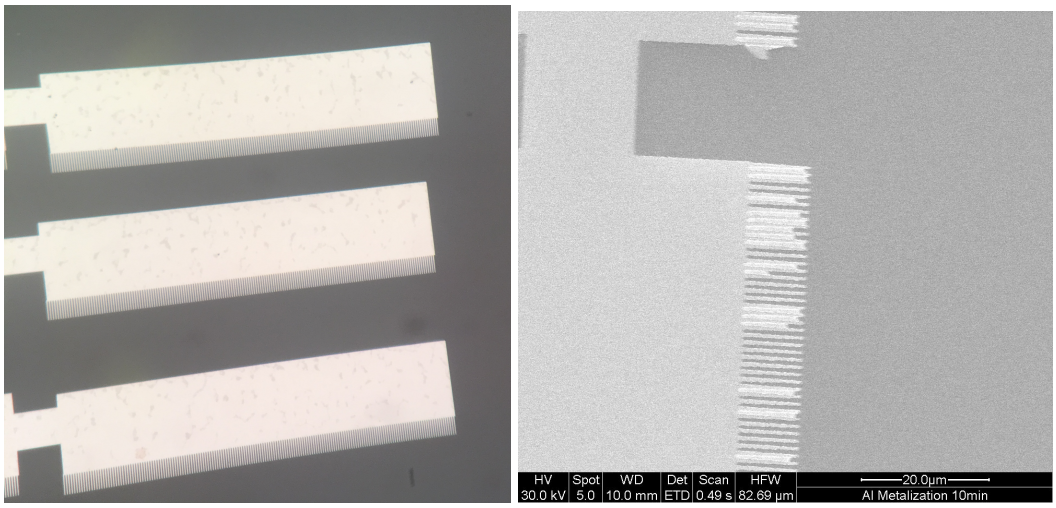

Figure 4.5: Optical microscope image (left) and SEM (right) of the original device metal contacts

Real world operation of solar cells does not operate under such a controlled environment, and hence during the testing we did not use the liquid cooling, apart from the fact that the cooling mechanism was also not functional. From the IR PL characterization of the quasi-1D graphene in Chapter 3, we have seen that the PL emission is higher at higher temperatures in the IR band, and hence it seems ideal to characterize our devices with solar induced heating. We also note that during the fabrication of nanoscale Bragg reflectors, there were some lift-off difficulties, as noted in the SEM image in Figure 4.5, where there was incomplete lift-off. Nonetheless, these imperfections should not affect the overall current collection of the device.

4.3 Experimental Results and Efficiency

For the following device characterization, vertically grown, quasi-1D graphene was synthesized with 40 W microwave plasma with H_2/CH_4 flow rates at 40 / 2.5 sccm for 10 minutes. Under these conditions, the thickness of the material was about 50 µm. This

material thickness range will be crucial for further experiments, because we have found that materials that are too thin would crack during device assembly, whereas materials that are too thick would quench the PL emission or act like a simple carbon photodetector without showing a significant dark current to light current change.

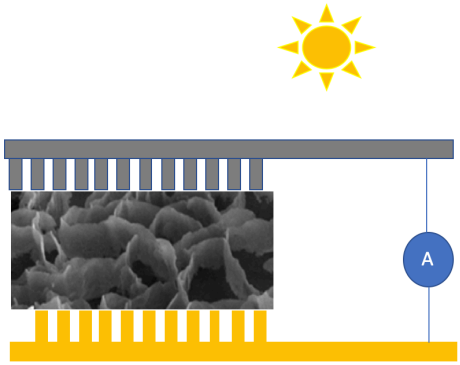

Figure 4.6: Schematic representation of the device with sandwiched quasi-1D graphene nanomaterial between aluminum and gold contact with Bragg gratings illustrated in Figure 4.3. The measurement used an ABET solar simulator to mimic the solar spectrum.

In all our measurements, we connected the device to a two-probe Keithley 2450 for sourcing a voltage and measuring a current (Figure 4.6). In our first sweep, we scanned the device from -40 mV to +40 mV to identify the possible working range of the device. To our surprise, we observed a very stable current out at almost -314.5 mA, as shown in Figure 4.7. The initial exponential tail, was also within the limits of -0.3145 to -0.316 A, with minor fluctuations. We repeated this measurement by inverting the bifacial device so that we could also identify the effect of metal-graphene junction effect, and the measurement led to a similar I-V plot, indicating that our observation was independent of the asymmetric metal contacts.

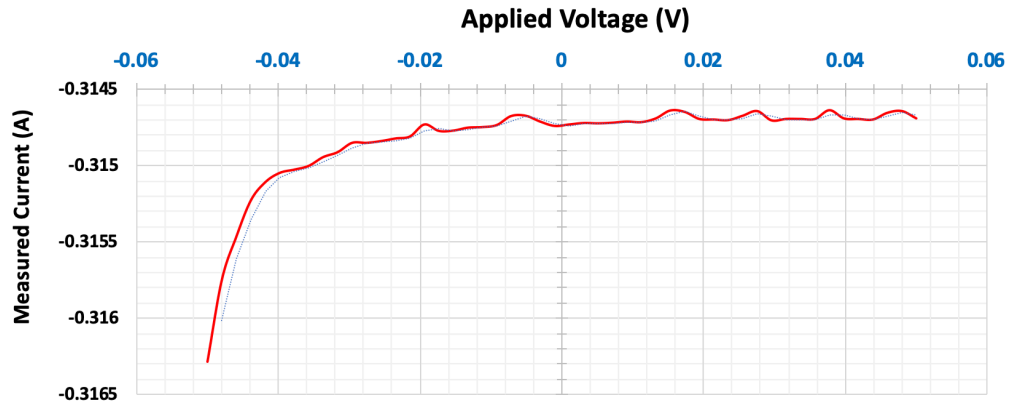

Figure 4.7: I-V measurement from quasi-1D graphene solar cell under 1-sun illumination using ABET solar simulator, with applied voltage sweep from -40 mV to +40 mV

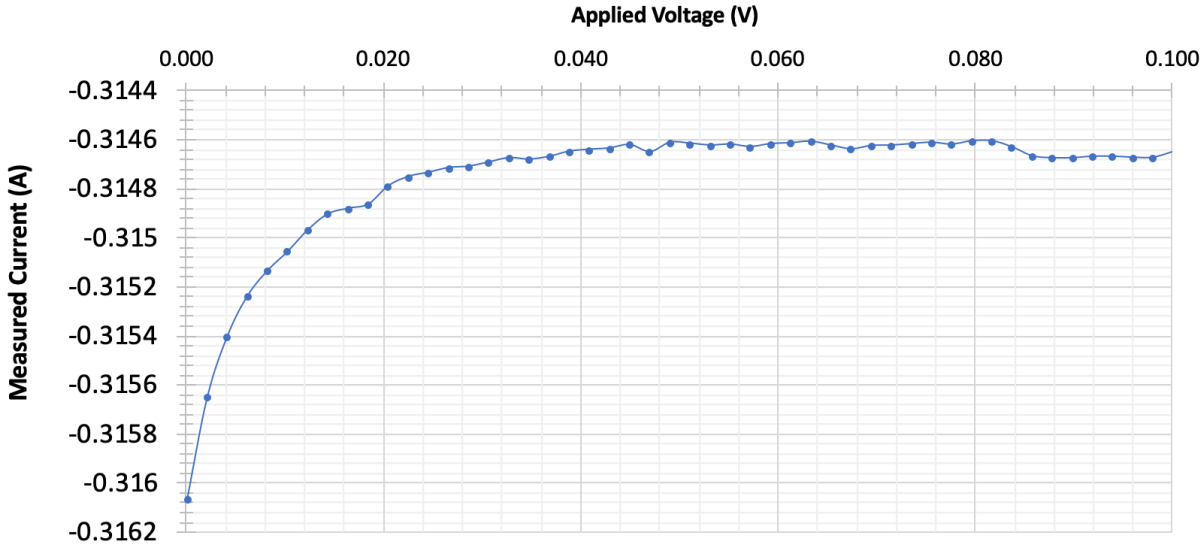

Figure 4.8: 1-sun illumination I-V characterization with voltage sweep from 0 to 100 mV, under 1-sun illumination using ABET solar simulator.

Next, when we cautiously increased the voltage sweep to +100 mV, we could still get the same current behavior with nearly constant current output. The above measurements indicated that for an input power of 1000 W/m^2 , we could estimate the power output at the operating point of the load by multiplying the voltage and current, with peak P_{out} = (– 0.04 V) × (– 313 mA) = 0.0125 Watts, or 12.5 mW. In these calculations, it is important to account for the area of active material, which in our case was less than 1 cm^2, which translated to 12.5 mW/cm^2. Next, we estimated the power output from 100 mV load,

supplied with – 0.3146A (negative sign indicating current is flowing into the Keithley rather than out of the KEITHLEY, which was what we expected when the device functions as solar cell acting like a current source) , or a power output of ~ 30 mW/cm^2. The results actually indicated some signature of a coherent photocurrent, where we obtained a constant output current as if we were collecting a coherent excited state of photoelectrons simultaneously, and this current collection was agnostic to the applied voltage load within certain bounds. At 100 mV, our device was already performing twice better than state-of-the-art silicon solar cells. More detailed I-V characterization data would be needed to verify the scalability of this large photocurrent generation throughout the sample. This proof-of-concept device and electrical characterizations demonstrates the feasibility of using quasi-1d-graphene with defect engineering for solar energy conversion.

4.4 Next Generation Designs for Graphene Solar Energy Harvesting

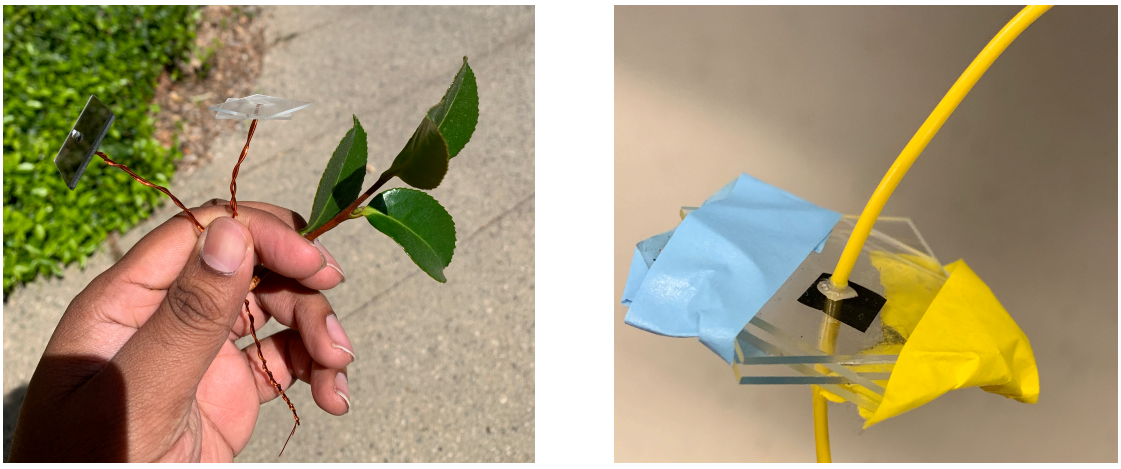

Figure 4.9: Next generation devices with transparent conductive oxide (TCO) contacts.

We are currently building and testing devices that eliminate the need for dual metal contacts (like gold and aluminum). We are also verifying the conjecture on whether a Bragg reflector is needed. Some preliminary results (not included at the moment) suggest that there is no mandatory requirement for having Bragg plasmonic contacts, although having such frequency selective reflectors allows for better light trapping within the quasi-1D

graphene nanomaterials. The dielectric sputter deposition tool at KNI, Caltech allows for quick deposition of low sheet resistance ITO conductive oxide [5] coatings from 30 nm to 50 nm with good transmission window in the visible, though the IR transmission is much lower. We are cautiously investigating the feasibility and viability of incorporating these expensive materials as contact metals into our solar devices.

4.5 Chapter Summary

Pristine quasi-1D graphene without any defects is a semi-metal without any bandgap and cannot create any photo voltage when illuminated with broadband sunlight. The sub-wavelength scattering effects of quasi-1D graphene nanomaterials enable strong broadband light trapping, and the presence of defects in these materials as color centers allows for a broad spectral excitations of the defect centers. The precise mechanism for stable photocurrent is not yet verified, but the presence of such photon harvesting regime invites more detailed studies on mapping the PL emission and photocurrent collections from different parts of the sample. One also needs to study whether the material is able to emit photons of a different spectral feature when illuminated by a solar simulator vs a laser source.

To verify the conjecture that the entropy reduction leads to larger work extraction, we need to measure the spatio-temporal coherence of the light emission under solar excitation, without making electrical contact. The polaritonic excitation decays can be studied as a photon if we use a photodetector, or the excitonic effect is captured when we make an electrical measurement. There are thus these open-ended questions that need to be addressed to conclude the mechanism of large photocurrent production. Our results from Chapter 3 only suggest some possible mechanism relating to local amplified spontaneous emission, or polaritonic emission.

References

[1] K. Masuko *et al.*, "Achievement of More Than 25% Conversion Efficiency With Crystalline Silicon Heterojunction Solar Cell," in *IEEE Journal of Photovoltaics*, vol. 4, no. 6, pp. 1433-1435, Nov. 2014, doi: 10.1109/JPHOTOV.2014.2352151.

[2] Green, M., Bremner, S. Energy conversion approaches and materials for high-efficiency photovoltaics. Nature Mater 16, 23–34 (2017). https://doi.org/10.1038/nmat4676

[3] Cusati, T., Fiori, G., Gahoi, A. *et al.* Electrical properties of graphene-metal contacts. *Sci Rep* **7,** 5109 (2017). https://doi.org/10.1038/s41598-017-05069-7

[4] Zheng, X., Jia, B., Lin, H. *et al.* Highly efficient and ultra-broadband graphene oxide ultrathin lenses with three-dimensional subwavelength focusing. *Nat Commun* **6,** 8433 (2015).

[5] Ikhmayies S.J. (2017) Transparent Conducting Oxides for Solar Cell Applications. In: Sayigh A. (eds) Mediterranean Green Buildings & Renewable Energy. Springer, Cham. https://doi.org/10.1007/978-3-319-30746-6_70

[6] Fahhad H. Alharbi, Sabre Kais, Theoretical limits of photovoltaics efficiency and possible improvements by intuitive approaches learned from photosynthesis and quantum coherence, Renewable and Sustainable Energy Reviews, Volume 43, 2015, Pages 1073-1089,

[7] Green, M. Commercial progress and challenges for photovoltaics. *Nat Energy* **1,** 15015 (2016). https://doi.org/10.1038/nenergy.2015.15

[8] Green, MA, Dunlop, ED, Hohl-Ebinger, J, Yoshita, M, Kopidakis, N, Hao, X. Solar cell efficiency tables (version 56). *Prog Photovolt Res Appl*. 2020; 28: 629– 638.

[9] Abrams, Z. R. (2012). Thermodynamics, Entropy, Information and the Efficiency of Solar Cells. UC Berkeley. ProQuest ID: Abrams_berkeley_0028E_12229. Merritt ID: ark:/13030/m52z19hg. Retrieved from https://escholarship.org/uc/item/60v8s91

Chapter 5

Conclusion and Outlook

Our demonstration of direct low-temperature PECVD synthesis of quasi-1D graphene on silicon substrates opens up new opportunities to investigate the nanoscale light-matter interaction further. Geometric engineering and defect landscape control of the nanostructured graphene may lead to more stable lasing, long coherence length / time, temperature resilient lasing, and multi-color lasing.

The preliminary observations in this thesis of novel optical effects in quasi-1D graphene, such as blue shifted photoemission, signatures of coherence, large photocurrent, CW pumped lasing-like emission opens up many applications in nanoscale optical energy generation for on-chip applications, optical powering of implantable devices for sensing and drug delivery, as well as feasible on-chip spectroscopy for biologically relevant chemicals. Such applications typically required large instrumentation, and the ability to produce laser lines in IR is typically more complex and has not been miniaturized to date.

Solar energy harvesting for the past several decades has focused on semiconductor light-matter enhancement approaches, from surface roughening, paraboloid light collectors, heterojunction stacking, high-mobility materials like GaAs, to dye based active absorbers. In this thesis, through detailed studies of the carrier dynamics, we have demonstrated that there may exist a new opportunity to harvest solar photons with semi-metallic, or metallic, graphene nanostructures with excitonic defects that can be synthesized directly by a low-temperature PECVD process on different substrates including silicon. The preliminary results presented in this thesis have shown a proof-of-concept demonstration and further experiments are needed to understand the origins of constant photocurrent.

Taking inspiration from studying the defects in our vertically grown graphene nanomaterials, we observed that the Ar plasma could etch layers of the materials at

different depths based on the etching conditions (*e.g.*, plasma power, growth time). Given the ease at which these ideas can be prototyped and fabricated under 10 minutes of PECVD growth, and the moderate complexity in modelling these graphene meta-surfaces, it is prudent to experimentally try various geometries and perform optical characterization to see if we can tune the laser output or modulate the comb characteristics.

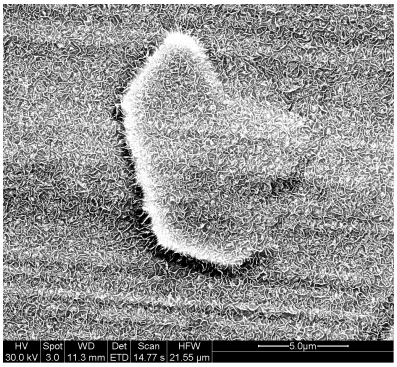

Figure 5.1: The effect of layer-by layer etching leaves large defects along the edges of the unetched portion of the vertically grown quasi-1D graphene nanostructures.

The SEM image in Figure 5.1 clearly shows no control in the etching process when the plasma was directly interacting with the bulk material, and we only observed the residual material towards the end of etching when the material remained exhibited the depth profile where we observed large photoluminescence signal from. The use of Ar plasma to completely remove or partially etch the graphene nanomaterials is highly advantageous in device fabrication scalability without the need for more complex methods. For instance, we may consider developing graphene nanomaterials into whispering gallery mode (WGM) type resonators by plasma etching of PECVD-grown quasi-1D graphene nanomaterials. Once we etch the graphene to a desired circular geometry, we can then mask the graphene and select open etch windows to undercut the quartz or oxide substrate to create supporting pillar structures for the graphene resonators, as illustrated in Figure 5.2.

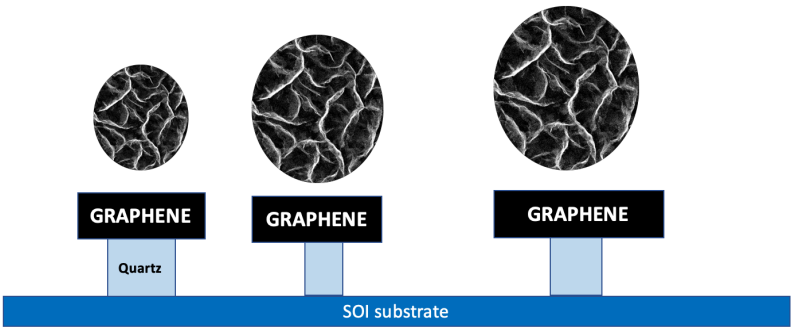

Figure 5.2: Proposed suspended structures of vertical graphene by undercutting the quartz with buffered HF etching, and masking the graphene, to create WGM type resonators

Apart from using pristine material for on-chip applications, exfoliated graphene nanomaterial can also serve as low-cost photodetectors. Preliminary results shown in Figure 5.3 have demonstrated changes in the photoconductivity when illuminated at 10 K with 365 nm light source.

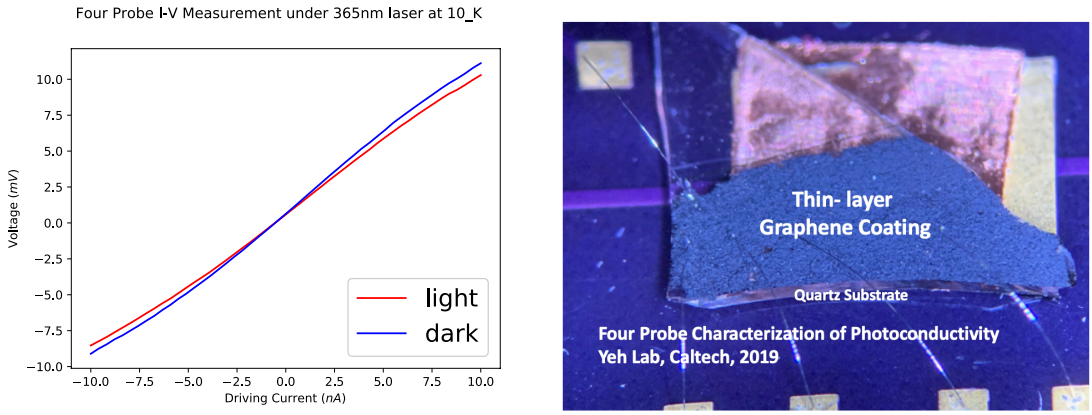

Figure 5.3: Thin-film deposited graphene nanomaterial for on-chip photo detection by photo-induced changes in the current-voltage characteristics.

Once we identify the suitable material synthesis parameters and substrate geometry that produce lasing-like amplified emission lines in a reproducible fashion, we can then fabricate Bragg gratings to act as an optical cavity to select the lasing wavelength of interest from the frequency comb output, as exemplified in Figure 5.4 and Figure 5.6.

Alternating stacks of AlGaAs/AlAs can be deposited on a thin quartz spacer placed directly above the vertically grown quasi-1D graphene nanomaterial to act as the gain mirror, similar to an optically pumped vertical cavity surface emitting laser, as depicted in Figure 5.6. These pairs of materials can be tuned to select laser wavelength from 800-920 nm. AlAs/GaAs pairs are typically used for the window of 920-1200 nm or AlAs/GaAs for the window of 1000 nm to 1550 nm.

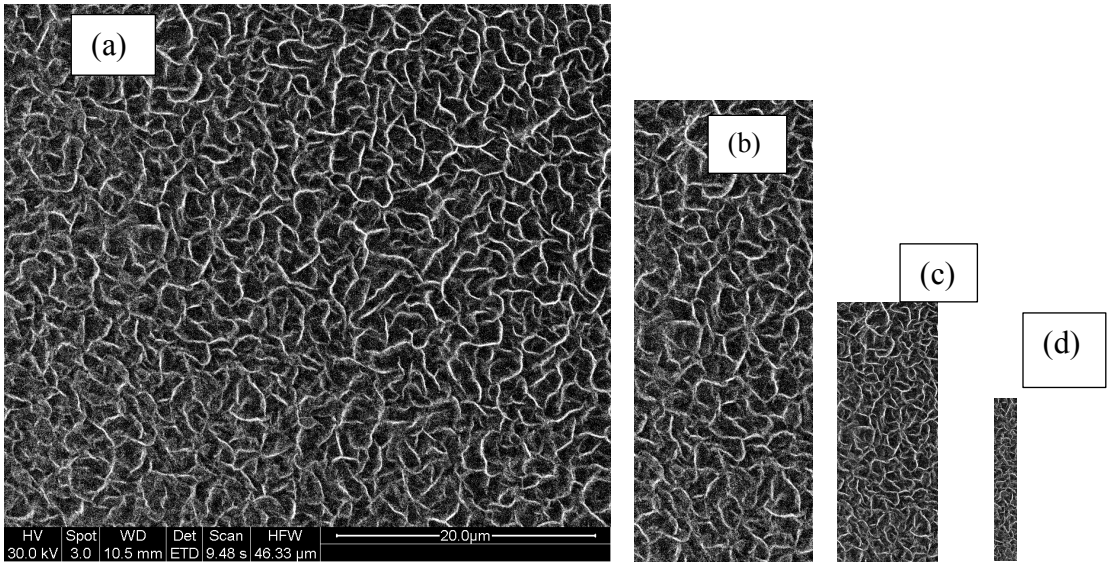

Figure 5.4: (a) Quasi-1D graphene nanomaterial directly grown on 1 cm × 1 cm copper foil. (b-d) The next three images show a few possible variations in the substrate size to directly study the effect of length scales on the light emission.

For instance, taking the value of refractive indices for n(GaAs) = 3.49 and n(AlAs) = 2.95, we can then simulate the reflectivity of the mirrors by solving the complex form of the Fresnel equation or using other techniques like the transfer matric method. For a center wavelength of 1064 nm, simulation results yield the optimum number of pairs of materials needed for single mode selection at 1064 nm to be about 18 pairs or better (as depicted in Figure 5.5). The as-grown vertical graphene can be placed above the DBR mirrors (gain mirrors).

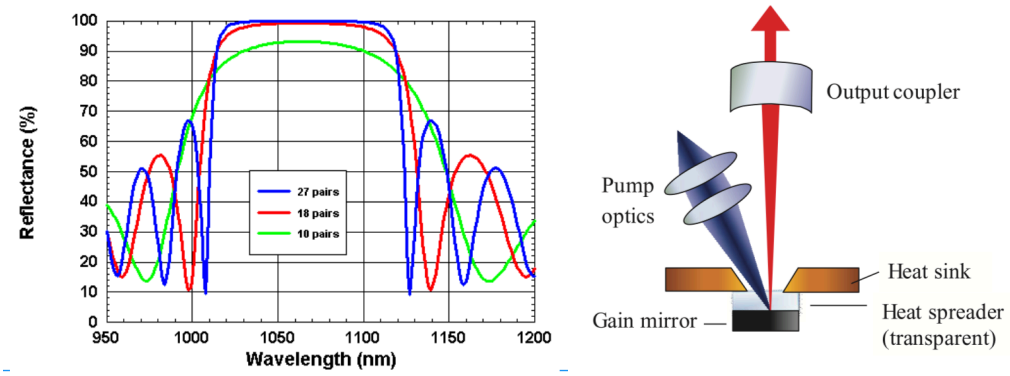

Figure 5.5: Bragg mirror selectivity (left) and optically pumped VCSEL (right). Source: J. Phys. D: Appl. Phys. 50 (2017) 383001.

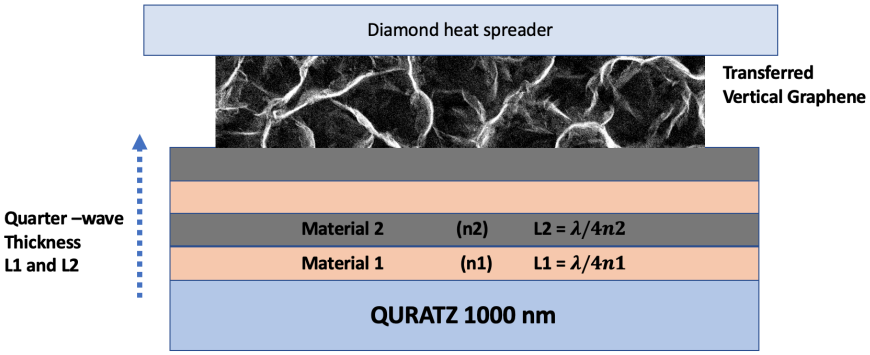

Figure 5.6: Schematic representation of DBR mirrors with just two pairs deposited on quartz substrate and graphene transferred on top with a diamond heat spreader placed above.

By carefully examining other material pairs such that n1 and n2 contrast is high, we can design DBR mirrors with more commonly available fabrication materials in the Kavli Nanoscience institute. This configuration in Figure 5.5 shows that the graphene laser can be pumped from above the diamond spacer and the mode selected by the DBR mirror that we design by careful material consideration and reflectivity estimation from simulation. We can also explore the possibility of directly synthesizing vertical graphene on novel substrates that are part of the DBR mirror materials, so that we can avoid the mechanical transfer step completely to improve output coupling of the laser. The applications of quasi-1d-graphene can be extended to other domains for bioimaging, or neural interfacing, electrochemical sensors, etc., by exploiting the light-matter interaction studies reported here.

APPENDIX

To corroborate the claim that we have the presence of C=O bonds in our pristine samples after exfoliation, we conducted EDS measurements and noticed a weak oxygen peak in the sample.

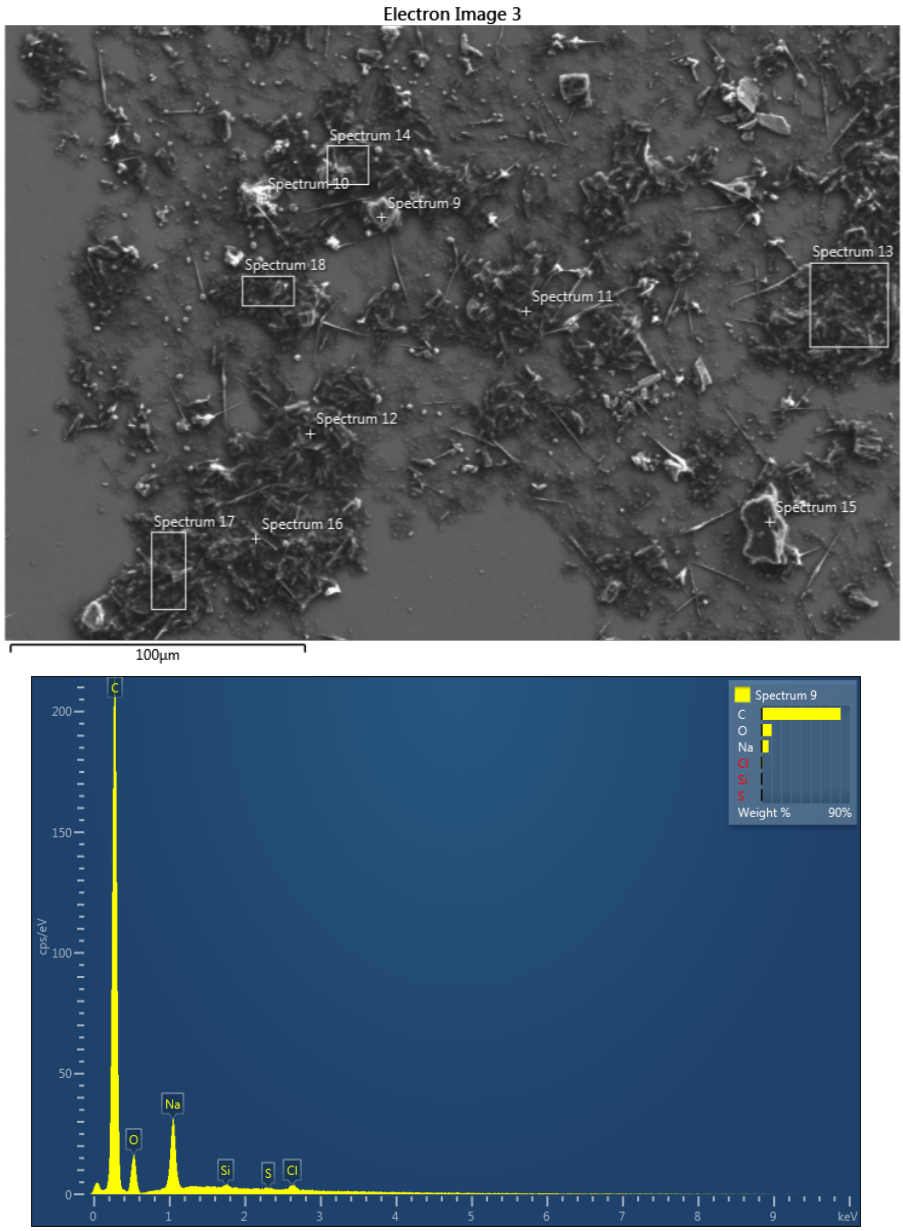

Figure A1: EDS spectrum (bottom panel) of liquid phase exfoliated quasi-1D graphene nanomaterials (top panel: SEM image), confirming sparse presence of oxygen.

Notes on Shockley Queisser (SQ) Limit

William Shockley and Hans Queisser published the “detailed balance limit” which states that the maximum electrical work that can be extracted from a solar cell is simply the difference between the absorbed and emitted radiation. The “ideal” solar cell, as described by Shockley and Queisser in their detailed balance model, is based on a certain number of assumptions: (1) Each absorbed photon generates one single electron-hole pair. (2) There is no absorption of photons with energy less than the semiconductor band gap. (3) The only recombination process within the cell is radiative recombination. The other non-radiative processes (Shockley-Read-Hall (SRH), Auger) are thus neglected. (4) The resistive losses are assumed to be zero. (5) The cell temperature is kept equal to the ambient temperature (300 K).

[1] William Shockley and Hans J. Queisser , "Detailed Balance Limit of Efficiency of p-n Junction Solar Cells", Journal of Applied Physics 32, 510-519 (1961)

[2] Xu, Y., Gong, T. & Munday, J. The generalized Shockley-Queisser limit for nanostructured solar cells. *Sci Rep* **5,** 13536 (2015).

[3] Luque, A. & Hegedus, S. Handbook of Photovoltaic Science and Engineering. (Wiley, 2011).

[4] Rau, U., Paetzold, U. W. & Kirchartz, T. Thermodynamics of light management in photovoltaic devices. Phys. Rev. B 90, 035211 (2014).

[5] Hirst, L. C. & Ekins-Daukes, N. J. Fundamental losses in solar cells. Prog. Photovolt. Res. Appl. 19, 286–293; 10.1002/pip.1024 (2011).

[6] A. De Vos & H. Pauwels (1981). "On the Thermodynamic Limit of Photovoltaic Energy Conversion". Appl. Phys. 25 (2): 119–125

[7] Green, M.A. (2001), Third generation photovoltaics: Ultra-high conversion efficiency at low cost. Prog. Photovolt: Res. Appl., 9: 123-135.

[8] Hirst, L.C. and Ekins-Daukes, N.J. (2011), Fundamental losses in solar cells. Prog. Photovolt: Res. Appl., 19: 286-293.